DISSERTATION

MICROARRAYS: BIOASSAY PERFORMANCE ON WAVEGUIDE SENSORS AND COMMERCIAL CAPTURE SURFACES

Submitted by

Peng Wu

Department of Chemistry

In partial fulfillment of the requirements

For the Degree of Doctor of Philosophy

Colorado State University

Fort Collins, Colorado

Summer 2006

COLORADO STATE UNIVERSITY

June 28, 2006

WE HEREBY RECOMMEND THAT THE DISSERTATION PREPARED UNDER OUR SUPERVISION BY PENG WU ENTITLED MICROARRAYS: BIOASSAY PERFORMANCE ON WAVEGUIDE SENSORS AND COMMERCIAL CAPTURE SURFACES BE ACCEPTED AS FULFILLING IN PART REQUIREMENTS FOR THE DEGREE OF DOCTOR OF PHILOSOPHY.

Committee on Graduate Work

Bruce A. Parkinson

Thomas Meersmann

Yian Shi

David S. Dandy

David W. Grainger/Advisor

Anthony K. Rappe/Department Head/Director

ABSTRACT OF DISSERTATION

MICROARRAYS: BIOASSAY PERFORMANCE ON WAVEGUIDE SENSORS AND COMMERCIAL CAPTURE SURFACES

Microarray technology allows for large-scale parallel analysis of thousands of parameters within a single experiment, representing a revolution in the field of both genomics and proteomics. While the DNA microarray has been extensively used in gene expression and genotyping studies during the past decade, protein microarrays are still in their early development stage mainly due to the fact that protein molecules are inherently more complex than DNA and respond to these microassay formats much differently. For both DNA and protein microarrays, substantial problems and challenges remain to obtain reliable, clinically useful formats, including microarray surface preparation, microarray agent printing/immobilization, on-array capture assay selectivity and reproducibility, and signal detection sensitivity.

The objective of this dissertation research is to investigate bioassay performance of nucleic acid and protein microarrays on various substrate surfaces including a silicon nitride waveguide sensor surface, model gold and commercial microarraying slides,providing new insight into the surface chemistry influences on DNA and protein immobilization during microarray printing, influences of different hydroxylated additives

in antibody microarray performance, and the relationship between surface capture feature size and analyte flux (surface capture efficiency).

New silicon nitride optical microfarbicated waveguide surfaces were silanized and modified with an organic hetero-bifunctional crosslinker. DNA oligonucleotides, streptavidin and murine anti-human interleukin-1β capture agents were successfully printed onto chemically modified silicon nitride surface in microarray formats, demonstrated by surface capture assays. X-ray photoelectron spectroscopy (XPS) was used to characterize each reaction sequence on the native silicon oxynitride surface. Various hydroxylated additives were added to capture antibody print buffers at different concentrations to stabilize printed antibodies during normal array spot dessication on commercial polymer-coated microarraying slides. Polyvinyl alcohol addition to print buffers produced the most regular spot morphologies, homogenous intra-spot antibody distribution, uniform fluorescence intensity, and improved analyte capture activity, maintaining capture activity against model analytes (anti-human IL-1β, IL-4 and TNFα) on these microarraying slides for up to 1 month under 4°C, dry storage conditions. Experimentally derived immobilized ligand and target capture densities as a function of microspot size for DNA probe oligomers on model gold substrates are compared directly with theoretical mass-transfer analysis, validating the inverse relationship between analyte flux and capture feature size under mass transfer limiting capture conditions that characterize many such assay formats.

Peng Wu
Chemistry Department
Colorado State University
Fort Collins, CO 80523
Summer 2006

ACKNOWLEDGEMENTS

I would like to thank my advisor, Prof. David Grainger, my advisor and mentor, without whose guidance, patience and encouragement this work would not have been possible.

Drs. Chad Greef, Mike Lochhead and others at Accelr8 Technology Corporation are greatly appreciated for their generous technical assistance in the microarray experiments. I thank Dr. David Dandy for his guidance on our cooperative waveguide biosensor project that runs across several groups at Colorado State University. Drs. Bruce Parkinson, Thomas Meersmann, Yianshi and David Dandy are acknowledged for reviewing and commenting on this dissertation.

I also want to thank members of the Grainger research group, Ping Gong, Jim Christie, Greg Harbers, Marisha Godek, Lisa Chamberlain and everybody else who inspired me to do better in my research projects.

DEDICATION

This dissertation is dedicated to my parents, Dazhi Wu and Jieying Peng, who have always given me love and support. Without them, I could not have possibly done all this. I also dedicate this to my wife, Xing Yin, who has always been by my side throughout this journey.

TABLE OF CONTENTS

PREFACE

This dissertation is written in a compiled "journals-format" style. It is based on two journal publications (Chapter 3 and appendix), two submitted journal manuscripts under review (Chapters 4 and 5), and an overview of DNA and protein microarray methods and progress (Chapter 2), each written in a format set by the American Chemical Society. A brief overview of each chapter is presented below.

Chapter 2 reviews DNA and protein microarray technology: their formats, surface chemistry coupling strategies with considerations for improved protein microarray immobilization strategies, and finally some common microarray detection methods, including conventional fluorescence and radiometric measurements, surface plasmon resonance (SPR) and waveguide methods, with a brief introduction to the concept of our cooperative waveguide biosensor research project running across several groups at Colorado State University.

Chapter 3 (published in *Biosensors and Bioelectronics, 2006*) describes immobilization of DNA oligonucleotides, streptavidin and anti-human interleukin-1β capture agents on chemically modified silicon nitride surfaces in microarray formats, demonstrated by surface capture assays [1]. X-ray photoelectron spectroscopy (XPS) was used to characterize each reaction sequence on the native silicon oxynitride surface.

Importance of covalent binding in both DNA and protein microarray immobilization and analyte capture performance on this two-dimensional microarray platform is also investigated.

Chapter 4 (submitted to *J. Proteomics Research, 2006*) describes the influences of various hydroxylated microarray printing additives on printed capture antibody (anti-human IL-1β, IL-4 and TNFα) microarray performance [2]. Differential interference contrast (DIC) images and fluorescence microscopy images of printed antibody microarray spots were used to compare influences of these hydroxylated printing additives on antibody printing and distribution in microspots on commercial polymer microarraying slides. Fluorescence intensities were also quantified to compare analyte surface capture activities of capture antibodies printed with different hydroxylated additives.

Chapter 5 (submitted to *Proc. Natl. Acad. Sci., 2006*) examines the relationships in microarray assays spots between analyte surface capture efficiency and capture feature size by comparisons of a full reaction-diffusion numerical model with actual DNA capture in an immobilized DNA oligomer/gold experiment system [3]. Both radiometric and fluorescence detection methods were used for validating the inverse relationship between DNA target analyte flux, DNA surface capture efficiency and capture feature size under mass transfer-limiting capture conditions that characterize many such assay formats.

Appendix 1 (published in *Biomaterials, 2006*) is a review of implantable combination devices-- those comprising drug-releasing components together with functional prosthetic implants [4]. This solicited review describes biomedical combination

devices including the drug-eluting cardiovascular stent device whose precedent FDA approval has proven to be landmark in both the regulatory requirements for such devices and the biomedical device industry. New anti-microbial catheters, orthopedic devices, cardiovascular implants, and wound coverings with new added capabilities from on-board or directly associated drug delivery systems will now be developed for improved clinical performance.

References:

(1) Wu, P.; Hogrebe, P.; Grainger, D. W. *Biosens. Bioelectron.* **2006**, *21*, 1252-1263.

(2) Wu, P.; Grainger, D. W. *Submitted to J Proteome Res.* **2006**.

(3) Dandy, D. S.; Wu, P.; Grainger, D. W. *in preview (Proc Natl Acad Sci)* **2006**.

(4) Wu, P.; Grainger, D. W. *Biomaterials* **2006**, *27*, 2450-2467.

CHAPTER I

AN OVERVIEW OF DNA AND PROTEIN MICROARRAY FORMATS AND PERFORMANCE ISSUES

This chapter is an overview of current DNA and protein microarray technology: their formats and surface chemistry coupling strategies with more considerations for improved protein microarray immobilization strategies, and finally some common microarray detection methods, including conventional fluorescence and radiometric measurements, surface plasmon resonance (SPR) and waveguide designs, with brief introduction to the CSU-based cooperative waveguide biosensor project currently involving several groups at Colorado State University.

Introduction to DNA and Protein Microarrays

The microarray is a two-dimensional multiplexed bioassay format comprising tens to thousands of microspots of capture agents with binding activity against libraries of soluble targets. Capture spots of nucleic acids (e.g., DNA), proteins, antibodies or other biomolecular agents are surface-immobilized in a predetermined spatial arrangement onto various solid substrates. [1]. Capture of analyte to each spot is monitored with a variety of detection technologies. Computer processing of the microarray signal set allows rapid, simultaneous determination of analyte presence in samples containing possibly thousands of analytes. The concept of the microarray was initiated by the ambient analyte model of Ekins and colleagues [2-6], which asserts that "microspot" assays that rely on the immobilization of capture agents on a few square microns should be capable of detecting target analytes in solution with much higher sensitivity than conventional macroscopic immunoassays. Boosted by the completion of whole-genome sequencing projects, DNA microarray technology rapidly became the first test of the R. Ekins hypothesis [7, 8]. Since then, DNA and other nucleic acid-based microarrays have made great advancements in facilitating gene expression and genotyping studies during the past decade. However, two other motivations have prompted more recent development of protein-based microarray assays. First, genetic profiling alone does not provide information sufficient to decipher complex cellular signaling pathways and communication networks. Lack of correlations between cellular gene up-regulation, resultant mRNA transcriptional products and translated protein abundance begs for a direct method to screen specific protein products. Second, accurate profiles of differentially expressed proteins by cells, tissue and indeed, whole organisms for better defining biomarkers for both normal

homeostasis, as well as distinguishing a wide range of diseases and responses to therapeutics required a convenient multiplexed format beyond the ELISA assay format. Protein-based microarrays have exhibited frenetic growth and diverse forms over the past few years as a requirement of increasing demand for these capabilities.

DNA Microarray

The DNA microarray exploits classic Watson-Crick (and Hoogsten) nucleotide base pairing interactions to pair target DNA in solution with its complementary printed probe on the array surface. While traditional nucleic acid analytical methods are limited

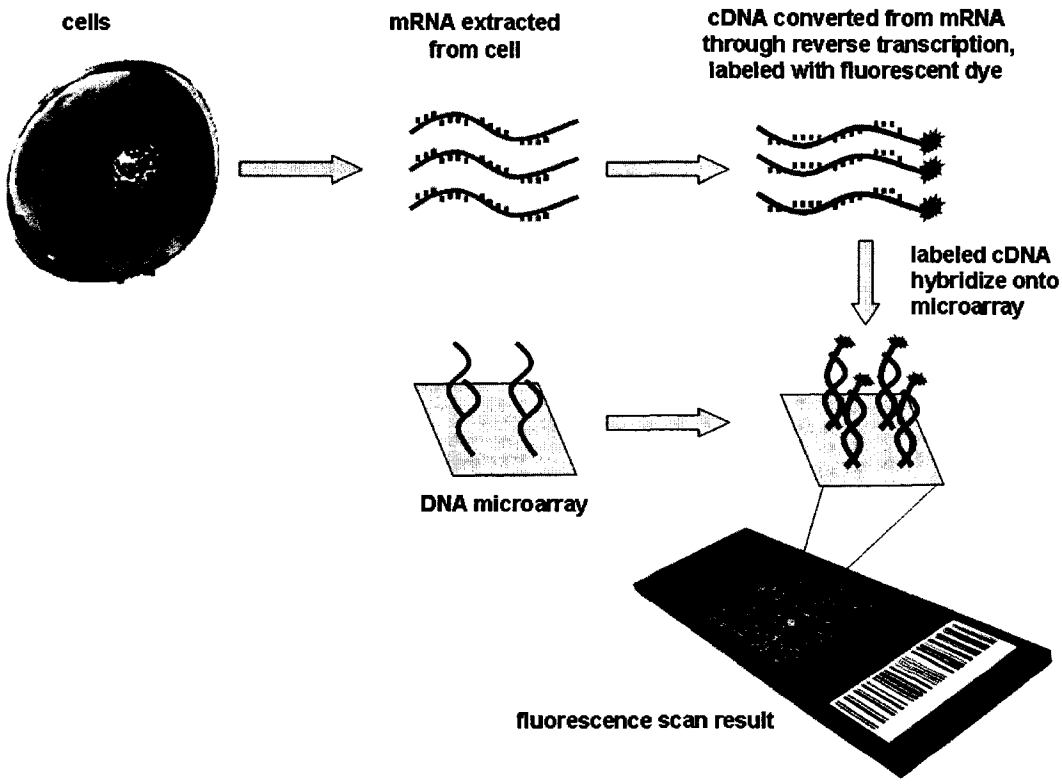

Figure 1. DNA microarray assay format: sample messenger RNA (mRNA) is extracted from a target cell or tissue, purified, and converted into complementary DNA (cDNA), using reverse transcriptase polymerase chain reaction (RT-PCR) that provides fluorescence labeling. Fluorescently labeled sample cDNAs are then exposed and hybridized to a DNA microarray.

to "one gene at a time", DNA microarray technology enables parallel processing of thousands of gene species concurrently by reducing individual assay features to sub-millimeter scales (50 ~ 200 μm) and putting them all on a single assay piece. This miniature assay format (Figure 1) greatly reduces sample consumption, assay time, and provides high-throughput assay technology for genomic studies profiling up to thousands of DNA targets in a single experiment.

Using a DNA microarray, libraries of DNA fragments representing a complete set (e.g., of the mouse or human), or a sub-set (e.g., inflammatory markers in humans) of the genes of an organism are microscopically spotted, often with a robotic ink-jet style or contact pin-type printer [9], to predetermined spatial locations on a solid substrate, usually a microscopic low-fluorescence glass slide. Robotic spotters pull aqueous solution samples of DNA probe fragments from individual wells on 384-well plates, depositing spot volumes of only a few nanoliters onto these supports. These spots usually dry within a few seconds onto the slide, forming circular dried DNA probe domains with diameters of 100-250 microns, spaced 100 microns on center. With successful development of highly accurate robotic spotters, tens of thousands of such DNA probe spots, each representing a unique nucleotide sequence, can be immobilized on a single slide in a few hours, allowing printing of virtually every gene present in a organismal genome. This constitutes the microarray.

Nucleic acid probes are either synthesized directly on the solid substrate or are synthesized by traditional methods and then printed onto substrates [10]. To date, the most popular to date microarray technology, Affymetrix GeneChip® microarrays comprise 25-mer probes synthesized directly on the solid support using a sequential, light-directed

photolithography process [11, 12]. The surface chemistry exploited for this strategy is a proprietary hydroxy-terminated organosilane layer on fused silica optimized for their particular synthesis approach [11, 12]. In many custom-made DNA microarrays, nucleic acid probes are usually obtained in a library from oligo-DNA vendors and printed onto solid substrate. Probes bind to surfaces either through direct attachment, or adsorption as insoluble aggregates.

In the typical DNA microarray assay format (see Figure 1), messenger RNA (mRNA) is extracted from a cell culture or tissue sample, purified, and converted into complementary DNA (cDNA) using reverse transcriptase polymerase chain reaction (RT-PCR) that includes incorporation of fluorescently tagged nucleotides to produce cDNA with fluorescence labels. Once labeled, the cDNA target samples are hybridized to a DNA microarray. Each spot of DNA microarray containing a single printed DNA sequence wherein single-stranded probe DNA fragments are strongly surface-bound, allowing cellular fluorescently labeled cDNA hybridize to a complementary spot on the array. After stringency rinsing of the hybridized array and drying, signal is detected by exposing the microarray to a fluorescence scanner or microscope: hybridized spots are identifiable as fluorescent array spots, while spots with no target hybridized will not be fluorescently visible. Microarray fluorescence data provide a relatively quantitative measurement of gene expression for each gene represented in the microarray (Figure 1). Detection limits vary, depending on substrate, probe length, target length, detection milieu, and spotting method, with femtomolar DNA target frequently reported [13].

In 2005, the first two microarray-based tools for cancer diagnosis gained U.S. Food and Drug Administration (FDA) approval. One test is for predicting the likelihood

of breast cancer recurrence in women with newly diagnosed, early-stage invasive breast cancer [14]. The other one tests a liver enzyme to predict how quickly a person metabolizes certain drugs, to help in prescribing proper amounts. Many more microarray-based tests are still in the development pipeline [14]. Numerous challenges remain in understanding the biological significance of the signal, screened data and various practical issues pertaining to reproducibility, quality control and correlations among different microarray methods and platforms [15]. Recent collaborative efforts have demonstrated much more positive, though certainly not perfect prospects, in performing reproducible microarray experiments between labs and across platforms by using standard methodologies that are adopted for best performance [16-18]. Even so, routine array use in clinical applications for human diagnostics and therapeutics is quite distant.

Protein Microarrays

Protein microarrays can refer to either the protein-based affinity capture agent used in the array, or to the proteinaceous analyte intended to be captured on-array, or both. These arrays offer an opportunity for analogous assay of a full spectrum of protein analytes similar to how DNA microarrays have already provided for genomic analytes in a massively parallel, miniaturized, and automated fashion. Representing a radical revolution from conventional "one protein at a time" methods such as ELISA, column chromatography and spectroscopic studies, protein microarrays promise exciting new capabilities for protein expression profiling, disease diagnosis and drug discovery [19-22].

The basic assay concept, processing steps, and microarray fabrication robotic systems used for DNA microarrays can all be directly applied to protein microarray

technology. However, because the fundamental difference between proteins and DNAs lies in their chemistry and associated higer order structural stability, protein microarrays remain in an early development stage. Proteins immobilized on array surfaces behave differently than nucleic acids in the same situation. Protein microarrays pose several other significant analytical challenges beyond those already known for nucleic acid arrays. First, the sheer number of targets in the human proteome (estimated 40,000 to 1,000,000) is several orders of magnitude more abundant than genes (20,000 to 25,000)[23]. Unlike DNA, which has relatively simple homogenous structure and electric properties, proteins have diverse chemical, structural and biological properties, producing widely different protein-protein, protein-antibody affinities and immobilized protein–microarraying surface interactions. The most common protein capture reagent printed into microarrays is the immunoglobulin G antibody. However, even with nanomolar ligand affinities typical of commercial monoclonal antibodies, analyte capture fidelity, sensitivity and shelf-life issues plague capture agents for protein arrays. High quality sources of specific antibodies or suitable protein binding ligands remain the critical limiting factor for bioassay performance, and starting point for protein microarray improvements. Second, the vast range of protein analyte concentrations of interest for clinical detection is 6 to 10 orders of magnitude between the most and least abundant proteins. In relevant bioassay milieu, however, low abundance analytes (femto- to atto-molar ranges) always exist in complex biological milieu (e.g., serum) containing a vast excess of other non-target proteins, producing high-cross reaction and unacceptable signal to background ratio [1]. Hence, improved capture surfaces and immobilization methods are of interest to enhance difficult-to-detect analyte capture. Third, no direct

amplification methods for protein analytes analogous to PCR for DNA exist, making adequate detection sensitivity (at least femtomolar range) in protein microarray assays a significant issue. Fourth, maintaining structural conformation and bioactivity of printed, desiccated immobilized capture proteins on microarraying surfaces remains a major issue in protein microarray technology. Unlike DNA oligomeric molecules that, because of their general lack of secondary structure in a single-strand state, remain stable under dry conditions and maintain activity after long periods in storage, proteins are known to be more susceptible to desiccation [24, 25 26, 27]. For all these reasons, protein microarrays are much more challenging than DNA microarrays and have not achieved a level of satisfactory performance comparable to DNA counterparts.

Protein microarrays have many diverse formats for protein analyte capture (Figure 2). Recombinant proteins, antibodies, short peptides, aptamers, and unique oligonucleotides can all be screened and used as protein-specific capture agents on the substrate surface according to different applications [28]. Microarrays fabricated using printed recombinant proteins have been used in protein-protein and protein-drug interaction studies [29-32]. Antibody microarrays provide an excellent format for protein expression profiling [33, 34]. Both formats have produced impressive results for the diagnosis of pathogenic bacteria and viruses, cancer, autoimmune disorders, food allergies and other diseases. [35-39] Additionally, different types of short peptides, oligonucleotides and aptamers have also been used in various areas, including diagnostics, epitope analysis and protein folding studies [1, 19, 21, 39-41].

Despite the many different types of protein microarrays reported, all the basic processing steps are the same as for DNA microarrays, including sample preparation and

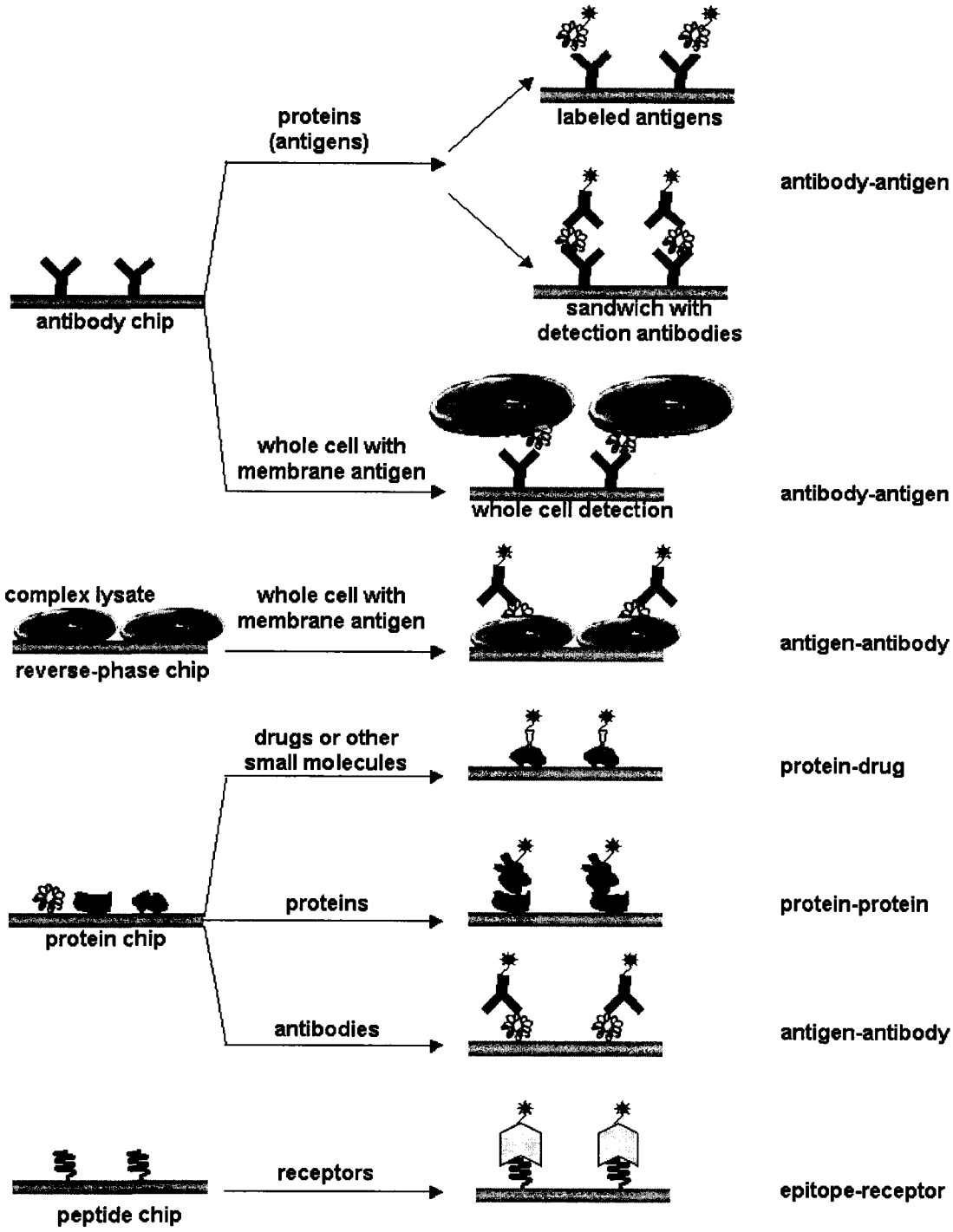

Figure 2. Different formats and applications of protein microarrays. Antigen and antibody microarrays have been used primarily in diagnostics, while protein microarrays have various potential in assaying a wide range of biochemical activities including protein-protein and protein-drug interactions [42]. Peptide microarray can be used in epitope analysis. Cell suspensions can also be incubated on microarrays of antibodies targeting cell surface antigens. Reverse-phase chips are fabricated by spotting complex cell lysates on substrate surfaces, then the presence of particular proteins in the lysates are quantified by incubation of antibodies targeting those proteins.

handling (probe and target), microarray fabrication, surface capture assay (complimentary DNA hybridization, antibody-antigen binding, protein-protein interaction, protein-drug interaction et al.), signal detection (see below, microarray detection technologies section) and data analysis.

Microarray surface chemistry and coupling schemes

Various strategies have been used for microarray construction on a wide range of substrates. DNA microarrays can be manufactured either by synthesis of oligonucleotides *in situ on chip,* or by microarray printing and other delivery techniques of pre-synthesized oligonucleotides and cDNAs from solutions using robotics. By contrast, most protein microarrays can only be delivered or printed onto substrates because the capture elements required for binding specificity exceed the size of peptides that can be synthesized *in situ* [43]. Approaches using modified capture biomolecules with tags to effectively anchor onto chemically reactive microarray or sensor substrates are becoming more popular because of low non-specific binding rates and higher surface coupling efficiency [44]. Nevertheless, many approaches for tailoring microarray surface properties for immobilization of unmodified biomolecules exist [10]. The advantage of this unmodified case is that the inherent biomolecular structure and interaction properties of the immobilized probes with substrate will not be adversely affected by capture molecule modifications. This is more important in protein microarray technologies.

Microarray substrates

Microarrays have been constructed on various substrates including glass, gold,

silicon, and filter paper. Essential practical features are quite simple: inexpensive solid supports or membranes that reliably immobilize printed nucleic acids and capture proteins and retain their specific analyte capture activity in various assay and detection formats over time, with some potential to archive this capture information. Glass slides are the most widely used microarray platform because they afford flexibility in array design and relative economy. Much of the current microarray processing and fabrication equipment, including robot microarray printers and microarray fluorescence scanners, is built around the standard 1" x 3" glass slide. Hence, most commercial available microarraying surfaces are based on glass substrates. Additionally, a rich history and extensively studied field of reactive organosilane coatings on glass and other hydroxylated solid surfaces [45, 46] bolsters the use of glass slides in microarray applications. More specifically, chemi- and physi-sorbed films of alkylchlorosilanes or alkylalkoxysilanes readily form on native oxide glass, silicon, titanium and many other substrates surfaces from solutions, permitting ready modification of glass surfaces to promote immobilization and uptake of printed affinity surface capture agents. Complex polysiloxane layers form spontaneously *in situ* via silane hydrolysis, achieving networks of inter-silane Si-O-Si bonds as shown in Figure 3, as well as silane-surface covalent and non-covalent associations. Surface reactivity to printed proteins and nucleic acids can be conveniently and inexpensively achieved using commercial alkylsilanes that bear terminal reactive groups, including epoxide, amine, carboxylate, vinyl, acrylate, and alkylyhalide functionalities.

Gold is another popular substrate for biomolecule immobilization and microarray fabrication. Spontaneous gold-thiol reactivity provides a convenient and reliable capability to modify gold surfaces from solutions with various thiolatred molecules. These gold thiolate bonds are reasonably strong (i.e., RS-Au bond dissociation energy is

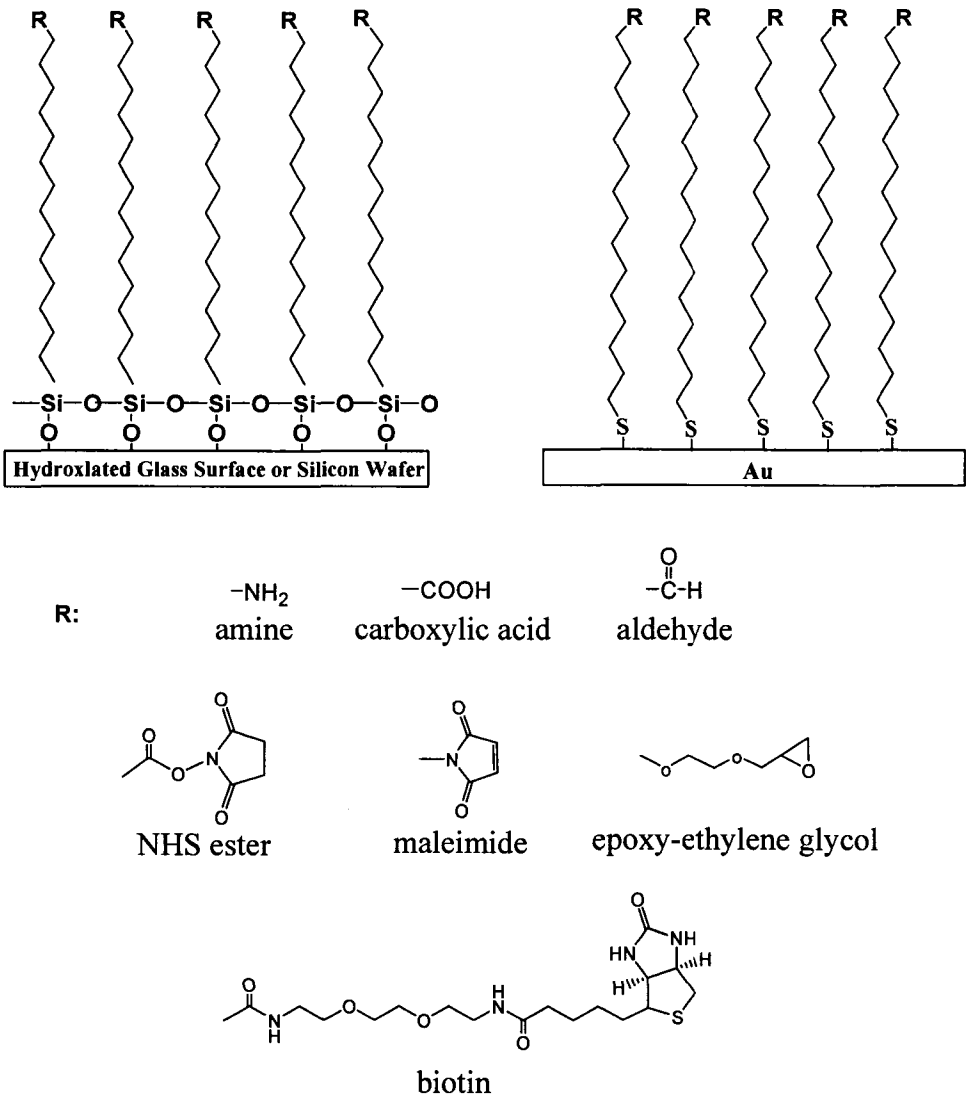

Figure 3. Schematic representation of polysiloxane layers formed from alkylsilanzation from solutions onto glass or silicon oxide wafers, and alkanethiol (SAM) monolayers on gold surface. Alkysilanes are well-known to form multi-layer networks on these surfaces in addition to monolayers shown (left). Various terminal functional groups can be introduced to these subtrate films for DNA and protein microarray immobilization.

~ 40 kcal/mol [47, 48]), and organosulfur compounds spontaneously form self-assembled monolayers (SAMs) on gold, extensively studied and well characterized now for decades [49-51]. Various terminal chemical functional groups can be introduced, as in the alkylsilane case, to yield different surface properties relevant to immobilization and microarray fabrication. Gold surfaces are easily fabricated by evaporation, sputtering , particle nucleation, or electroless redox chemistry, and remain relatively stable (i.e., non-oxidized) under normal microarray fabrication conditions. Despite these advantages and abundant fundamental academic studies [52-56], widespread commercial use of gold-based microarrays is limited by their cost and low adlayer (e.g., RS-Au) thermal stability (unsuitable for high temperature wash conditions) as well as by gold-fluorescence quenching, on many microarray formats not appropriate for fluorescence detection. However, gold's intrinsic metallic properties permit use of label-free technologies such as surface plasmon resonance (SPR) for surface capture detection [57].

Three-dimensional surfaces, including porous bulk phases (e.g., zeolites) and porous membranes, are increasingly popular in microarray technologies, especially in protein microarrays. These three-dimensional formats might provide a more friendly biological environment than two-dimensional surfaces for biomolecules, especially more delicate proteins. Theoretically, three-dimensional formats also provide larger surface area and higher biomolecule probe loading capacities, hence higher signal capture potential. Polymer membranes such as aminated nylon [58] and nitrocellulose [59] were examples of first commonly used substrates for microarray preparation and have been widely employed in microbiology laboratories as protein and DNA blotting supports. Gel-based immobilization studies in combination with mass spectrometry have been

routinely used in proteomics investigations [44,60]. Arrays fabricated on thin hydrogels on gold substrates have dominated real-time protein interaction studies for the past decade because widespread application of SPR and SPR imaging (SPRI) technology [61-64]. Polymer films and hydrogels fabricated on glass substrates have been extensively used for conventional DNA and protein microarray formats [65]. These are considered "three-dimensional" since the organic film thickness used for capture agent immobilization is much larger than the molecules being immobilized and are not classic organic monolayers. Many commercial available microarray formats are based on three-dimensional reactive polymer films and hydrogels for array immobilization [65].

Surface coupling chemistry for array bio-immobilization

Various chemical functional groups for coupling DNA probes and affinity capture proteins onto glass, silicon and gold through self-assembled monolayer of organosulfur and silane compounds are shown in Figure 3. Functional groups on both these substrate surfaces, and also DNA and proteins responsible for the surface attachment are also listed out in Table 2.1. It should not be presumed, however, that biomolecules are only immobilized by covalent forces. Covalent coupling appears to be a major (but not exclusive) component of nucleic acid surface interactions but this is not the case for printed proteins where substantial non-covalent forces are involved [66].

Cationic surfaces

Amine-terminated organosilane-coated slides provide cationic surfaces for binding anionic DNA probes through electrostatic interactions. Because a terminal primary amine functional group carries a net positive charge when exposed to aqueous

solutions below approximately pH 9, anionic oligonucleotides or cDNA in the aqueous print buffer are electrostatically immobilized to this basic, cationic surface during microarray printing. This feature is the basis for several popular commercial silane-based glass microarray substrates. A post-print UV or thermal cross-linking step is often used to achieve covalent linkage between printed DNA molecules and the surface, via thymidine nucleotide's known photochemical reactivity [67]. Protein microarrays have also been generated on an aminosilane cationic surfaces through non-covalent binding [68]. Poly-L-lysine (PLL)-modified slides also provide cationic immobilization of DNA probes and proteins. PLL, a basic, synthetic, positively charged poly(aminoacid) polyelectrolyte, adsorbs from aqueous solution to the negatively charged surface of glass and also binds DNA and proteins through electrostatic interactions. Because the binding of DNA and proteins on the cationic surface is only based on non-covalent electrostatic adsorption, such microarrays have relatively low stability, especially for protein microarrays. Another downside of these cationic surface formats is that they lack requisite non-specific binding properties during assay [10]. Negatively charged analytes and other assay reagents from solutions, especially abundant in physiological milieu, also adsorb onto these cationic surfaces through electrostatic interactions.

Amine-reactive surfaces

Surfaces with capabilities for covalent binding of DNA and proteins have advantages of better stability and generally lower assay background compared to cationic surfaces. Many microarray substrates are designed to be amine-reactive for covalent immobilization of many synthetic printable oligonucleotide probes and native peptides and proteins containing terminally labeled or amino acid-derived nucleophilically

reactive primary amine groups, respectively. Well-known amine-reactive immobilization chemistries (Table 2.1) include epoxides, aldehydes (Schiffs base formation), isothiocyanate and reactive esters including p-nitrophenyl and N-hydroxysuccinimide (NHS) reactive esters [69]. Epoxide reactivity leaves residual secondary hydroxyl groups; aldehyde coupling with amines requires an additional reduction step for stability; isothiocyante is relatively unstable in aqueous conditions and should be stored desiccated in refrigerator or freezer; NHS groups exhibit high intrinsic reactivity to nucleophiles and are available in many bioconjugation formats for surfaces, but also suffers from competitive hydrolysis under ambient conditions [69]. Although the NHS ester hydrolysis side reaction is usually slow below pH 9, it causes significant loss of surface covalent binding reactivity for oligonucleotides after two months [70]. A one-step reaction to regenerate NHS-reactive chemistry in situ on microarray surfaces has been reported to perform equally to freshly prepared microarray slides in print-immobilization of oligonucleotides [70].

Thiol-reactive surfaces

DNA oligonucleotides and proteins bearing thiol groups can be covalently immobilized onto thiol-reactive surfaces. In proteins, thiol groups are present in cysteine residues, but can also be generated by selectively reducing cystine disulfides with appropriate reagents such as dithiothreitol, 2-mercaptoethanol (β-mercaptoethanol) or tris-(2-carboxyethyl) phosphine (TECP). Available surface chemistries for covalent thiol coupling include maleimide, other activated vinyl groups, pyridyl disulfide and vinyl sulfone chemistries. Reaction of any of these functional groups with thiols usually proceeds rapidly at or below room temperature in the physiological pH range

Table 2.1 Various methods of coupling DNA and proteins on a microarray platform [44]

Functional side group on protein/peptide and DNA/oligonucleotide		Available surface functional groups	Type of binding
protein/peptide	DNA/oligonucleotide		
	polyphosphate backbone	Amino	Electrostatic
-COOH (carboxylic acid) Asp			Electrostatic Covalent amide (after carboxy activation)
	polyphosphate backbone	Poly-L-lysine	Electrostatic
-COOH (carboxylic acid) Asp			Electrostatic Covalent amide (after carboxy activation)
$-NH_2$ (amino) Lys, Gln, Arg	$-NH_2$	Carboxylic acid, active ester, epoxide, aldehyde, isothiocyanate	Covalent amide
-SH (thiol) Cys	-SH	Maleimide, disulfided, vinyl sulfone	Covalent thiol ether
		gold	gold-thiol bond
-OH Ser, Thr		Epoxide	Covalent ether
Synthetic His-Tag		Metal complex	Coordination complex
Biotin		Streptavidin	Supramolecular complex
$-NH_2$ (amino) Lys, Gln, Arg	$-NH_2$	Azidophenyl	Covalent bond (photochemical coupling)

(pH 6.5–8.0) to yield chemically stable thioethers. Biomolecules modified with thiol terminal groups can also be immobilized directly onto gold substrates. Oligonucleotides immobilized on gold provide a simple two-dimensional model for studying DNA surface density, probe orientation and hybridization efficiency of immobilized DNA oligonucleotides [53-56, 71-73].

Photochemical coupling

Photochemistry has been widely used in bimolecule patterning on substrate surfaces [74-77 78]. Photo-induced coupling can be used in fabricating both surface chemistry patterning and biomolecule reactions with surfaces. In the former case, a surface pattern can be created using spatially selective or masked photochemistry to produce reactive functional groups only at specific surface sites for binding proteins, DNA and other biomolecules. In the latter case, photo-actively derivatized biomolecules can be deposited uniformly onto surfaces bearing homogeneous films of reactive functional groups, followed by exposure to light of appropriate wavelength – through a mask if desired. Only biomoleucles exposed to light will covalently attach to surfaces; unexposed biomolecules can be washed off the surface.

Azidophenyl-functionalization is a prominent example of photochemistry used to

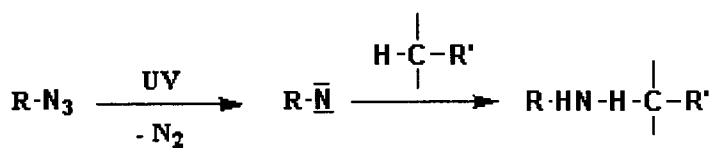

Figure 4. Schematic representation of the insertion reaction into C-H bonds of the nitrene radical (R-N), formed upon irradiation of azidophenyl-functionalized compound ($R-N_3$). R' can be protein, DNA, and organic surfaces and other organic molecules.

immobilize DNA and proteins through photochemical coupling. The excitation wavelength of the photoreaction can be adjusted using additional substitutents on the azidophenyl ring [79, 80]. Upon irradiation, these compounds generate a nitrene radical that readily inserts into various chemical bonds (C-H, O-H, N-H, N-O, etc.) (Figure 4). This compound has been widely employed in reactions with organic surfaces and conjugations with proteins and DNA [76]. Another example of photochemical coupling of biomolecules uses an anthraquinone linker (AQ) developed by Exiqon (Vedbaek, Denmark) permitting coupling to a wide variety of organic substrates upon irradiation (e.g. polystyrene, polypropylene, PMMA) and conjugation with biomolecules, ligands and small reactive groups (carboxylic acids or amines) [81]. AQ photoreagents can even be recycled via photochemical reduction and air oxidation (Figure 5).

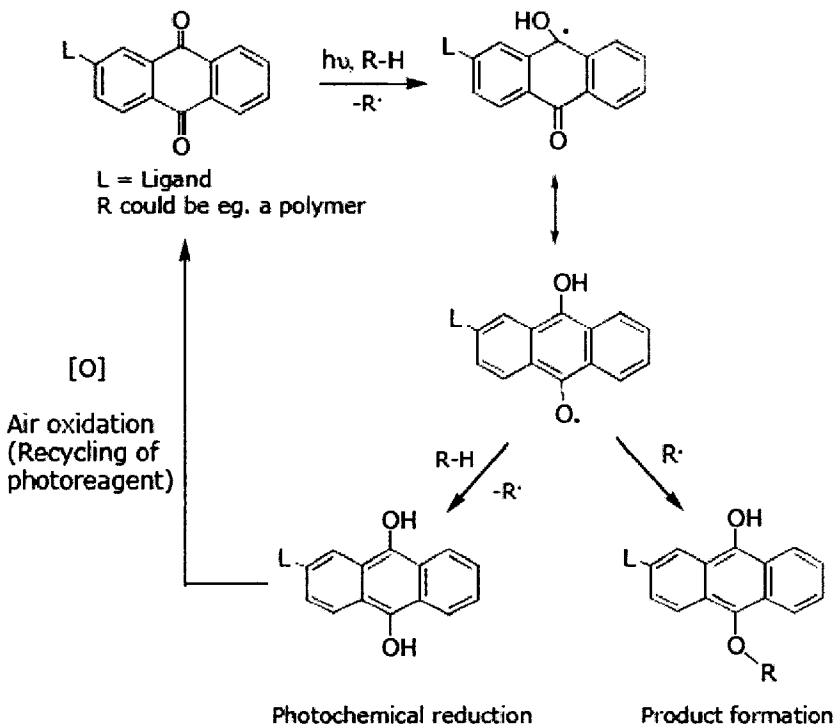

Figure 5. Exiqon's patented anthraquinone (AQ) photochemical attachment method.

Photoaptamer techniques used by SomaLogic (Boulder, CO) represent another versatile method for photochemical cross-linking of captured proteins to surfaces. Aptamers are synthetically manufactured, single-stranded DNA and RNA molecules that can bind target molecules with extraordinary affinity and specificity through large contact area between the aptamer and its target protein. SomaLogic's photoaptamer contains 5-bromodeoxyuridine (BrdU) instead of deoxythymidine. These halogenated bases provided photo-reactive sites that can specifically cross-link to target proteins. Aptamer arrays are printed, exposed to analyte targets and then irradiated. Upon exposure to UV light, the photocrosslinking of the BrdU of the photoaptamer to an electron-rich amino acid side chain of the captured target protein adds a second dimension of specificity to the normal aptamer-protein binding event. Photoaptamers are able to recognize both the complex shape and charge distribution of their targets and the presence of specific amino acid residues at specific sites, representing the next step in the evolution of aptamer technology [82].

Complex binding

The biotin-streptavidin binding architecture has been widely used for immobilizing of biomolecules to surfaces. Biotin binds to one of four streptavidin binding sites with strong binding energy (~ 20 kcal/mol [83]) in aqueous solutions. Two pairs of binding sites lie on opposite faces of streptavidin, allowing crosslinking of biotinylated surfaces [84, 85]. With developments in the area of biotinylation of biomelcules, biotin-streptavidin technology for stable non-covalent biomolecule surface binding is growing rapidly [86] [87-89]. Biotinylation kits (Pierce, Inc, IL) allow facile modification of nucleic acids, proteins and even cells with biotin.

Another well-known label in protein chemistry is the 6XHis affinity tag [90, 91]. This tag comprises approximately six histidine residues introduced artificially near the N- or C-terminus of a protein, generally using fusion protein technology. Nickel ion-chelate nitrolotriacetic acid (Ni-NTA) complexes can be introduced onto biochip surfaces for immobilization of 6XHis-tagged proteins [44, 92, 93 94]. One advantage of these metal chelate systems is their reusability. After capture assay experiments, immobilized proteins can be removed by the addition of a strong metal-complexing agent such as ethylenediaminetetraacetic acid (EDTA), or changing pH, or competitive elution using histidine. However, the binding between nickel ion chelates and His-tagged proteins is not very stable and is often susceptible to interference by commonly used salts and chemicals [95]. Several commercial suppliers provide Ni ion-based products for biomolecular screening such as Greiner (Frickenhausen, Germany) and Qiagen (Valencia, CA).

Strategies for improving protein microarray immobilization

Microarray printing: non-equilibrium immobilization

In typical microarray printing applications, pins deliver 1 to 2 nanoliter volume drops of printing solution onto microarraying slides. Under normal conditions on the print deck (room temperature, relative humidity 50~70%), such small volumes evaporate in a few seconds. The printing solution never reaches equilibrium with the surface in this short period. The question really is, what chemistry between printed solution and surface reactive groups can occur before spot drying? Immobilization of DNA and proteins from

these nanodrops onto substrate surfaces under non-equilibrium conditions have not been thoroughly investigated or clearly described, yet appears to be an unavoidable consequence of microarray printing/fabrication formats.

Our investigations of capture agent printing on two-dimensional maleimide-modified silicon nitride surfaces and commercial three-dimensional amine-reactive polymer microarraying slides revealed that covalent reactions were important for reliable DNA microarray immobilization, but not necessary for protein/antibody microarray immobilization [66, 96]. The difference between printed DNA oligonucleotide and protein immobilizations result from this fast evaporation, non-equilibrium microarray printing condition, and the inherent differences between DNA and protein structural interactions with surfaces under drying conditions. Proteins contain substantially more higher order structure than DNA, and a wider diversity of monomer chemistry with many more physical interactions possible between peptides and peptide-surface interactions. Diffusion coefficients for DNA 20-mers (used in our microarray experiments in Chapters 2 through 4, molecular weight from 5 to 7kDa) is approximately 5.7×10^{-7} cm^2/s [97], compared to ~10^{-9} to 10^{-10} cm^2/s for immunoglobulin (IgG) antibody (molecular weight: ~150 kDa) [98]. Generally, DNA diffuses to the surface much faster than protein molecules, imparting higher probability to covalently react with surface reactive groups. However, a reaction-diffusion model for microarray immobilization systems in such non-equilibrium conditions is difficult to establish as salt and biomolecule concentrations change dramatically during evaporation over a few second period. Additionally, compared to DNA (3~ 14 nm^2 for DNA 20-mer) [53], IgG has a much larger footprint on the microarray surface (~100 nm^2) [99], producing substantially stronger physical

adsorption and becoming almost irreversibly adsorbed after complete evaporation. Amounts of antibodies or proteins in printed nanoliter droplets for microarray spots (~ 10^{-15} mole) greatly exceed that required for an immobilized antibody/protein monolayer. After complete evaporation in the few seconds following microarray printing, stacked, aggregated multi-layers of antibody/protein form on each microarray spot. There is no control over either deposited thickness, antibody immobilization modes, molecular orientation, or intermolecular aggregation. This is important for the resulting antibody analyte capture performance and it is puzzling that so little research has been directed at this issue. Dried antibodies aggregate extensively [100, 101] and adsorb onto surfaces in random orientations through multi-point contacts by mixtures of surface covalent bonds, hydrogen bonds, electrostatic interactions or other physical forces. Rapid spot drying onto array surfaces promotes irreversible surface adhesion of printed proteins [66], resulting from uncontrolled protein denaturation, aggregation and conformational changes in drying proteins on all surfaces. During microarray processing and blocking steps, loosely attached printed proteins are washed from the surface, with only strongly adsorbed antibodies remaining [66]. In later surface capture assays, target analyte solution is usually incubated on-array from 30 min. to 12 h. However, capture antibodies immobilized in microspots are only able to capture specific analytes from sample solutions if their specific F_v binding domains are (1) exposed to external milieu containing analyte, and (2) remain structurally active to recognize and bind ligand. Actual antibody dispostion on-array has not been reported with much regularity. Additionally, physically attached printed capture antibodies or proteins in array spots can also desorb from microarray surfaces after extended immersion in incubation sample solutions [102]. With so many

uncontrollable parameters, poor reproducibility between different batches of printed microarrays and preparation methods, variance from spot to spot, and difficulties to produce consistent results between different laboratories and different platforms of microarray systems are endemic problems plaguing the capabilities of these arrays as quantitative, metric platforms.

Site-specific protein microarray immobilization

With so many challenges in current protein microarray technologies, one key focus in protein microarray technology is the ability to immobilize proteins in their optimized analyte-recognizing orientation, especially for antibodies. Surfaces designed for attaching antibodies of IgG idiotypes selectively through their heavy chain Fc-domains of the heavy chains allow their two identical Fab-domains (antigen binding fragments) to be oriented outward, away from the surface, and accessible to antigens in sample solutions.

A poly-His tag [92, 103] or biotin tag [104] can be engineered into either the C- or N-terminus of the protein molecule: these tags generally do not interfere with the structure or biofunction of the protein, nor adversely affect the secretion, compartmentalization, or folding of fusion proteins within cells [92, 103]. Nitroliotriacetic acid- (NTA) [93, 102] or streptavidin- functionalized array surfaces [104] then can be used for the immobilization of oriented protein molecules bearing poly-His tags or biotin tags, respectively [94].

Protein A and protein G are known to bind the Fc region of most mammalian IgG subclones. Protein A is a cell wall component produced by several strains of *Staphylococcus aureus,* and protein G is a bacterial cell wall component isolated from

group *G streptococci* [105]. Protein A and protein G have different capabilities for binding particular species of IgG. Protein G also exhibits some non-specific binding characteristics. Both proteins are used for affinity purification of antibodies or for an oriented immobilization of antibodies [106, 107]. Another genetically engineered Fc-binding fusion protein, known as protein A/G, is recombinantly expressed in *Bacillus sp.* Protein A/G is produced by gene fusion of the Fc-binding domains of protein A and protein G, possessing a more extended binding specificity than either protein A or protein G alone [108, 109]. Surfaces coated with protein A, protein G and protein A/G can all be used for site-specific IgG antibody immobilization [106, 107]. As each protein A or protein G molecule multiple binding sites for antibody IgG_c domains, reliable, high-density orientation of immobilized protein A or G on surfaces is likely. This leads to accessibility of antibody Fab-domains for protein analytes [110].

Commercialized surface chemistry called Mix&Go® (Bio-Layer, Brisbane, Australia) comprises polymeric coatings directly applied to microbeads or other substrates, combining two different proprietary approaches for capturing and orienting antibodies, respectively [111]. The first approach uses small molecule ligands screened and selected to reliably bind antibody Fc domains as an anchoring point. These small molecules create antibody binding domain comprising two different small ligands mimicking binding domains of protein A and protein G, respectively, and extending as two adjacent side chains from a polymer backbone. Antibodies in solution are recognized and interact with this synthetic binding pocket through Fc domains. However, since this interaction is low affinity, a second approach adds another dimension to antibody binding stability on these surfaces. In this approach, metal complexes

(created using combinatorial chemistry selection methods) are integrated into polymer chains, further binding Fc domains already attracted in the synthesized binding pocket. The combination of these two approaches has exhibited substantial improvements over either surface approach alone. In a multiplex flow cytometry assay for TNFα cytokine, a 70-fold signal enhancement was achieved compared to amide-coupled beads. Dramatic improvements were also demonstrated for over a dozen of other assays, including a membrane-based microarray immunoassay [111]. Additionally, structure-activity relationships for tailoring interactions between surfaces and other molecules might also be predicted for thousands of surface coatings using such a strategy to generate large libraries of novel polymer surfaces predicted to have superior characteristics for specific applications [111].

Printing additives to improve protein microarray performance

Stabilization of the structure and maintainance of the bioactivity of immobilized proteins or antibodies after microarray printing remains a substantial challenge essential for improving assay sensitivity, capture bioactivity and microarray shelf-life. Studies in this regard will be discussed in detail in Chapter 4.

Microarray detection technologies

Nucleic acid and protein microarrays require signal detection to produce results. Microarray signals are detected using a variety of technologies including directly fluorescently labeled target [24, 42], sandwich assay using secondary fluorescent detection agents [112], radioactive labeling [113], surface plasmon label-free resonance [114], waveguide

methods [33], and mass-based piezoelectric techniques [115]. Typically, analytical sensitivities in these detection methodologies extend to the femtomolar (~pg/ml) range [57, 110]. To improve the sensitivity of these techniques, improvements in all other aspects of microarray fabrication, surface capture assay and biomolecular interactions must be considered (e.g., affinity of interactions, use of labels with outstanding optical properties and microarray surfaces with intrinsically low non-specific binding/backgrounds, resulting in high signal-to-noise ratios). It is also possible to combine multiple techniques to provide overall information regarding the orientation of biomolecules, packing densities and also kinetic information not possible from a single detection technology [52].

Fluorescence detection

Fluorescence is the dominant detection method applied for microarray technologies due to its ease of use, standardized fluorescent label-biomolecule conjugation techniques, commercial availability and variety, fast detection and multicolor fluorescence detection modes. The 1″ x 3″ microscope glass slide has been established as standard format for most microarray printers and microarray fluorescence scanners. Despite its popularity in microarray technologies, the fluorescence detection strategy has several inherent disadvantages. Fluorescence signal is a semi-quantitative output, not able to provide absolute information on surface densities of capture agents or target analytes. Second, stability of fluorescent dyes are still problematic with regard to reproducibility of experiments executed at different times. Fluorescence intensities of dyes or labeled biomolecules usually decrease after a long periods in storage. Also,

autofluorescence from substrates and components in analyte solutions, especially in complex milieu, lower assay sensitivity and cause false positive signals. Specialized glass slides with low autofluorescence are usually used in industry for microarray slides.

In microarray systems, fluorescence intensities for each microarray spot are not solely dependent on target analyte abundance. Additional confounding sources of signal variability include the effects of (1) concentrations of printed capture agents, (2) variability in biomolecule affinities, (3) printing efficiencies, (4) variability in spot diameters, (5) fluorescence quenching, (6) dye-dye interference (especially in conditions of high concentrations of fluorescently labeled biomolecules), and (7) fluorescent dye conjugation efficiencies. To address these uncertainties, microarray analysis proceeds by computing the ratio of intensities between the two different fluorescence colors in each assay spot to control for differential hybridization or comparisons of two samples on the array, canceling out other unknown sources of variability [116]. The ratiometric strategy has been routinely used in cDNA microarrays. Two DNA or mRNA samples or targets (e.g., reference sample and experimental samples) are labeled using different fluorescent dyes (usually a red fluorescent dye, Cyanine 5 (Cy5), and a green fluorescent dye, Cyanine 3 (Cy3)), then mixed in equal proportions and hybridized on array to printed DNA probes. Ratios of red and green fluorescence intensities in this competitive hybridization for each spot reflects relative abundance of the corresponding gene sequence in the two nucleic acid target samples [117].

This ratiometric format has also been successfully used in protein and antibody microarrays [118 66]. After surface sandwich assay, microarrays are exposed to mixtures of two fluorescently labeled detection reagents. One binds to printed capture agents on the

surface, while the other label is used to monitor the sandwich assay signal (activity). The ratio of these two signals from two fluorescence channels during detection analysis is proportional to the fraction of receptor that is available in the sandwich assay. However, because fluorescent efficiencies (e.g., intensities, local environmental effects) are dye- and detection instrument dependent, absolute analyte abundance or capture bioactivity cannot be asserted. Nonetheless, this strategy can be used to standardize measurements among and within experiments, and minimize uncontrollable sources of assay variability, when positive and negative controls as well as fiduciary markers are implemented appropriately [118]. Formats similar to cDNA ratiometric microarrays could also be used to quantify protein analyte abundance using competitive incubation of experimental and reference samples on array. However, in multiplexed high-density protein microarrays, standard analyte reference sets analogous to inexpensive standards for cDNA microarrays are not available.

Conventional microarray fluorescence detection reaches ~pM detection limits for both DNA and protein analytes [20, 119]. While PCR and other forms of target amplification are available for detecting and quantifying DNA targets, comparable target amplification methods for protein analytes do not yet exist [120]. Picomolar detection limits are sufficient for some protein analytes but not sufficiently sensitive for others, considering the vast range of protein analyte concentrations of interest.

Radiometric detection

Radiometric measurement is a very sensitive immunoassay detection technique (fM~pM) capable of reporting absolute surface densities of both capture agents and target

analytes [53, 54, 56, 79 121]. DNA oligonucleotides can be labeled with ^{32}P on either 3' or 5' in presence of terminal transferase enzymes. Proteins can be labeled with ^{32}P [121, 122] and ^{125}I [123, 124] using various techniques. Gamma radio emission (e.g., ^{125}I or ^{131}I labels) allows for direct quantification by scintillation or gamma counting. For low energy beta emitters (^{32}P), substrate quenching is an issue. Hence, gray-scale pixelated images of surface radiolabel density are obtained using a radio-sensitive imaging scanner. Direct quantification of radio-labeled DNA/protein surface density using gray-scale image analysis is not possible. Nonetheless, this limitation can be overcome by constructing calibration curves for each labeling reaction.[53, 54]

Disadvantages of radiometric measurements include the handling of hazardous radioactive materials and waste disposal. Also, radiolabeled DNA or proteins can only be printed in conventional robotic microarray printers dedicated to this use. In a recent study, sensitive ^{32}P-DNA radiometric density measurements were calibrated with more routine fluorescence measurements and X-ray photoelectron spectroscopy (XPS) DNA surface signals for both probes and targets on gold, facilitating future DNA density determinations in this format without the use of hazardous radioactive assay [53].

Surface plasmon resonance detection

Surface plasmon resonance (SPR) is a popular label-free surface sensing technique used to directly detect binding of biomolecules onto substrate surfaces via changes in the local surface index of refraction upon analyte adsorption [57, 110]. In the past decade, SPR has grown to become an exceedingly powerful and quantitative probe of a wide variety of biomolecular interactions, including protein-ligand, protein-protein,

protein-DNA, DNA-surface and protein-surface binding [125-127]. It provides a detection technology not only for identifying these interactions, but also quantifying their equilibrium constants, kinetic constants and underlying energetics [125-127].

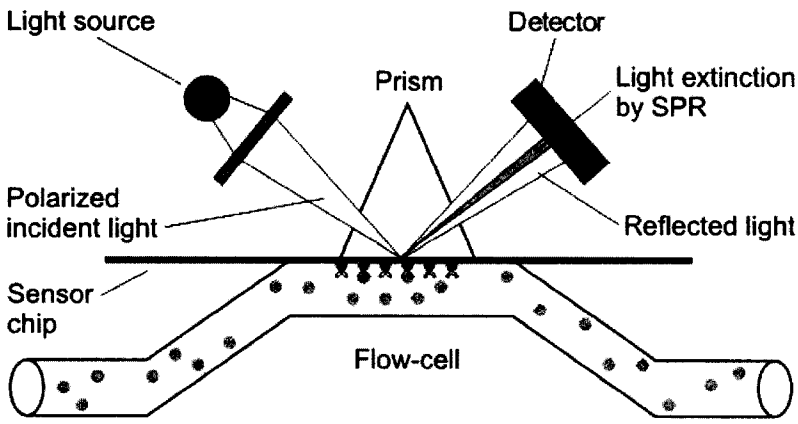

Figure 6. Principle of SPR spectroscopy. Capture agents are immobilized on the surface of a sensor chip in a flow cell. The other binding partner is flowing over the surface of the sensor chip and allowed to interact with the immobilized molecules. A binding event on the surface of the sensor chip is monitored by a change in refractive index close to the surface of the sensor chip [128].

Figure 6 shows the principle of SPR spectroscopy. Common to many waveguided methods where incident light is totally reflected, the electromagnetic field component of the incident a reflected light creates a standing wave external to the optically reflected medium that penetrates into a medium of a lower refractive index. This creates an exponentially detenuating evanescent wave. In SPR spectroscopy, the interface between the media is coated with a thin layer of metal (gold), and incident light is both monochromatic and p-polarized. The intensity of the reflected light is reduced sharply at a specific incident angle due to the resonance energy transfer between evanescent wave and surface plasmons residing in the polarizing metal films. Mass entering or exiting the evanescent field adjacent to the gold film changes the local optical

conditions, altering the reflected intensity or the angle of maximum or minumum reflected optical intensity, both of which become experimental monitors. Satisfactory linear relationship is found between resonance energy detected or transferred and mass concentration of biochemically relevant biomolecules within the evanescent field. The SPR signal, expressed in resonance units, is therefore a measure of mass concentration at the sensor chip surface. This means that the analyte and probe association and dissociation constants can be observed and equilibrium constants can be calculated.

SPR measurements are usually performed in a flow cell format that can handle only a few analytes simultaneously. SPR imaging (SPRI) is a method that offers multiplexed detection capability compatible with DNA and protein microarrays [129]. SPRI has already been applied to a wide variety of bioaffinity interactions and microarray formsts [130-135].

Several limitations to SPR and SPRI detection technology are currently being addressed. Gold substrates limit wide spread use of SPR and SPRI in terms of economic efficiency and practical sensing applications. Detection limits (~nM to ~ hundreds of nM) are insufficient for many clinical, food or environmental analytes. Additionally, SPR is analyte non-specific: any substance encountering the evanescent field produces the same optical signal, dependent only upon refractive index. Non-specific binding and cross-interactions must therefore be minimized to increase SPR detection reliability and sensitivity. Microarrays with different capture agents (especially those with vastly different molecular sizes) are also a challenge for SPRI imaging to establish suitable standard curves [136-138].

Optical waveguide detection

Combinations of optical analysis and direct immunosensing, frequently exploited in integrated optical waveguides (IOWs), represent an attractive sensing modality for applications in rapid detection, diagnostic and sensing area because of their high sensitivity and selectivity [139-145]. First described by Marcuse as thin film dielectrics [146], IOWs currently comprise three major subclasses: (1) IOW-attenuated total reflection (ATR) spectrometry, (2) waveguide Raman spectroscopy (WRS), and (3) IOW-fluorosensing (IOW-FS) [144]. All three modes have substantial history and current interest in biosensing using immobilized capture agents, including nucleotides and antibodies [147-150]. Femtomolar (fM) detection limits were proven feasible using a dual channel

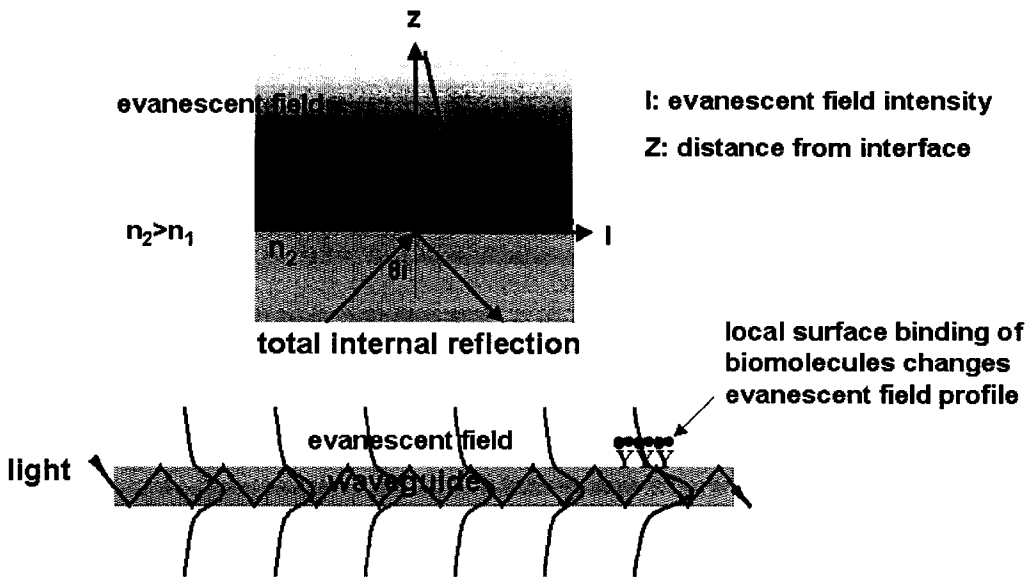

Figure 7. Schematic of integrated optical waveguide (IOW). Light is interfaced with, propogated within and repeatedly reflected (total internal reflection) along the waveguide material. The evanescent field penetrates into the external media with lower refractive index and its intensity decays exponentially away from interface. Local surface binding of biomolecules is detected by detecting changes in the evanescent field profile or intensity within the evanescent field integrated along the waveguide. Localized or spatially resolved detection zones can be monitored by external detectors along the waveguide (e.g., CCD cameras).

fluorescent evanescent field sensing thin film IOW [151], although these are far from routine.

As shown in Figure 7, IOW guides light by repeatedly reflecting (total internal reflection) it along the IOW length, and offers the best possibility for mass production with flexibility in both design and dimension [57]. The guided light field is mainly confined to the IOW core. While the incident optical field is reflected, as described for SPR (vida infra), the resulting evanescent wave penetrates outside core region into media directly adjacent to the IOW with lower refractive index and decays exponentially with increasing distance from the interface according to

$$I(z) = I(0)e^{-z/d}, \qquad (1)$$

where *I* is the evanescent field intensity; *I(0)* is the intensity at the interface; *z* is the vertical distance from the interface. The characteristic penetration depth *d* at $\lambda(0)$, the wavelength of incident light in a vacuum, is given by

$$d = \lambda(0)/4\pi(n_1^2 \sin\theta i^2 - n_2^2)^{-1/2}. \qquad (2)$$

While conventional absorption or interferometric waveguide sensors detect small changes in the intensity or phase of light remaining in the waveguide, we have proposed a novel IOW approach [152, 153] that senses the change in optical power transferred out of the waveguide (Figure 7). Because only relative changes in power outside the waveguide are detected, accurate knowledge of exact power levels in the waveguide are not required, and thus are insensitive to variation in light coupling efficiency or media heterogeneity. Spatial isolation of assay detection platforms of distinct analytes and multiplexed spatially resolved detection formats can be combined with surface chemistry and

patterning to produce microarray-based multi-analyte IOW formats. Even with improvement of IOW optical properties and novel detection mechanism, the real performance of IOW in bioassays is still limited by surface capture performance issues (vida infra), either poor surface immobilization of affinity capture reagents (e.g., antibodies), unacceptable maintenance of surface-bound bioactivity, or unacceptable non-specific non-analyte surface adsorption (noise) [66].

Nanotechnology approaches

Reducing dimensionality of assay components may provide performance advantages (e.g., detection limits, reagent consumption, speed-to-answer, and remote field deployment) for certain assay designs. Microfluidics and nanoparticles have received substantial attention for these purposes. Colorimetric properties of gold-nanoparticles depend on the particle sizes and spacing provides highly selective detection technology for microarrays [120, 154-161]. Detection principles, methods and various applications are described in a detailed review of nanostructures in biodiagnostics [157]. In a recent study, a 30 aM detection limit is reported for a nanoparticle-based bio-bar method for the detection of prostate-specific antigen (PSA) in goat serum [120]. Technical potential and opportunities for these approaches remain to be seen, as most approaches reported must be further developed and applied betyond proof of concept.

Conclusions

Microarray technology is now fairly mature, facilitating high-throughput parallel semi-quantitative assessment of analyte abundance relevant to many useful applications.

While DNA microarrays have been extensively used in gene expression and genotyping studies, they remain unapproved for clinical use in most formats. Despite some commercial presence for research use, protein microarrays are still in early proof of concept stages. Substantial technological issues remain to bring these array formats to widespread practical use, including surface and materials performance problems, affinity reagent reliability and stability, and cross-reactivity, and detection sensitivity, quantitative capabilities, and ease of use. For both microarray platforms, numerous challenges also plague understanding of the biological significance of the screened data (e.g., results). Intrinsic differences between protein and DNA structure, chemistry and interfacial behavior require careful distinctions between specific approaches to each format: protein microarrays appear to face many more difficult challenges and problems to bring this format into routine use than DNA microarrays. These challenges present at every stage of microarray technology from sample purification to microarray fabrication, analyte capture assay and signal detection. Hence, new strategies integrated across several disciplines that can design, apply and troubleshoot new assay reagents, materials, methods, detection techniques, and data analyses might best be brought to bear on this field.

Referneces

(1) Schena, M. In *Protein Microarrays*; Schena, M., Ed.; Jones and Bartlett Publishers: Sudbury, MA, 2005, pp 1-12.

(2) Ekins, R.; Chu, F.; Biggart, E. *Ann Biol Clin (Paris)* **1990**, *48*, 655-666.

(3) Ekins, R.; Chu, F.; Biggart, E. *Clin. Chim. Acta* **1990**, *194*, 91-114.

(4) Ekins, R. P.; Chu, F. W. *Clin Chem* **1991**, *37*, 1955-1967.

(5) Ekins, R.; Chu, F. *Ann Biol Clin (Paris)* **1992**, *50*, 337-353.

(6) Ekins, R.; Chu, F. W. *Trends Biotechnol* **1999**, *17*, 217-218.

(7) Pease, A. C.; Solas, D.; Sullivan, E. J.; Cronin, M. T.; Holmes, C. P.; Fodor, S. P. *Proc Natl Acad Sci U S A* **1994**, *91*, 5022-5026.

(8) Schena, M.; Shalon, D.; Davis, R. W.; Brown, P. O. *Science* **1995**, *270*, 467-470.

(9) Delehanty, J. B.; Ligler, F. S. *BioTechniques* **2003**, *34*, 380-385.

(10) Gong, P.; Grainger, D. W. In *Microarrays: Method in Molecular Biology - Methods and Protocols,* 2 ed.; Rampal, J. B., Ed.; Humana Press: NJ, 2006 (in press).

(11) McGall, G.; Labadie, J.; Brock, P.; Wallraff, G.; Nguyen, T.; Hinsberg, W. *Proc Natl Acad Sci U S A* **1996**, *93*, 13555-13560.

(12) McGall, G. H.; Christians, F. C. *Adv Biochem Eng Biotechnol* **2002**, *77*, 21-42.

(13) Ferguson, J. A.; Boles, T. C.; Adams, C. P.; Walt, D. R. *Nat Biotechnol* **1996**, *14*, 1681-1684.

(14) http://mednews.stanford.edu/stanmed/2005fall/microarray.html.

(15) Sherlock, G. *Nat Methods* **2005**, *2*, 329-330.

(16) Bammler, T.; Beyer, R. P.; Bhattacharya, S.; Boorman, G. A.; Boyles, A.; Bradford, B. U.; Bumgarner, R. E.; Bushel, P. R.; Chaturvedi, K.; Choi, D.; Cunningham, M. L.; Deng, S.; Dressman, H. K.; Fannin, R. D.; Farin, F. M.; Freedman, J. H.; Fry, R. C.; Harper, A.; Humble, M. C.; Hurban, P.; Kavanagh, T. J.; Kaufmann, W. K.; Kerr, K. F.; Jing, L.; Lapidus, J. A.; Lasarev, M. R.; Li, J.; Li, Y. J.; Lobenhofer, E. K.; Lu, X.; Malek, R. L.; Milton, S.; Nagalla, S. R.; O'Malley J, P.; Palmer, V. S.; Pattee, P.; Paules, R. S.; Perou, C. M.; Phillips, K.; Qin, L. X.; Qiu, Y.; Quigley, S. D.; Rodland, M.; Rusyn, I.; Samson, L. D.; Schwartz, D. A.; Shi, Y.; Shin, J. L.; Sieber, S. O.; Slifer, S.; Speer, M. C.; Spencer, P. S.; Sproles, D. I.; Swenberg, J. A.; Suk, W. A.; Sullivan, R. C.; Tian, R.; Tennant, R. W.; Todd, S. A.; Tucker, C. J.; Van Houten, B.; Weis, B. K.; Xuan, S.; Zarbl, H. *Nat Methods* **2005**, *2*, 351-356.

(17) Irizarry, R. A.; Warren, D.; Spencer, F.; Kim, I. F.; Biswal, S.; Frank, B. C.; Gabrielson, E.; Garcia, J. G.; Geoghegan, J.; Germino, G.; Griffin, C.; Hilmer, S. C.; Hoffman, E.; Jedlicka, A. E.; Kawasaki, E.; Martinez-Murillo, F.; Morsberger,

L.; Lee, H.; Petersen, D.; Quackenbush, J.; Scott, A.; Wilson, M.; Yang, Y.; Ye, S. Q.; Yu, W. *Nat Methods* **2005**, *2*, 345-350.

(18) Larkin, J. E.; Frank, B. C.; Gavras, H.; Sultana, R.; Quackenbush, J. *Nat Methods* **2005**, *2*, 337-344.

(19) Angenendt, P. *Drug Discov Today* **2005**, *10*, 503-511.

(20) Cahill, D. J. *J. Immunol. Methods* **2001**, *250*, 81-91.

(21) Glokler, J.; Angenendt, P. *J Chromatogr B Analyt Technol Biomed Life Sci* **2003**, *797*, 229-240.

(22) Yu, W.; Sun, Y.; Gu, N.; Wu, J. *Shengwu Huaxue Yu Shengwu Wuli Jinzhan* **2002**, *29*, 491-494.

(23) Chen, G. Y.; Uttamchandani, M.; Lue, R. Y.; Lesaicherrea, M. L.; Yao, S. Q. *Curr Top Med Chem* **2003**, *3*, 705-724.

(24) Angenendt, P.; Glokler, J.; Murphy, D.; Lehrach, H.; Cahill Dolores, J. *Anal. Biochem.*, *309*, 253-260.

(25) Hill, J. J.; Shalaev, E. Y.; Zografi, G. *J. Pharm. Sci.* **2005**, *94*, 1636-1667.

(26) Kambhampati, D. *Protein microarray technology*; Wiley-VCH Verlag GmbH & Co. KGaA: Weinheim, Germany, 2003.

(27) Schena, M. *Protein Microarrays*; Jones and Bartlett Publishers: Sudbury, MA, 2005.

(28) Mitchell, P. *Nat Biotechnol* **2002**, *20*, 225-229.

(29) Zhu, H.; Bilgin, M.; Bangham, R.; Hall, D.; Casamayor, A.; Bertone, P.; Lan, N.; Jansen, R.; Bidlingmaier, S.; Houfek, T.; Mitchell, T.; Miller, P.; Dean, R. A.; Gerstein, M.; Snyder, M. *Science* **2001**, *293*, 2101-2105.

(30) Templin, M. F.; Stoll, D.; Schrenk, M.; Traub, P. C.; Vohringer, C. F.; Joos, T. O. *Drug Discov Today* **2002**, *7*, 815-822.

(31) MacBeath, G.; Schreiber, S. L. *Science* **2000**, *289*, 1760-1763.

(32) Stoll, D.; Templin, M. F.; Schrenk, M.; Traub, P. C.; Vohringer, C. F.; Joos, T. O. *Front Biosci* **2002**, *7*, c13-32.

(33) Pawlak, M.; Schick, E.; Bopp, M. A.; Schneider, M. J.; Oroszlan, P.; Ehrat, M. *Proteomics* **2002**, *2*, 383-393.

(34) Sreekumar, A.; Nyati, M. K.; Varambally, S.; Barrette, T. R.; Ghosh, D.; Lawrence, T. S.; Chinnaiyan, A. M. *Cancer Res.* **2001**, *61*, 7585-7593.

(35) Xu, L.; Aha, P.; Gu, K.; Kuimelis, R. G.; Kurz, M.; Lam, T.; Lim, A. C.; Liu, H.; Lohse, P. A.; Sun, L.; Weng, S.; Wagner, R. W.; Lipovsek, D. *Chem Biol* **2002**, *9*, 933-942.

(36) Woodbury, R. L.; Varnum, S. M.; Zangar, R. C. *J Proteome Res* **2002**, *1*, 233-237.

(37) Beyer, K. *Curr Opin Allergy Clin Immunol* **2003**, *3*, 189-197.

(38) Mezzasoma, L.; Bacarese-Hamilton, T.; Di Cristina, M.; Rossi, R.; Bistoni, F.; Crisanti, A. *Clin Chem* **2002**, *48*, 121-130.

(39) Robinson, W. H.; DiGennaro, C.; Hueber, W.; Haab, B. B.; Kamachi, M.; Dean, E. J.; Fournel, S.; Fong, D.; Genovese, M. C.; de Vegvar, H. E.; Skriner, K.; Hirschberg, D. L.; Morris, R. I.; Muller, S.; Pruijn, G. J.; van Venrooij, W. J.; Smolen, J. S.; Brown, P. O.; Steinman, L.; Utz, P. J. *Nat Med* **2002**, *8*, 295-301.

(40) Robinson, W. H.; Fontoura, P.; Lee, B. J.; de Vegvar, H. E.; Tom, J.; Pedotti, R.; DiGennaro, C. D.; Mitchell, D. J.; Fong, D.; Ho, P. P.; Ruiz, P. J.; Maverakis, E.; Stevens, D. B.; Bernard, C. C.; Martin, R.; Kuchroo, V. K.; van Noort, J. M.; Genain, C. P.; Amor, S.; Olsson, T.; Utz, P. J.; Garren, H.; Steinman, L. *Nat Biotechnol* **2003**, *21*, 1033-1039.

(41) Collett, J. R.; Cho, E. J.; Ellington, A. D. *Methods* **2005**, *37*, 4-15.

(42) Zhu, H.; Snyder, M. *Curr Opin Chem Biol* **2003**, *7*, 55-63.

(43) Schena, M.; Heller, R. A.; Theriault, T. P.; Konrad, K.; Lachenmeier, E.; Davis, R. W. *Trends Biotechnol* **1998**, *16*, 301-306.

(44) Schaferling, M.; Kambhampati, D. In *Protein microarray technology*; Kambhampati, D., Ed.; Wiley-VCH Verlag GmbH & Co. KGaA: Weinheim, Germany, 2003, pp 1-9.

(45) Mittal, K. L. *Silanes and other coupling agents*; VSP: Utrecht ; Boston, 1992.

(46) Leyden, D. E.; Collins, W. T. *Silylated Surfaces*; Gordon and Breach Science Publishers: New York, 1978.

(47) Nuzzo, R. G.; Dubois, L. H. D.; Allara, D. L. *J. Am. Chem. Soc.* **1990**, *112*, 558 - 569.

(48) Love, J. C.; Estroff, L. A.; Kriebel, J. K.; Nuzzo, R. G.; Whitesides, G. M. *Chem Rev* **2005**, *105*, 1103-1169.

(49) Vericat, C.; Vela, M. E.; Salvarezza, R. C. *Physical Chemistry Chemical Physics* **2005**, *7*, 3258-3268.

(50) Everhart, D. S. *Handbook of Applied Surface and Colloid Chemistry* **2002**, *2*, 99-116.

(51) Flink, S.; van Veggel, F. C. J. M.; Reinhoudt, D. N. *Sensors Update* **2001**, *8*, 3-19.

(52) Gong, P.; Harbers, G. M.; Grainger, D. W. *Anal. Chem.* **2006**, *78*, 2342-2351.

(53) Gong, P.; Lee, C.-Y.; Gamble, L. J.; Castner, D. G.; Grainger, D. W. *Anal. Chem.* **2006**, *78*, 3326-3334.

(54) Steel, A. B.; Levicky, R. L.; Herne, T. M.; Tarlov, M. J. *Biophys. J.* **2000**, *79*, 975-981.

(55) Petrovykh, D. Y.; Kimura-Suda, H.; Tarlov, M. J.; Whitman, L. J. *Langmuir* **2004**, *20*, 429-440.

(56) Herne, T. M.; Tarlov, M. J. *J. Am. Chem. Soc.* **1997**, *119*, 8916-8920.

(57) Ince, R.; Narayanaswamy, R. *Analytical Chimica Acta* **2006**, *569*, 1-20.

(58) Gershoni, J. M.; Palade, G. E. *Anal. Biochem.* **1982**, *124*, 396-405.

(59) Towbin, H.; Staehelin, T.; Gordon, J. *Proc Natl Acad Sci U S A* **1979**, *76*, 4350-4354.

(60) Gavin, I. M.; Kukhtin, A.; Glesne, D.; Schabacker, D.; Chandler, D. P. *BioTechniques* **2005**, *39*, 99-107.

(61) Nelson, B. P.; Grimsrud, T. E.; Liles, M. R.; Goodman, R. M.; Corn, R. M. *Anal. Chem.* **2001**, *73*, 1-7.

(62) Goodrich, T. T.; Lee, H. J.; Corn, R. M. *J Am Chem Soc* **2004**, *126*, 4086-4087.

(63) Jung, J. M.; Shin, Y. B.; Kim, M. G.; Ro, H. S.; Jung, H. T.; Chung, B. H. *Anal. Biochem.* **2004**, *330*, 251-256.

(64) Ro, H. S.; Koh, B. H.; Jung, S. O.; Park, H. K.; Shin, Y. B.; Kim, M. G.; Chung, B. H. *Proteomics* **2006**, *6*, 2108-2111.

(65) Gong, P.; Grainger, D. W. In *Microarrays: Method in Molecular Biology - Methods and Protocols,* 2 ed.; Rampal, J. B., Ed.; Humana Press: NJ, 2006 (in press).

(66) Wu, P.; Hogrebe, P.; Grainger, D. W. *Biosens. Bioelectron.* **2006**, *21*, 1252-1263.

(67) Wang, H. Y.; Malek, R. L.; Kwitek, A. E.; Greene, A. S.; Luu, T. V.; Behbahani, B.; Frank, B.; Quackenbush, J.; Lee, N. H. *Genome Biol* **2003**, *4*, R5.

(68) Martin, B. D.; Gaber, B. P.; Patterson, C. H.; Turner, D. C. *Langmuir* **1998**, *14*, 3971-3975.

(69) Hermanson, G. T. *Bioconjugate techniques*; Academic Press: San Diego, 1996.

(70) Gong, P.; Grainger, D. W. *Biomed Sci Instrum* **2004**, *40*, 18-23.

(71) Peterson, A. W.; Heaton, R. J.; Georgiadis, R. M. *Nucleic Acids Res.* **2001**, *29*, 5163-5168.

(72) Peterson, A. W.; Wolf, L. K.; Georgiadis, R. M. *J Am Chem Soc* **2002**, *124*, 14601-14607.

(73) Wolf, L. K.; Gao, Y.; Georgiadis, R. M. *Langmuir* **2004**, *20*, 3357-3361.

(74) Liu, A. P.; Fletcher, D. A. *Nano Lett* **2005**, *5*, 625-628.

(75) Liu, X. H.; Wang, H. K.; Herron, J. N.; Prestwich, G. D. *Bioconjug Chem* **2000**, *11*, 755-761.

(76) Hengsakul, M.; Cass, A. E. *Bioconjug Chem* **1996**, *7*, 249-254.

(77) Blawas, A. S.; Reichert, W. M. *Biomaterials* **1998**, *19*, 595-609.

(78) Sundarababu, G.; Gao, H.; Sigrist, H. *Photochem. Photobiol.* **1995**, *61*, 540-544.

(79) Ciesiolka, J.; Gornicki, P.; Ofengand, J. *Biochemistry* **1985**, *24*, 4931-4938.

(80) Rinke, J.; Meinke, M.; Brimacombe, R.; Fink, G.; Rommel, W.; Fasold, H. *J Mol Biol* **1980**, *137*, 301-304.

(81) http://www.exiqon.com.

(82) http://www.somalogic.com/.

(83) Miyamoto, S.; Kollman, P. A. *Proteins* **1993**, *16*, 226-245.

(84) Green, N. M. *Adv Protein Chem* **1975**, *29*, 85-133.

(85) Blankenburg, R.; Meller, P.; Ringsdorf, H.; Salesse, C. *Biochemistry* **1989**, *28*, 8214-8221.

(86) Pavlickova, P.; Hug, H. *Methods in Molecular Biology (Totowa, NJ, United States)* **2004**, *264*, 73-83.

(87) Kotlin, R.; Dyr, J. E. *Chemicke Listy* **2006**, *100*, 178-183.

(88) Skerra, A.; Schmidt, T. G. M. *Biomolecular Engineering* **1999**, *16*, 79-86.

(89) Turkova, J. *Journal of Chromatography, B: Biomedical Sciences and Applications* **1999**, *722*, 11-31.

(90) Terpe, K. *Appl. Microbiol. Biotechnol.* **2003**, *60*, 523-533.

(91) Nishiya, Y.; Kitabayashi, M.; Ikeda, K. *Jikken Igaku* **2002**, *20*, 479-482.

(92) Hochuli, E.; Dobeli, H.; Schacher, A. *J Chromatogr* **1987**, *411*, 177-184.

(93) Sigal, G. B.; Bamdad, C.; Barberis, A.; Strominger, J.; Whitesides, G. M. *Anal. Chem.* **1996**, *68*, 490-497.

(94) Zhen, G.; Falconnet, D.; Kuennemann, E.; Voros, J.; Spencer, N. D.; Textor, M.; Zurcher, S. *Advanced Functional Materials* **2006**, *16*, 243-251.

(95) Lesaicherre, M. L.; Lue, R. Y.; Chen, G. Y.; Zhu, Q.; Yao, S. Q. *J Am Chem Soc* **2002**, *124*, 8768-8769.

(96) Wu, P.; Grainger, D. W. *Submitted to J Proteome Res.* **2006**.

(97) Lukacs, G. L.; Haggie, P.; Seksek, O.; Lechardeur, D.; Freedman, N.; Verkman, A. S. *J Biol Chem* **2000**, *275*, 1625-1629.

(98) Perry, R. H.; Chilton, C. H.; Perry, J. H. *Chemical engineers' handbook*, 5th ed.; McGraw-Hill: New York,, 1973.

(99) Nichkova, M.; Dosev, D.; Perron, R.; Gee, S. J.; Hammock, B. D.; Kennedy, I. M. *Analytical and Bioanalytical Chemistry* **2006**, *384*, 631-637.

(100) Duddu, S. P.; Zhang, G.; Dal Monte, P. R. *Pharm. Res.* **1997**, *14*, 596-600.

(101) Gombotz, W. R.; Pankey, S. C.; Phan, D.; Drager, R.; Donaldson, K.; Antonsen, K. P.; Hoffman, A. S.; Raff, H. V. *Pharm. Res.* **1994**, *11*, 624-632.

(102) Cha, T.; Guo, A.; Jun, Y.; Pei, D.; Zhu, X. Y. *Proteomics* **2004**, *4*, 1965-1976.

(103) Porath, J.; Carlsson, J.; Olsson, I.; Belfrage, G. *Nature* **1975**, *258*, 598-599.

(104) Lue, Y.-P. R.; Yeo, S.-Y. D.; Tan, L.-P.; Uttamchandani, M.; Chen, G. Y.-J.; Yao, S. Q. In *Protein microarrays*; Schena, M., Ed.; Jones and Bartlett: Sudbury, Mass., 2005, pp 13-42.

(105) Sauer-Eriksson, A. E.; Kleywegt, G. J.; Uhlen, M.; Jones, T. A. *Structure* **1995**, *3*, 265-278.

(106) Dodge, A.; Fluri, K.; Verpoorte, E.; de Rooij, N. F. *Anal. Chem.* **2001**, *73*, 3400-3409.

(107) Oh, B. K.; Kim, Y. K.; Park, K. W.; Lee, W. H.; Choi, J. W. *Biosens Bioelectron* **2004**, *19*, 1497-1504.

(108) Naserke, H. E.; Bonifacio, E.; Ziegler, A. G. *J Clin Endocrinol Metab* **1999**, *84*, 1239-1243.

(109) Bhide, M. R.; Curlik, J.; Travnicek, M.; Lazar, P. *Comp Immunol Microbiol Infect Dis* **2004**, *27*, 191-199.

(110) Bilitewski, U. *Anal. Chim. Acta* **2006**, *568*, 232-247.

(111) http://www.bio-layer.com/.

(112) Li, Y.; Nath, N.; Reichert, W. M. *Anal. Chem.* **2003**, *75*, 5274-5281.

(113) Kambhampati, D. In *Protein microarray technology*; Kambhampati, D., Ed.; Wiley-VCH Verlag GmbH & Co. KGaA: Weinheim, Germany, 2003, pp 1-9.

(114) Stenlund, P.; Babcock, G. J.; Sodroski, J.; Myszka, D. G. *Anal. Biochem.* **2003**, *316*, 243-250.

(115) Wu, G.; Datar, R. H.; Hansen, K. M.; Thundat, T.; Cote, R. J.; Majumdar, A. *Nat Biotechnol* **2001**, *19*, 856-860.

(116) DeRisi, J. L.; Iyer, V. R.; Brown, P. O. *Science* **1997**, *278*, 680-686.

(117) Yang, Y. H.; Speed, T. *Nat Rev Genet* **2002**, *3*, 579-588.

(118) Nielsen, U. B.; Cardone, M. H.; Sinskey, A. J.; MacBeath, G.; Sorger, P. K. *Proc Natl Acad Sci U S A* **2003**, *100*, 9330-9335.

(119) Goldsmith, Z. G.; Dhanasekaran, N. *Int J Mol Med* **2004**, *13*, 483-495.

(120) Nam, J. M.; Thaxton, C. S.; Mirkin, C. A. *Science* **2003**, *301*, 1884-1886.

(121) Ge, H. *Nucleic Acids Res.* **2000**, *28*, e3.

(122) Riese, M. J.; Barbieri, J. T. *Infect. Immun.* **2002**, *70*, 2230-2232.

(123) Foo, L. H.; Fraser, D. R.; Greenfield, H.; Trube, A.; Simpson, J. M. *Asia Pac J Clin Nutr* **2004**, *13*, S151.

(124) Motie, M.; Schaul, K. W.; Potempa, L. A. *Drug Metab Dispos* **1998**, *26*, 977-981.

(125) Rich, R. L.; Myszka, D. G. *Curr. Opin. Biotechnol.* **2000**, *11*, 54-61.

(126) Buckle, M.; Williams, R. M.; Negroni, M.; Buc, H. *Proc Natl Acad Sci U S A* **1996**, *93*, 889-894.

(127) McDonnell, J. M. *Curr Opin Chem Biol* **2001**, *5*, 572-577.

(128) http://www.fz-juelich.de/ibi/ibi-1/protein-protein_interaction.

(129) Smith, E. A.; Corn, R. M. *Appl. Spectrosc.* **2003**, *57*, 320A-332A.

(130) Kanda, V.; Kariuki, J. K.; Harrison, D. J.; McDermott, M. T. *Anal. Chem.* **2004**, *76*, 7257-7262.

(131) Kyo, M.; Usui-Aoki, K.; Koga, H. *Anal. Chem.* **2005**, *77*, 7115-7121.

(132) Wegner, G. J.; Lee, H. J.; Corn, R. M. *Anal. Chem.* **2002**, *74*, 5161-5168.

(133) Wegner, G. J.; Lee, H. J.; Marriott, G.; Corn, R. M. *Anal. Chem.* **2003**, *75*, 4740-4746.

(134) Wegner, G. J.; Wark, A. W.; Lee, H. J.; Codner, E.; Saeki, T.; Fang, S.; Corn, R. M. *Anal. Chem.* **2004**, *76*, 5677-5684.

(135) Wolf, L. K.; Fullenkamp, D. E.; Georgiadis, R. M. *J Am Chem Soc* **2005**, *127*, 17453-17459.

(136) Iwasaki, Y.; Tobita, T.; Horiuchi, T.; Seyama, M. *NTT Technical Review* **2006**, *4*, 21-29.

(137) Perez-Luna, V. H. *Surfaces and Interfaces for Biomaterials* **2005**, 248-270.

(138) Homola, J.; Vaisocherova, H.; Dostalek, J.; Piliarik, M. *Methods (San Diego, CA, United States)* **2005**, *37*, 26-36.

(139) Bradshaw, J. T.; Mendes, S. B.; Saavedra, S. S. *Anal. Chem.* **2005**, *77*, 28A-36A.

(140) Brecht, A.; Klotz, A.; Barzen, C.; Gauglitz, G.; Harris, R. D.; Quigley, G. R.; Wilkinson, J. S.; Sztajnbok, P.; Abuknesha, R.; Gascon, J.; Oubina, A.; Barcelo, D. *Anal. Chim. Acta* **1998**, *362*, 69-79.

(141) Klainer, S. M.; Coulter, S. L.; Pollina, R. J.; Saini, D. *Sensors and Actuators, B: Chemical* **1997**, *B38*, 176-182.

(142) Ligler, F. S.; Breimer, M.; Golden, J. P.; Nivens, D. A.; Dodson, J. P.; Green, T. M.; Haders, D. P.; Sadik, O. A. *Anal. Chem.* **2002**, *74*, 713-719.

(143) Misiakos, K.; Kakabakos, S. E. *Biosens. Bioelectron.* **1998**, *13*, 825-830.

(144) Plowman, T. E.; Saavedra, S. S.; Reichert, W. M. *Biomaterials* **1998**, *19*, 341-355.

(145) Prieto, F.; Sepulveda, B.; Calle, A.; Llobera, A.; Dominguez, C.; Abad, A.; Montoya, A.; Lechuga, L. M. *Nanotechnology* **2003**, *14*, 907-912.

(146) Marcuse, D. *Theory of dielectric optical waveguides*; Academic press: New York, 1974.

(147) Clerc, D.; Lukosz, W. *Sensors and Actuators, B: Chemical* **1997**, *B40*, 53-58.

(148) Gao, H.; Saenger, M.; Luginbuehl, R.; Sigrist, H. *Biosens. Bioelectron.* **1995**, *10*, 317-328.

(149) Haron, S.; Nabok, A. V.; Ray, A. K. *Proceedings of SPIE-The International Society for Optical Engineering* **2003**, *5119*, 100-108.

(150) Trummer, N.; Adanyi, N.; Varadi, M.; Szendroe, I. *Fresenius. J. Anal. Chem.* **2001**, *371*, 21-24.

(151) Plowman, T. E.; Reichert, W. M.; Peters, C. R.; Wang, H. K.; Christensen, D. A.; Herron, J. N. *Biosens. Bioelectron.* **1996**, *11*, 149-160.

(152) Yuan, G.; Lear, K. L.; Stephens, M. D.; Dandy, D. S. *Appl. Phys. Lett.* **2005**, *87*, 191107/191101-191107/191103.

(153) Yuan, G. W.; Stephens, M. D.; Dandy, D. S.; Lear, K. L. *IEEE Photonics Technology Letters* **2005**, *17*, 2382-2384.

(154) Han, M. S.; Lytton-Jean, A. K.; Oh, B. K.; Heo, J.; Mirkin, C. A. *Angew Chem Int Ed Engl* **2006**, *45*, 1807-1810.

(155) Nam, J. M.; Park, S. J.; Mirkin, C. A. *J Am Chem Soc* **2002**, *124*, 3820-3821.

(156) Park, S. J.; Taton, T. A.; Mirkin, C. A. *Science* **2002**, *295*, 1503-1506.

(157) Rosi, N. L.; Mirkin, C. A. *Chem Rev* **2005**, *105*, 1547-1562.

(158) Stoeva, S. I.; Lee, J. S.; Thaxton, C. S.; Mirkin, C. A. *Angew Chem Int Ed Engl* **2006**, *45*, 3303-3306.

(159) Festag, G.; Steinbruck, A.; Wolff, A.; Csaki, A.; Moller, R.; Fritzsche, W. *J Fluoresc* **2005**, *15*, 161-170.

(160) Minard-Basquin, C.; Kugler, R.; Matsuzawa, N. N.; Yasuda, A. *IEE Proc Nanobiotechnol* **2005**, *152*, 97-103.

(161) Wang, Z.; Lee, J.; Cossins, A.; Brust, M. *IEE Proc Nanobiotechnol* **2005**, *152*, 85-88.

CHAPTER II

DNA AND PROTEIN MICROARRAY PRINTING ON SILICON NITRIDE WAVEGUIDE SURFACES

Reprinted with permission from Wu, P.; Hogrebe, P.; Grainger, D. W. *Biosensors & Bioelectronics* **2005**.

This chapter contains the manuscript of a full paper published in *Biosensors & Bioelectronics*, formatted according to requirement of *Biosensors & Bioelectronics*. References are formatted according to the Harvard system (i.e. using Author(s) name(s) and date), with a reference list, in alphabetical order, at the end of the paper. This manuscript was written by Peng Wu, and edited by David W. Grainger. This chapter describes immobilization of DNA oligonucleotides, streptavidin and anti-human interleukin-1β capture agents on chemically silicon nitride surface in microarray formats, demonstrated by surface capture assays. X-ray photoelectron spectroscopy (XPS) was used to characterize each reaction sequence on the native silicon oxynitride surface. Importance of covalent binding in both DNA and protein microarray immobilization on this two-dimensional microarray platform is also investigated. Surface modification experiments were planned by Peng Wu and executed by Peng Wu and Paul Hogrebe. Microarray experiments were planned and executed by Peng Wu.

DNA and Protein Microarray Printing on Silicon Nitride Waveguide Surfaces

Peng Wu, Paul Hogrebe, David W. Grainger

Abstract

Sputtered silicon nitride optical waveguide surfaces were silanized and modified with a hetero-bifunctional crosslinker to facilitate thiol-reactive immobilization of contact-printed DNA probe oligonucleotides, streptavidin and murine anti-human interleukin-1β capture agents in microarray formats. X-ray photoelectron spectroscopy (XPS) was used to characterize each reaction sequence on the native silicon oxynitride surface. Thiol-terminated DNA probe oligonucleotides exhibited substantially higher surface printing immobilization and target hybridization efficiencies than non-thiolated DNA probe oligonucleotides: strong fluorescence signals from target DNA hybridization supported successful DNA oligonucleotide probe microarray fabrication and specific capture bioactivity. Analogously printed arrays of thiolated streptavidin and non-thiolated streptavidin did not exhibit noticeable differences in either surface immobilization or analyte capture assay signals. Non-thiolated anti-human interleukin-1β printed on modified silicon nitride surfaces reactive to thiol chemistry exhibited comparable performance for capturing human interleukin-1β. analyte to commercial amine-reactive microarraying polymer surfaces in sandwich immunoassays, indicating substantial non-specific antibody-surface capture responsible for analyte capture signal.

Keywords: immobilization; hybridization; sandwich immunoassay; optical waveguide; silicon nitride; microarray

Introduction

Rapid detection and accurate monitoring of various trace biomolecular targets and interactions remain formidable bioanalytical challenges in developing assays for clinically relevant agents in physiological fluids, hazardous environmental agents, biological warfare agents and high-throughput drug screening. Combinations of optical analysis and direct immunosensing, frequently exploited in integrated optical waveguides (IOWs), represent an attractive sensing modality for these applications because of their high sensitivity and selectivity (Bradshaw et al., 2005; Brecht et al., 1998; Klainer et al., 1997; Ligler et al., 2002b; Misiakos and Kakabakos, 1998; Plowman et al., 1999; Prieto et al., 2003). First described by Marcuse as thin film dielectrics (Marcuse, 1974), IOWs currently comprise three major subclasses: (1) IOW-attenuated total reflection (ATR) spectrometry, (2) waveguide Raman spectroscopy (WRS), and (3) IOW-fluorosensing (IOW-FS) (Plowman et al., 1998). All have history and current interest in biosensing using immobilized capture agents, including nucleotides and antibodies (Clerc and Lukosz, 1997; Gao et al., 1995; Haron et al., 2003; Trummer et al., 2001). Frequently, however, IOW performance in bioassays is limited by surface capture performance, either poor surface immobilization of affinity capture reagents (e.g., antibodies), unacceptable maintenance of surface-bound bioactivity, or unacceptable non-specific non-analyte surface adsorption (noise).

Silicon-based oxides, nitrides and oxynitrides are common IOW materials (Sahu et al., 2000), more robust than polymer waveguides and easily fabricated using conventional silicon microfabrication techniques from bulk silicon substrates, allowing miniaturization and integration of multiplexed, active features within the same optically matched substrates (Valette, 1988). Refractive indices of these materials can be varied from 1.46 (SiO_2) to 2.2 (Si_3N_4) by altering the nitrogen mass fraction in the source compound during material deposition. Thus, optical waveguide mode size can be controlled without changing the waveguide geometry (Chelnokov et al., 1994). Also, the native silicon oxide surfaces on these nitrogenated materials facilitates organo-silane coupling, one popular initial step in device chemical surface modification to accommodate biomolecule immobilization (i.e., DNA, proteins) (Brennan et al., 1993; Cass and Ligler, 1998; Henke et al., 1997).

Immobilization of biosensing capture agents (e.g., DNA, antibodies, streptavidin) on silicon oxide IOWs is widely reported (Clerc and Lukosz, 1997; Gao et al., 1995; Haron et al., 2003; Trummer et al., 2001). Less is reported concerning analogous modification of potentially useful silicon nitride/oxynitride IOWs. Immunoassay using immobilized rabbit capture antibody and fluorescent-labeled anti-rabbit antibody (10 nM model analyte) on a silicon nitride optical waveguide was exploited to study a three-dimensional microfluidic confinement method (Hofmann et al., 2002). An integrated optical Mach-Zehnder interferometer has been developed for biosensing using a silicon oxynitride waveguide surface functionalized to bind to streptavidin and a biotinylated antibody (Busse et al., 1999). Immobilization of human IgG and goat anti-human IgG antibodies as well as their specific affinity reactions have also been studied using planar

polarization interferometry comprising a silicon wafer with a silicon nitride layer sandwiched between two silicon oxide layers. Specific binding of 0.3 ng/ml human IgG model analyte was reported (Nabok et al., 2000).

To impart improved IOW sensing specificity and sensitivity, DNA and protein affinity capture agent immobilization on silicon oxide IOWs using silane coupling agents has also been widely investigated (Hermanson, 1995; Ligler and Rowe Taitt, 2002a). Additionally, nine hetero-bifunctional crosslinkers were investigated for their ability to immobilize active antibodies onto glass. Carbohydrate-reactive crosslinkers exhibited higher antibody immobilization activity than those with reactive succinimide esters but required a procedure that adversely affected antibody bioactivity (Shriver-Lake et al., 1997). The hetero-bifunctional N-hydroxysuccinimide (NHS)-maleimide coupling agent, succinimidyl 4-[N-maleimidomethyl]-cyclohexane-1-carboxylate (SMCC), is a popular crosslinker used to immobilize DNA or proteins to silanized silicon-based substrates (Hermanson, 1995; Lateef et al., 2002; Rezania et al., 1999). The thiol-reactive maleimide group coupling by Michael addition is more stable than the amine-reactive succinimide group reacted by nucleophilic displacement, with the latter NHS displacement reaction very susceptible to non-specific hydrolysis even under high humidity environments (Gong and Grainger, 2004; Hermanson, 1995; Tilstone, 2003). Using maleimide coupling for thiol-terminated DNA or thiolated proteins permits SMCC-activated substrates to be stored for relatively long periods before DNA/protein immobilization, avoiding considerable shelf-life stability issues known for NHS (Gong and Grainger, 2004; Metzger et al., 2002). Recently, DNA oligonucleotide printing onto 1,4-phenylene diisothiocyanate-activated silanized glass and silicon nitride in a printed

microarray format has been reported (Manning et al., 2003; Manning and Redmond, 2005). Combinations of array-based sensing and IOWs are of interest for multiple-analyte screening in real-time assays using the IOW surface-capture detection (Bradshaw et al., 2005) and size-based analytical chemistry advantages (Ekins and Chu, 1991).

We report characterization of microarrayed bioassay formats on sputtered silicon nitride films suitable for IOW applications, use of SMCC-silane hetero-bifunctional coupling to immobilize standard nucleic acid and protein affinity capture agents in printed microarray formats, and their resulting target capture capabilities from simple solutions. Comparison of specific versus non-specific capture agent binding to silicon nitride, and subsequent analyte assay performance is described for DNA oligomers, streptavidin, and anti-cytokine antibodies. The intent is to optimize surface-printed microarray capture formats for silicon nitride IOW-based affinity sensing of analytes from solution.

Materials and Methods

Materials

N-(2-aminoethyl)-3-aminopropyl-trimethoxysilane (EDS) was obtained from Gelest (Morrisville, PA) and used as received. Sulfosuccinimidyl 4-[N-maleimidomethyl]-cyclohexane-1-carboxylate (sulfo-SMCC) was obtained from Pierce (Rockford, IL). Dye-labeled thiol terminated 5'-Cy3-DNAoligo1-SH 3'(DNAoligo1 = CTGAACGGTAGCATCTTGAC-$(CH_2)_6$) and unlabeled 5'-DNAoligo1-SH 3' were purchased from TriLink Biotechnologies (San Diego, CA). Analogous fluorescent dye-labeled non-thiol-modified DNA oligomers of identical sequence, 5'-Cy3-DNAoligo1-3' and non-thiolated, unlabeled DNAoligo1, were both obtained from MWG Biotech (High

Point, NC). Complementary matched DNAoligo2 (DNAoligo2 = 5'-GTCAAGATGCTACCG TTCAG-3') with a 3'-Cy5 dye tag was purchased from IDT (Coralville, IA). Murine anti-human interleukin-1β (anti-hIL-1β) and anti-hIL-1β-biotin were obtained from Antibody Solutions (Palo Alto, CA). Recombinant human interleukin-1β target and goat anti-mouse secondary antibody were purchased from Pierce (Rockford, IL). Biotinylated goat anti-mouse antibody and streptavidin-Alexa Fluor® 647 conjugate were both obtained from Molecular Probes (Eugene, OR). Streptavidin was thiolated using a protein coupling kit from Pierce using their recommended protocols. Murine anti-Flag® M2-Cy3 conjugated antibody (Flag® octapeptide: Asp-Tyr-Lys-Asp-Asp-Asp-Asp-Lys) was obtained from Sigma (Milwaukee, WI) for use as model protein analyte for sandwich assay. Phosphate buffer and saline sodium citrate (SSC) saline salts were purchased from IGN Biomedicals (Aurora, Ohio). DNA assay buffer 1X SSC contains 150mM sodium chloride, 15mM sodium citrate, pH = 7.0; 4X SSC is 600mM sodium chloride, 60mM sodium citrate. Bovine serum albumin (BSA) and Tween 20 were obtained from Sigma (Milwaukee, WI). Polyethylene glycols (PEG, mol. wt. 150, 750, 2000, 6000, 20000) were purchased from Aldrich (St. Louis, MO). 2-Mercaptoethanol and ethanolamine, used to block unreacted surface-bound reactive groups on microarray printed slides, were obtained from Acros Organics (Morris Plains, NJ) and Aldrich (St. Louis, MO), respectively. A commercial polymer-coated amine-reactive microarraying slide surface (Codelink™, Amersham, Piscataway, NJ) was used to compare anti-hIL-1β print loading and target capture activity in antibody sandwich immunoassays to silanized silicon nitride surfaces.

Silicon nitride substrate preparation

Silicon borosilicate microscope 1" x 3" glass slides were subjected to argon plasma cleaning for 1 min (gas pressure = 0.1 Torr, power = 100W), followed by reactive ion sputtering deposition to produce 50-100 nm homogeneous silicon nitride overlayers. This process was performed at Thermo Electron Corporation (Boulder, CO) using ThermoElectron (West Palm Beach, FL) deposition equipment (TPDRO 1100). In this overlayer process, a nitrogen-containing plasma fragments a solid silicon substrate target, sputtering target material onto the substrate. Nitrogen plasma (either N_2 or NH_3 used as a nitrogen source) reacts with sputtered silicon material enroute to the substrate, forming a silicon nitride deposited film on the substrate. When the desired film thickness is achieved, the shutter is closed, plasma power is terminated and the sample is removed. A native siliconoxynitride surface forms upon exposure to air (Castanho et al., 1997).

Surface chemistry for oligo-DNA probe and capture antibody immobilization on silicon nitride

Silicon nitride-modified materials were cleaned with repeated acetone washing, a 5-minute sonication in acetone, re-rinse in acetone and final drying under a stream of nitrogen. Immediately prior to silanization, both silicon nitride substrates were subjected to argon/oxygen plasma cleaning for 5 min (gas pressure = 0.3 Torr, power = 100W). Slides were then immediately silanized in an acidic methanol solution (pH=5.2; adjusted using glacial acetic acid) containing 5% water and 1% (v/v) EDS under continuous agitation for 20 minutes, rinsed repeatedly with methanol and Millipore water (18.2 MΩ), dried under nitrogen, and then cured ambiently at 110°C (15 min.). Silanized substrates were activated for either DNA oligonucleotide probe or capture antibody covalent

attachment using a hetero-bifunctional crosslinker (sulfo-SMCC) dissolved at a concentration of 0.2 mg/ml in sodium borate buffer (pH = 7.5) using reaction conditions modified from Rezania et al., 1999. Silanized substrates agitated in this sulfo-SMCC crosslinker solution for 2 hours were promptly removed, rinsed repeatedly in fresh sodium borate buffer and Millipore water, dried under nitrogen, and stored under nitrogen until DNA oligonucleotide or antibody immobilization could be performed (typically not more than 2 weeks).

Figure 1 shows a schematic representation of the covalent immobilization process. Each immobilization step was characterized using X-ray photoelectron spectroscopy (XPS) employing a Physical Electronics 5800 instrument equipped with a monochromatic Al K X-ray source (1486.6eV) and a hemispherical analyzer (Chanhassen, MN). High-resolution C1s and N1s spectra were acquired with an analyzer pass energy of 23.50eV. Elemental composition wide scans were acquired with an analyzer pass energy of 187.85eV. A low-energy electron flood gun was used to neutralize electrically non-conductive samples. To assess compositional variation with depth, angle-dependent XPS data were collected at nominal photoelectron take-off angles of 45° and 15°, where take-off angle is defined as the angle between the surface and the axis of the analyzer lens system. Using published electron mean free paths equations from Seah and Dench,(Seah and Dench, 1979) the sampling depth (three times the mean free path) should decrease from ~4.5 nm to ~1.5 nm as the take-off angle decreases from 45° to 15°. All spectra binding energies were referenced to the C1s hydrocarbon peak at 285eV. Peaks from all high-resolution core spectra were fitted using XPSPeak software

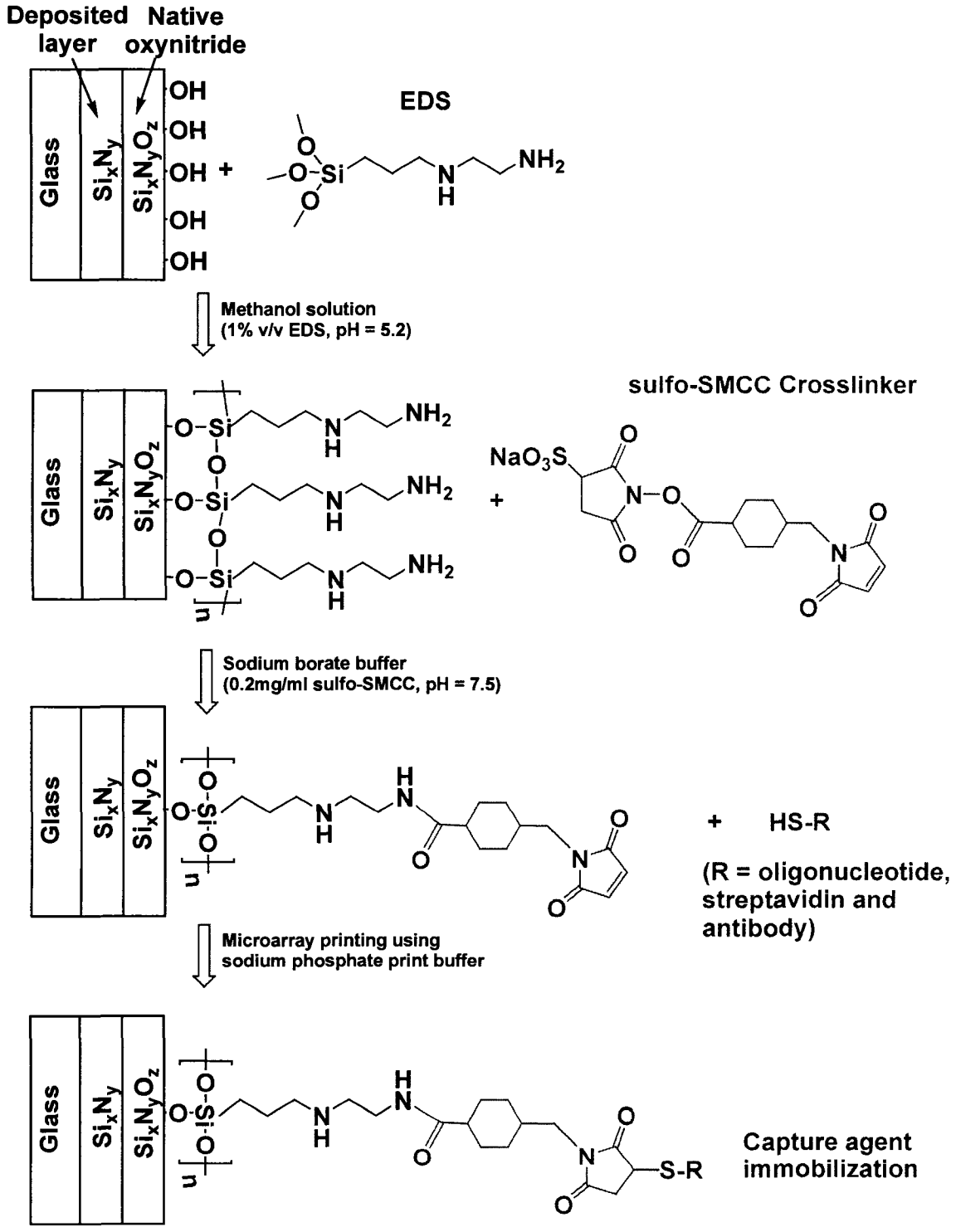

Figure 1. Idealized schematic for the surface reactions used to immobilize array-printed capture agents on sputtered silicon nitride surfaces.

(written by R. Kwok, Chinese University of Hong Kong, http://www.phy.cuhk.edu.hk/~surface/XPSPEAK/). A 100% Gaussian line shape was used to fit XPS high-resolution peaks, and a Shirley function was used to model the background (May et al., 2004).

DNA oligonucleotide probe surface printing and array hybridization with solution-phase target

Mechanical pin contact printing was used to print oligo-DNA probes and proteins into spotted arrays on silane-derivatized silicon nitride surfaces on commercial glass slides. Oligomer/antibody spots (1.1~1.8 nl) were deposited using a SpotBot™ microarrayer equipped with SPM4 and SMP6 Stealth™ microarray spotting pins (Telechem, Sunnyvale, CA). 5'-Cy3-DNAoligo1-SH-3', 5'-DNAoligo1-SH-3', 5'- Cy3-DNAoligo1 and DNAoligo1 probes were printed from 20μM stock solutions in 100mM sodium phosphate (pH=6.6) print buffer. Ambient humidity within the printing chamber was ~ 45%. Average DNA spot size after drying was approximately 100-150μm in diameter with spot center-center distances of 350–400 μm. Following printing, substrates were incubated in a 75% humidity chamber for 6 hours, then immersed in a solution of 50mM 2-mercaptoethanol in 50mM sodium phosphate buffer (pH=6.6) for 30 min to block unreacted surface-bound maleimide groups. Substrates were then rinsed repeatedly with 150mM phosphate buffered saline (PBS) and Millipore water, immediately placed in vials containing 4X SSC (4-fold concentrated 1X SSC, pH=7.0) and 0.1wt% sodium dodecyl sulfate (SDS) solution, submerged in a 50°C water bath for 30 minutes to remove non-specifically bound DNA oligonucleotide probes, then rinsed with Millipore water and dried under nitrogen.

DNA probe-printed microarrays were assessed for surface capture bioactivity by hybridization with 1μM fluorescently labeled complementary DNAoligo2 (3'-Cy5-DNAoligo2) in 4X SSC and 0.1% SDS solution using a LifterSlip™ cover glass (Erie Scientific, Portsmouth, NH) in a 100% humidity chamber for 4 hours. After incubation, slides were rinsed again with 4X SSC and placed in vials containing solutions of 2X SSC and 0.1wt% SDS. This vial was then placed in a 50°C bath for 5 min, followed by a series of SSC rinses of decreasing concentration. After a final rinse with Millipore water and nitrogen drying, hybridized substrates were imaged for fluorescence intensity.

Streptavidin and anti-hIL-1β capture antibody array printing and analyte surface-capture assays

Streptavidin-Alexa Fluor®647 was thiolated with a standard protein thiolation kit (product 23460, Pierce Biotechnology Inc., Rockford, IL, USA). Deprotection of protein-bound derivatives by hydroxylamine to thiol groups occurred immediately before array printing. Approximately 25 sulfhydryl groups per protein molecule were obtained according to Ellman's assay using Pierce-recommended protocols (data not shown). Streptavidin-Alexa Fluor®647 (50μg/ml) and thiolated streptavidin-Alexa Fluor®647 (50μg/ml) were printed onto maleimide-activated substrates and control slides (maleimide-activated silicon nitride on glass blocked with mercaptoethanol, see section 2.4 for conditions) in sodium phosphate print buffer (250mM $NaPO_4$ (pH=7.5) and 0.005% Tween 20). Anti-hIL-1β (non-thiolated, 400μg/ml) was printed directly onto both maleimide-activated silicon nitride substrates and commercial-sourced amine-reactive polymer-coated microarray glass slides (Codelink™, Amersham, Piscataway, NJ) using the same print buffer. PEG additives with different molecular weights (150, 750, 2000,

6000, 20000) and at different concentrations (0.5%, 5% w/v), were added to the anti-hIL-1β printing buffer to assess their possible effects to protect/maintain/improve capture antibody bioactivity. An environment of ~65% humidity was maintained throughout the printing process. Unreacted surface-bound maleimide groups were blocked immediately after printing using mercaptoethanol as previously described in section 2.4. Residual amine-reactive groups on commercial polymer-coated microarray slides were quenched using ethanolamine (1:500 v/v) in 50mM sodium borate buffer (pH=9.1). Slides were then rinsed with PBS and Millipore water, and finally dried under nitrogen.

Protein analyte capture assay on printed streptavidin microarrays

Printed, fully dried streptavidin microarray slides were rinsed with PBST (150 mM phosphate buffered saline with 0.01wt% Tween 20) and Millipore water, and dried under nitrogen. Biotinylated goat anti-mouse capture antibody and non-biotinylated control goat anti-mouse antibody were each dissolved in PBS + 0.05wt% Tween20 + 0.1wt% BSA buffer at 5 μg/ml and incubated on-array separately using Secure Seal™ hybridization chambers (Grace Bio-Labs Inc., Bend, OR) for 1 hour under 100% humidity. Slides were then rinsed repeatedly with PBST solution and Millipore water, and dried with nitrogen. Immediately thereafter, these surfaces were incubated with murine anti-Flag® M2-Cy3 conjugated antibody (used as a fluorescent target protein analyte) in PBS + 0.05wt% Tween20 + 0.1wt% BSA buffer at 1μg/ml for 2 hours. After final rinsing and drying, microarray slides were imaged for fluorescence intensity representing analyte capture signal.

Anti-hIL-1β sandwich immunoassay

Human IL-1β was assayed using sandwich immunoassay format with array-printed anti-human IL-1β antibodies on solid supports (Blawas and Reichert, 1998; Li et al., 2003). Recombinant human IL-1β model analyte (molecular weight ~ 17kDa), a clinically relevant inflammatory cytokine, was diluted in PBS + 0.05wt% Tween20 + 0.1wt% BSA buffer at 10 ng/ml and incubated on-array for 1 hour using Lifterslips™ under 100% humidity. Slides were then rinsed with PBST and water, and dried with nitrogen. Biotinylated secondary antibody (anti-hIL-1β-biotin) was diluted to ~6.6 μg/ml in PBS + 0.05wt% Tween20 + 0.1wt% BSA solution from 1 mg/ml frozen stock and incubated on-array for 30 minutes. After repeated rinsing and drying, arrays were finally incubated for 30 minutes with streptavidin-Alexa Fluor® 647 conjugate (diluted to 20μg/ml from 1mg/ml stock solutions using PBS + 0.05wt% Tween20 + 0.1wt% BSA solution). Dye-conjugated streptavidin fluorescence imaging was used to verify antigen capture and activity of the biotinylated sandwich assay antibodies.

Microarray fluorescence detection and image processing

All substrates were imaged using a Packard BioChip fluorescence imager using appropriate filters for each respective dye. Resolution was set to 10 microns. All microarray scanned fluorescence images were processed with ScanAlyze™ software (Dr. M. Eisen, Univ. California-Berkeley, see http://rana.lbl.gov/EisenSoftware.htm). Intensities from spotted replicates (n = 10 or 20) were averaged and standard deviations calculated. Statistical analysis was performed to distinguish significance using paired Student's *t*-tests.

Results and Discussion

Surface characterization using XPS

XPS results from analyses of surface-modified silicon nitride-coated glass substrates determined after each reaction step are shown in Table 1. Sonication and plasma cleaning steps greatly reduced adventitious carbon and other trace element surface contamination on as-deposited silicon nitride substrates prior to silanization. A highly oxygenated silicon oxynitride surface layer was detected on plasma-cleaned un-derivatized silicon nitride films. Whether this was a mixed oxynitride or a thin layer of silicon oxide over a basal layer of silicon oxynitride cannot be distinguished by depth-dependent XPS analysis. This native silicon oxynitride surface confirmed by XPS (Table 1) was used to chemically react with EDS for subsequent bio-immobilization per Figure 1. XPS evidence supports surface coupling reactions to silicon nitride consistent with the proposed reaction scheme (Figure 1). Table 1 demonstrates significant increases (p <0.001) in carbon atomic% composition on plasma-cleaned glass after EDS silanization and sulfo-SMCC modification, accompanied by decreases in silicon and oxygen substrate signals attenuated by the EDS and sulfo-SMCC crosslinker overlayers. Deposited EDS is not a homogeneous monolayer, demonstrated by large deviations in atomic% composition (Table 1). The C/N atomic% ratios of EDS silanization and sulfo-SMCC modification reaction steps were compared with theoretical values assuming a 100% pure EDS monolayer and 100% reaction of sulfo-SMCC with amino groups on EDS as shown in the proposed reaction scheme (Figure 1). The C/N atomic percent ratio obtained at 1.5 nm sampling depth is close to theoretical values whereas C/N ratios obtained at 4.5 nm

sampling depth are much lower. This is due to greater XPS contributions from substrate silicon nitride at deeper sampling depth versus that at shallower sampling depth.

Table 1. XPS elemental surface composition of silicon nitride before and after sequential modification steps from survey scans. Atomic percent was measured on at least 4 different spots from 2 to 3 substrates (avg. ± S.D. shown).

surface (sampling depth)	XPS atomic%			
	C1s	**N1s**	**O1s**	**Si2p**
untreated silicon nitride (as received) (4.5 nm)	19.7 ± 2.3	18.3 ± 0.6	37.8 ± 1.5	24.3 ± 0.5
plasma cleaned silicon nitride (4.5 nm)	2.4 ± 0.3	16.4 ± 0.2	50.2 ± 0.2	31.0 ± 0.3
EDS silane on silicon nitride (4.5 nm)	21.0 ± 2.0	12.5 ± 0.6	44.3 ± 1.3	22.6 ± 0.9
EDS silane on silicon nitride (1.5 nm)	29.9 ± 2.2	11.2 ± 0.9	41.5 ± 1.3	17.5 ± 1.2
sulfo-SMCC + EDS on silcon nitride (4.5 nm)	37.9 ± 0.6	11.5 ± 0.5	34.0 ± 0.7	16.6 ± 0.3
sulfo-SMCC + EDS on silcon nitride (1.5 nm)	51.9 ± 0.4	10.0 ± 0.2	28.2 ± 0.3	10.0 ± 0.6
	C/N ratio			
EDS silane on silicon nitride (4.5 nm)	1.7 ± 0.2			
EDS silane on silicon nitride (1.5 nm)	2.7 ± 0.3			
100% EDS on silcon nitride (theoretical)	2.5			
sulfo-SMCC + EDS on silcon nitride (4.5 nm)	3.3 ± 0.2			
sulfo-SMCC + EDS on silcon nitride (1.5 nm)	5.2 ± 0.1			
100% sulfo-SMCC + EDS on silcon nitride (theoretical)	5.7			

The XPS C1s high-resolution spectra of silicon nitride after plasma cleaning, EDS silanization and sulfo-SMCC modification (Figure 2(a)) clearly shows emergence of the C-N peak at 286.4eV (Shibata and Miyazaki, 2002) after EDS silanization, and the amide peak at 288.2eV (Hitchcock et al., 2002) resulting from the sulfo-SMCC-amine reaction. These spectra are similar to those published previously on silicon and titanium oxide

surfaces (Rezania et al., 1999), confirming successful EDS silanization and modification with the hetero-bifunctional sulfo-SMCC crosslinker.

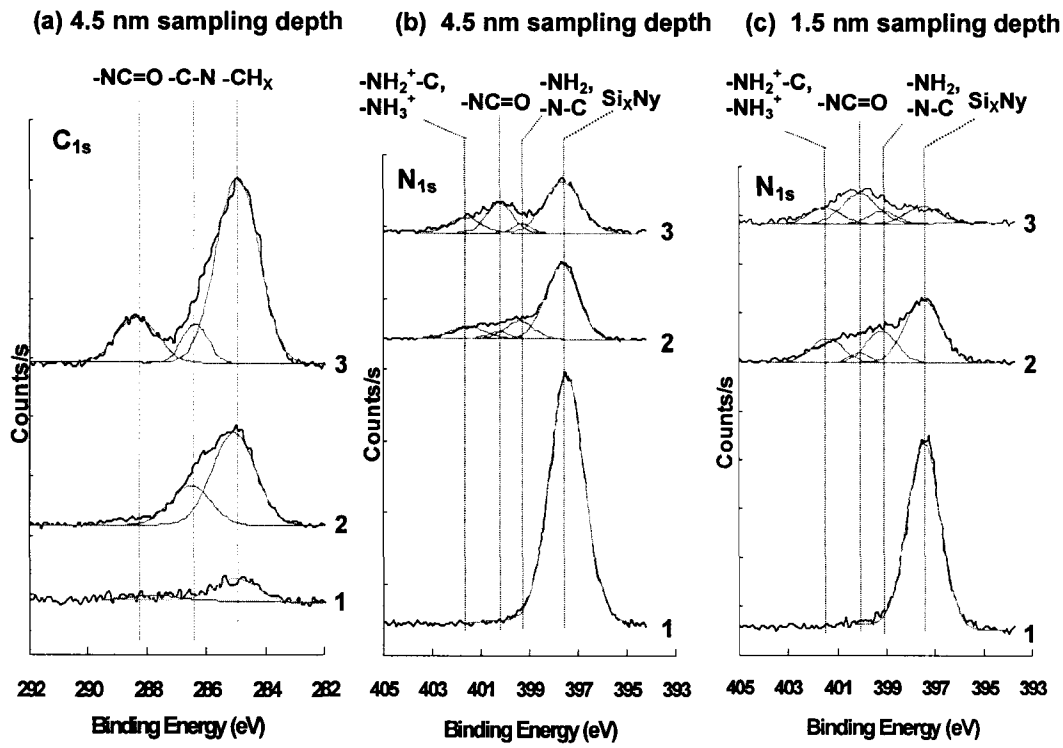

Figure 2. XPS high-resolution spectra of (a) carbon C1s, and (b-c) nitrogen N1s regions for (1) plasma-cleaned silicon oxynitride, (2) EDS, (3) EDS + sulfo-SMCC on silicon oxynitride substrate over glass ((a-b) spectra measured at 45° take-off angle, ~ 4.5 nm sampling depth; (c) spectra measured at 15° take-off angle, ~ 1.5 nm sampling depth).

The XPS N1s high-resolution spectra (Figure 2(b)-(c)) demonstrate emergence of -N-C- and $-NH_2$ peaks at 399.2eV (Weng et al., 1995) after EDS silanization and the amide peak at 400.2eV (Lin and Lin, 2001) after sulfo-SMCC modification, with attenuation of the substrate Si_xN_y component peak at 397.5 eV (Choi et al., 1999) after each surface reaction step. Small amide peaks appearing in these N1s spectra after EDS silanization may be attributed to minor surface contaminants (e.g., adventitious oxidized

carbon species). Peaks at 401.5eV are proposed to be due to protonated amine groups produced under acidic surface-silanization conditions (Ganapathy et al., 2001).

Changing XPS take-off angle (sampling depth) changes the N1s contributions from substrate silicon nitride and amine/amide in organic adlayers, clearly demonstrated in Figures 2 (b) and (c). Specifically, decreasing photoelectron take-off angles from 45° to 15° (XPS sampling depth from 4.5 nm to 1.5 nm) decrease the substrate Si_xN_y contribution from the component peak at 397.5eV, while contributions from higher binding energy nitrogen peaks from organic adlayers increases at shallower sampling depth. The N1s spectra for maleimide-activated silicon nitride exhibited significant contributions from the Si_xN_y peak at 397.5eV at a sampling depth of 4.5 nm, and lower contributions from organic adlayers (EDS, sulfo-SMCC) at higher binding energies. These N1s component contributions reverse at the shallower 1.5 nm sampling depths. Overall, these XPS data shown together in Table 1 and Figure 2 confirmed successful deposition of EDS and sulfo-SMCC crosslinker onto silicon nitride-sputtered glass substrates.

Oligonucleotide probe microarray spotting and target surface hybridization from solution

After EDS silanization and sulfo-SMCC modification of silicon nitride, thiolated oligonucleotide probes and thiolated streptavidin were reacted with substrate-immobilized maleimide functional groups via Michael addition (Rezania et al., 1999). Figure 3 shows the printed oligonucleotide microarray experimental lay-out, scanned fluorescence images, and image analysis results. To analyze the effectiveness of probe printing, immobilization, and complementary oligonucleotide target hybridization,

fluorescence intensity readings (i.e., mean intensity minus median background) were calculated for 20 spots from two identical microarrays per slide (10 spots/array) and were repeated using other similarly activated glass slides (all data not shown). The Cy3 fluorescence scanner channel was used to monitor the surface immobilization efficiency of Cy3-oligonucleotide single-strand probe, while the Cy5 channel was used to investigate Cy5 dye-labeled DNA target double-strand hybridization efficiency. Data in Figure 3 indicate that thiolated-oligonucleotide, 5'-Cy3-DNAoligo1-SH-3', exhibits significantly higher (p <0.001) relative fluorescence units (RFUs) than the non-thiolated oligonucleotide printed control, 5'-Cy3-DNAoligo1, in both Cy3 (print) and Cy5 (capture) channels. Unlabeled 5'-DNAoligo1-SH-3' and non-thiolated 5'-DNAoligo1-3' controls printed for comparison and hybridized with labeled 3'-Cy5-DNAoligo2 target showed the same trend in the Cy5 (capture) channel (p <0.001). This indicates that thiol-derivatized DNA probe demonstrates specific coupling efficiency to the surface maleimide group, an observation that while intuitive, is not always true for microvolume printing/rapid drying of nucleotides onto surfaces where non-specific surface capture effects are significant upon drying (Gong and Grainger, 2004). The data show that oligonucleotide printed probes lacking Cy3 fluorescent tags are likely better indicators of the real differences between specific and non-specific DNA target binding since possible interference (both steric and electronic) from bulky fluorescence dyes on both probe binding to substrates and short target oligonucleotide hybridization are eliminated.

Covalent reaction between DNA terminal thiol groups and surface maleimide groups improves printed oligonucleotide probe signal on maleimide functionalized silicon nitride. However, non-specific binding of the printed non-thiolated

oligonucleotide control was 50 times higher than surface background fluorescence and cannot be neglected. Similar non-specific printing residual issues with reactive DNA oligomers have been reported recently using commercial polymer-coated DNA microarray surfaces (Gong and Grainger, 2004). Levels of non-specific DNA probe binding to these surfaces are correlated with high DNA probe concentrations in print buffers and the rapid non-equilibrium drying/sorption occurring within seconds for 1~2 nl probe liquid spots upon printing in the ~45% humidity print chamber. It is not well understood how functionalized oligonucleotides specifically react with functionalized surfaces within such short time periods under non-equilibrium reaction conditions while ionic strength and probe concentrations are both rapidly changing under evaporation and surface sorption. Other than covalent reactions, ubiquitous van der Waals forces, acid-base and electrostatic interactions, and irreversible surface energetics all likely play roles in specific and non-specific probe surface binding during the microarray print process as the three-phase line moves across the printed spot during evaporation. A further interesting observation is that unlabeled 5'- DNAoligo1-SH-3' probe exhibited significantly higher (~ 50% higher RFU) (p <0.01) than labeled 5'-Cy3-DNAoligo1-SH-3' probe in the Cy5 target signal channel after 5'-DNAoligo2-Cy5-3' hybridization. This indicates some dye interference between Cy3 on the DNAoligo1 probe 5' end and Cy5 on the DNA-oligo2 target 3' end, introducing likely steric barriers during hybridization of these short complimentary probe-target pairs.

Analyte capture assay on printed thiolated streptavidin microarrays

As shown in Figure 4(a), streptavidin-Alexa Fluor® 647 and thiolated streptavidin-Alexa Fluor® 647 were printed in identical microarray formats to investigate

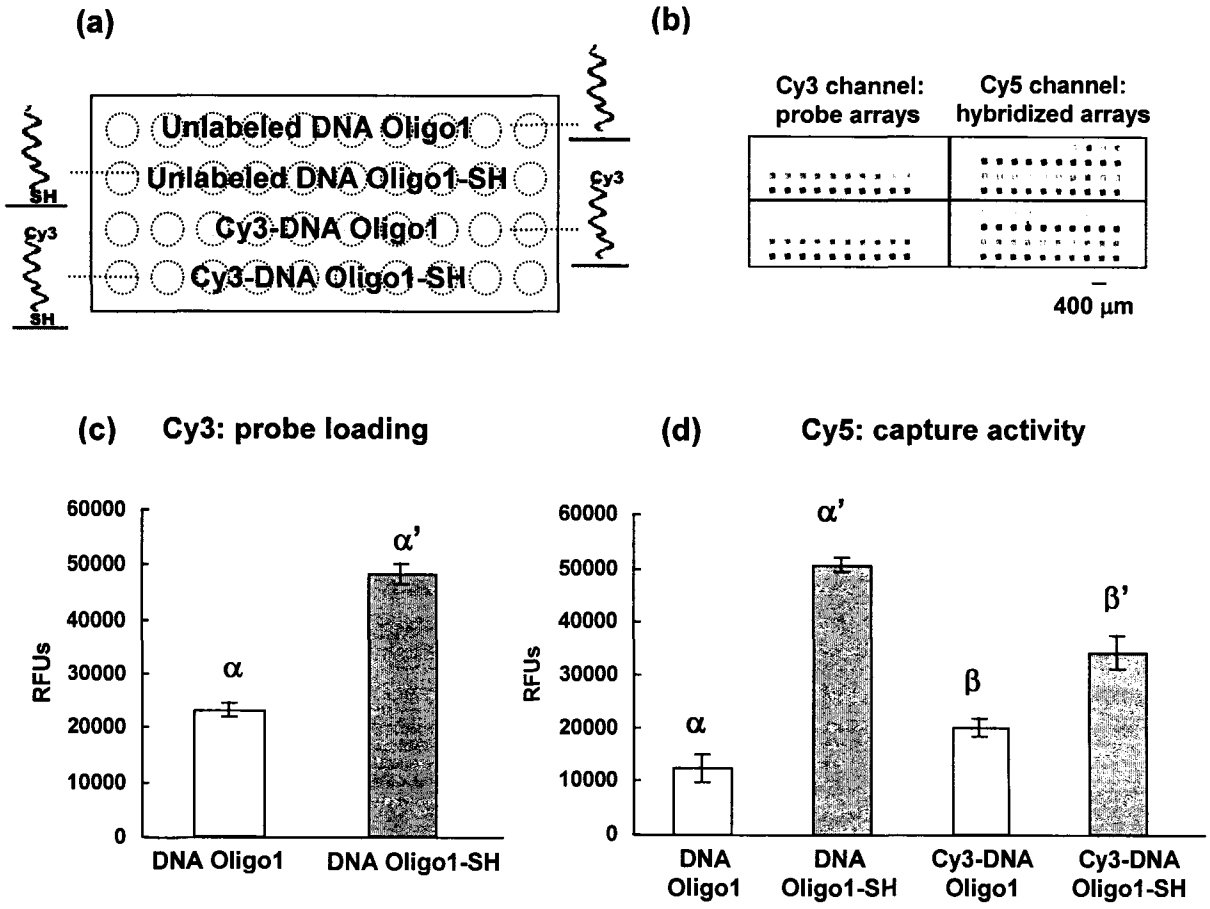

Figure 3. Microarray DNA print and target hybridization fluorescent signals on maleimide-activated surfaces: (a) microarray experimental lay-out; (b) actual fluorescence scanned images (upper/lower = 2 identical arrays) for printed DNA probes formatted as in (a), and hybridized with Cy5-DNAoligo2 targets; (c) quantified Cy3 labeled DNAOligo1 probe print fluorescence intensity (avg. ± S.D. for n = 20 spots) comparing thiolated versus non-thiolated DNA probes on maleimide-activated surfaces (α & α' statistically different, $p < 0.001$); and (d) quantified Cy5-DNA target capture spot fluorescent intensities after array hybridization with 1µM Cy5-DNAOligo2 target (avg. ± S.D. for n = 20 spots) on oligo1-printed arrays shown in (b) (α & α', β & β'and α' & β' statistically different, $p < 0.001$). DNAoligo1 is printed from 20µM stock DNA probe solutions in 100mM sodium phosphate (pH=6.6) print buffer and hybridized with 1µM complementary 3'-Cy5-DNAoligo2 in 4X SSC and 0.1wt% SDS solution as described in text.

protein capture bioactivity after immobilization (printing, drying) on maleimide-activated silicon nitride on glass substrates. Four identical streptavidin arrays were printed per activated glass slide and onto a mercaptoethanol pre-blocked control slide with the array lay-out shown in Figure 4(a). The intended analyte capture and reporting design in schematically shown in Figure 5. After printing, each streptavidin printed microarray was incubated under different conditions using four isolated capture assay chambers. As shown in Figure 4(b), none of the control print buffer-only arrays show any signal in the Cy5 (protein print) channel, indicating low background fluorescence. Additionally, the first streptavidin printed control array (b1) was incubated without antibody analyte: the scanner loading channel shows fluorescence only from printed rows of streptavidin-Alexa Fluor® 647. The second streptavidin control array (b2) was incubated only with anti-Flag® M2-Cy3 conjugate murine antibody target directly for 2 hours, exhibiting no signal in the Cy3 (capture) channel, indicating little non-specific analyte capture. The third streptavidin control array (b3) was incubated with non-biotinylated goat anti-mouse capture antibody for 1 hour, then with anti-Flag® M2-Cy3 conjugate murine antibody target analyte for 2 hours. Negligible signal here demonstrates no observable non-specific antibody reactivity. The last streptavidin array (b4) represents the complete assay, incubated with biotinylated goat anti-mouse capture antibody for 1 hour, then with anti-Flag® M2-Cy3 conjugate murine antibody target analyte for 2 hours (see complete sandwich capture assay scheme in Figure 5). Only this last array shows significant Cy3 fluorescence signal indicative of the intended capture sandwich assay design: biotinylated goat anti-mouse capture antibody binding to printed streptavidin-Alexa Fluor® 647 via biotin-streptavidin interactions, followed by Cy3-labeled mouse antibody (anti-Flag®

M2-Cy3 conjugate murine antibody) target capture by the biotinylated goat anti-mouse antibody.

Importantly, differences observed in Cy5-probe loading signals either between printed thiolated streptavidin-Alexa Fluor® 647 and non-thiolated streptavidin-Alexa Fluor® 647, or between maleimide-activated and pre-blocked control surfaces (see intensity data, Figure 4(c)) are substantially less than differences observed between thiolated oligonucleotide and non-thiolated oligonucleotide probes printed as described in Figure 3. Significant non-specific (non-covalent) surface binding must exist between non-thiolated streptavidin and maleimide-activated silicon nitride surfaces, and also between streptavidin and pre-blocked control surfaces to account for these differences. These effects could be exacerbated by non-equilibrium rapid drying of spotted nanoliter droplets, producing irreversible non-covalent surface aggregation and binding as witnessed to a lesser extent for probe nucleotides (c.f., section 3.3 above). Interestingly, this non-specific streptavidin capture produces no substantial difference in Cy3-target analyte capture signals (see intensity data, Figure 4(d)) indicating that streptavidin thiolation to produce surface covalent binding via maleimide-thiol coupling during streptavidin printing does not improve immobilization to modified silicon nitride compared to other non-specific streptavidin-surface adsorption factors. This reflects the importance of creating sensing surfaces designed for capture assays, either in macro- or microarray formats, that facilitate specific immobilization of capture agents, preserve their efficient analyte recognition activity after drying, and retain low non-specific adsorption interference from non-analyte species. The distinction between nucleotide and protein immobilization behavior and requirements upon rapid, non-equilibrium

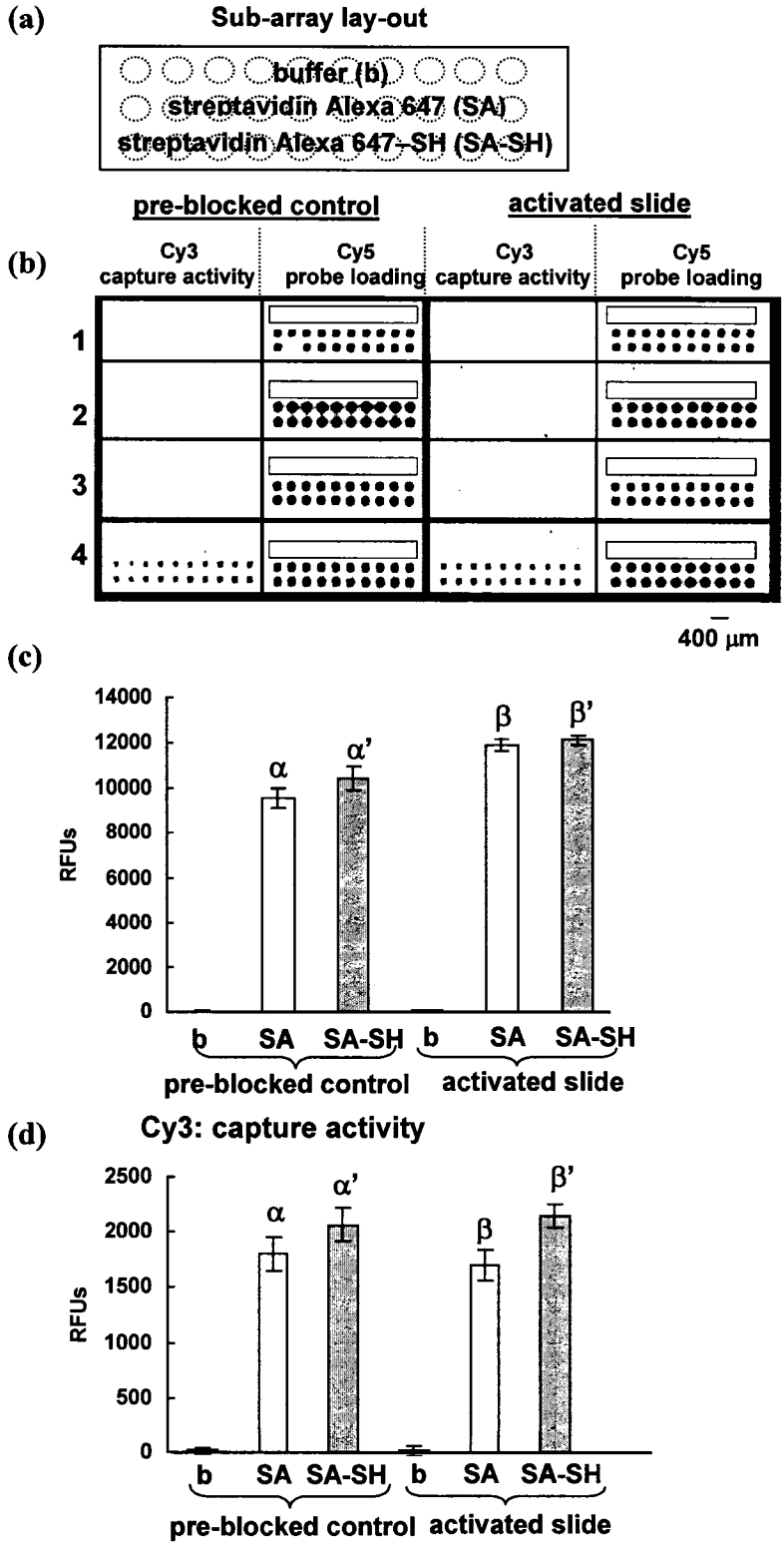

Figure 4. Printed streptavidin-Alexa 647 microarrays on maleimide-activated silicon nitride-sputtered surfaces: (a) experiment microarray print lay-out showing buffer-only, non-thiolated streptavidin and thiolated streptavidin rows; (b) actual fluorescence

scanned images of print and capture results (four identical streptavidin arrays **1-4** printed as shown in lay-out scheme in (a); open boxes in row 1 of each array identifies printed buffer control spot rows as negative control); Array **1** (control) was not incubated with analyte, array **2** (control) incubated only with anti-Flag® M2-Cy3 conjugate murine antibody (1μg/ml), array **3** (control) was incubated with non-biotinylated goat anti-mouse IgG (5 μg/ml) and anti-Flag® M2-Cy3 conjugate murine antibody target (1μg/ml), array **4** (complete assay) was incubated with biotinylated goat anti-mouse IgG (5μg/ml) and anti-Flag® M2-Cy3 conjugate murine antibody target (1μg/ml); (c) quantified streptavidin-Alexa 647 print fluorescence intensities (avg. ± S.D. for n = 10 spots) of array **4** (α & α' statistically different, $p = 0.025$; β & β' statistically not different $p > 0.05$; α & β and α' & β'statistically different $p < 0.001$); and (d) quantified Cy3-target antibody fluorescence intensities after biotinylated antibody and Cy3-target antibody capture (avg. ± S.D. for n=10 spots) of array **4** (α & α' statistically different, $p = 0.013$; β & β' statistically different, $p < 0.001$; a & β and α' & β' statistically not different $p > 0.05$) (**b**: buffer, **SA**: streptavidin-Alexa 647, **SA-SH**: thiolated streptavidin-Alexa 647).

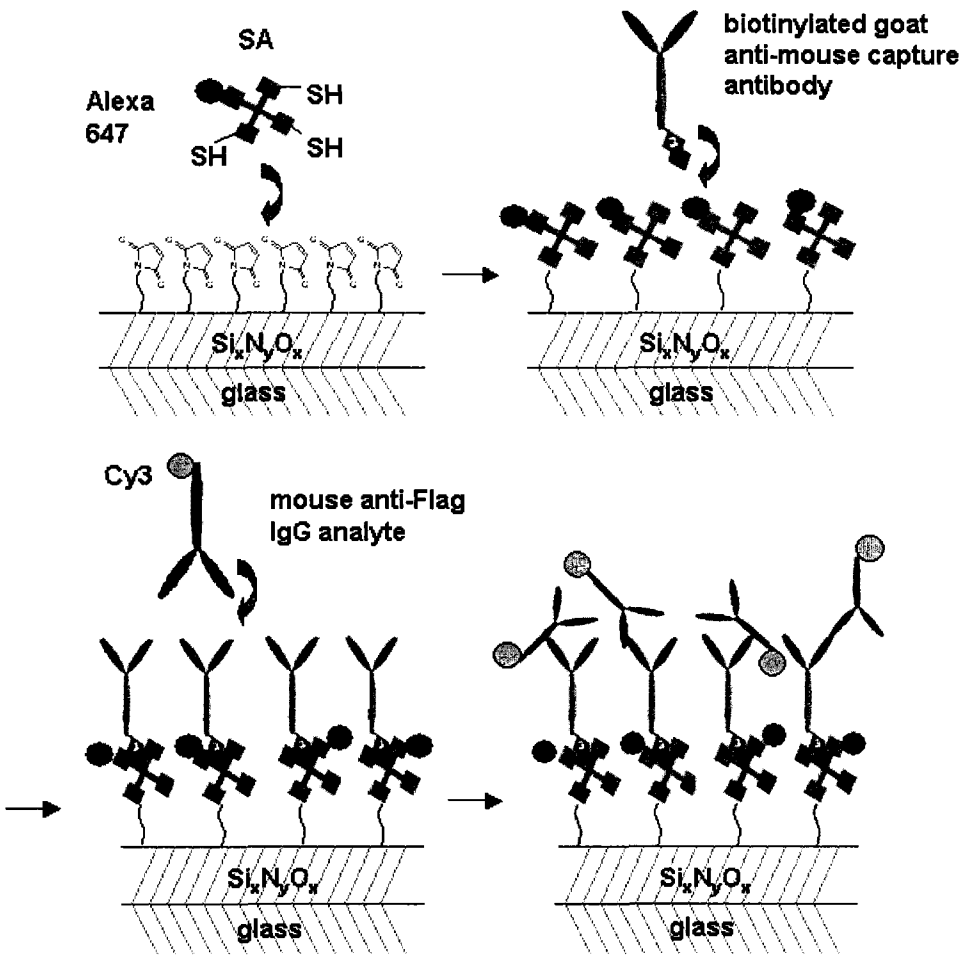

Figure 5. Sandwich capture assay design on printed streptavidin microarray.

drying after printing are empirically evident from comparing print and capture yields between these two affinity agents in Figures 3-4. However, specific strategies to accommodate each chemistry with specific surface properties to optimize reagent activity are not known. To further study this aspect, an anti-hIL-1β cytokine sandwich capture assay using non-thiolated anti-hIL-1β antibodies printed onto thiol-reactive maleimide-modified silicon nitride was compared to printing on amine-reactive commercial polymer-coated microarrays slides marketed for this purpose (Codelink™, Amersham, Piscataway, NJ).

Comparing anti-hIL-1β sandwich microarray assays on silanized silicon nitride versus commercial polymer-coated microarray slides

Polyethylene glycols are benign, hygroscopic, highly hydrated excipients often used in protein-based formulations to preserve protein hydration, structure stability and bioactivity (Carpenter et al., 1993; Harris, 1992). Soluble PEG additives at different dilute concentrations and molecular weights were added into antibody print buffers to examine their influence on the performance of anti-hIL-1β antibody print and analyte capture efficiency after printing and drying onto silicon nitride-sputtered surfaces. Figure 6 shows anti-hIL-1β antigen capture activity in a sandwich format: comparable bioactivity was observed on both the maleimide-activated silicon nitride specific for thiol reactivity and commercial polymer surfaces designed to be chemically amine-reactive, despite our observation that most antibodies have few surface-exposed cyteine thiols and may have over 100 surface-resident lysines containing ε-amino groups (analysis of various antibody crystal structures, Protein Data Bank, data not shown). This surface comparison supports a primary non-specific antibody-surface binding interaction upon

printing and drying, that is, independent of covalent antibody-surface chemistry or functionalization. Biotinylated goat anti-mouse antibody was chosen as a positive control because of its direct interactions with the streptavidin-Alexa Fluor® 647 sandwich tag without significant concern about lost antibody bioactivity influencing fluorescence signal in the Cy5 channel (immobilization is biotin-streptavidin mediated). Buffer without anti-hIL-1β antibody capture served as a negative printed control. Printed without PEG additives, anti-hIL-1β arrays exhibited much higher sandwich assay fluorescence signal on commercial polymer microarray slides than on maleimide-modified silicon nitride after antigen capture. This is likely due both to higher surface binding capacity by the commercial three-dimensional hydrophilic polymer gel coating versus more planar, less polar, non-sorptive silane surface, and a higher covalent binding efficiency between more abundant surface lysine amine groups of printed capture antibodies and amine-reactive groups on the commercial polymer slide versus fewer surface-exposed free thiols for maleimide reaction with these antibodies. However, IL-1β antigen capture signals can be significantly enhanced with PEG additives in the print buffer: 5% (w/v) PEG 6000 ($p < 0.001$), 5% (w/v) PEG 2000 ($p < 0.001$) for anti-hIL-1β printed on maleimide-activated silicon nitride, and 0.5% (w/v) PEG 20000 ($p < 0.001$) for anti-hIL-1β printed on commercial polymer microarray slides. Plausibly, the PEG additives help preserve antibody structure and bioactivities after printing and drying on solid array surfaces, as several poorly controlled print factors other than surface covalent binding (e.g., rapid non-equilibrium drying, surface-induced conformational influences, and possible salting-out) significantly influence the observed bioactivity of immobilized desiccated microarrayed capture proteins on activated silicon nitride.

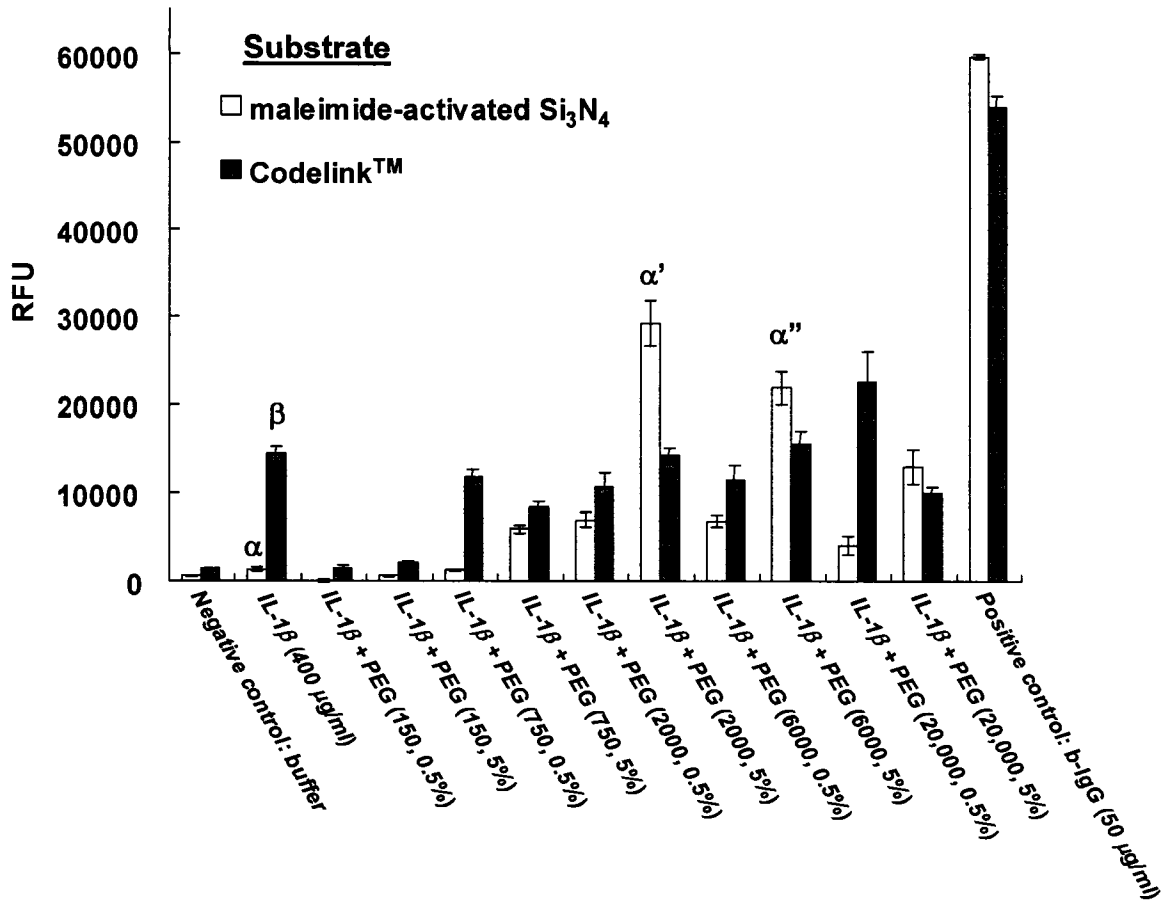

Figure 6. Comparison of printed microarray fluorescence image analysis for native anti-human IL-1β microarray sandwich assay activity on maleimide-activated silicon nitride-sputtered glass versus commercial polymer-coated amine-reactive microarray slides. Additives including PEG of different molecular weight (150, 750, 2000, 6000, 20,000) and concentrations (0.5%, 5% w/v) were added to print buffers to examine their influence on capture efficiency of anti-human IL-1β post-printing and drying. Intensity of captured antigen, cytokine IL-1β, from biotinylated sandwich antibody assay design with fluorescent streptavidin shown (avg. ± S.D. for n = 5 spots). Negative control (left): print buffer only; positive control (right): biotinylated goat anti-mouse IgG (b-IgG) (α, α' & α'' and β & β' statistically different, $p < 0.001$).

Conclusions

Silicon nitride surfaces were immobilized with microarrayed nucleic acid and antibody affinity capture agents for potential applications in optical waveguide biosensing. The oxynitride surface facilitates silane-modification as reported extensively

for analogous organo-coupling to native silicon oxide, silica, glass, alumina, and titania (Jin et al., 2003; Matinlinna et al., 2004; Plueddemann, 1982). Comprehensive surface characterization of silicon nitride model surfaces intended for IOW applications supports the ability to modify these surfaces to reliably attach DNA oligonucleotides, streptavidin and capture antibodies in printed, dried microarray formats. Printed DNA oligonucleotides, streptavidin and antibodies all retained reasonable (i.e., detectable by conventional fluorescence assay methods) capture bioactivity, confirmed either by DNA hybridization or sandwich assays and fluorescence imaging. Probe DNA oligonucleotides bearing terminal thiol end groups exhibited significantly improved printing efficiency over non-thiolated analogous oligonucleotides using thiol-maleimide surface coupling. This led to improved hybridization performance in surface-capture assays with complementary DNA target solutions. However, significant target hybridization from non-specific binding of printed non-thiolated oligonucleotide probes was also observed. Printed streptavidin and anti-human IL-1β capture proteins showed little difference in surface retention between covalent and non-covalent attachment modes, demonstrating the fundamental differences between DNA oligomer and protein printing influences on array bioactivity, and the importance of producing surface chemistries that might exploit these differences to improve protein-based microarray assays. Print additives (PEG polymers) showed some ability to improve analyte capture sensitivity for printed proteins, consistent with their known important role in cryo- and dessicant-protection in protein therapeutics. Surface chemistries that respond to the distinctly different specific immobilization requirements of nucleotides versus protein affinity reagents to preserve

high capture activity in reproducible, spatially controlled microarray formats in each case will contribute to improving capabilities of IOWs in advanced assay designs.

Acknowledgements

The authors acknowledge support from NIH EB00726 and the National Science Foundation's Research Experience for Undergraduates (REU) program. Technical guidance from S. S. Saavedra (Univ. of Arizona) and G. Harbers (CSU) are both gratefully acknowledged. Further assistance for fluorescence scanning from Dr. W. H. Hanneman (CSU), silicon nitride sputter coating by M. Stephens (CSU), L. Rea and H. Cross (Thermo Electron Corp., Boulder, CO), and reproducible spotting protocols from Dr. C. Greef (Accelr8, Denver, CO) are all gratefully acknowledged.

References

Blawas, A.S., Reichert, W.M. 1998. Protein patterning. Biomaterials 19, 595-609.

Bradshaw, J.T., Mendes, S.B., Saavedra, S.S. 2005. Planar integrated optical waveguide spectroscopy. Anal. Chem. 77, 28A-36A.

Brecht, A., Klotz, A., Barzen, C., Gauglitz, G., Harris, R.D., Quigley, G.R., Wilkinson, J.S., Sztajnbok, P., Abuknesha, R., Gascon, J., Oubina, A., Barcelo, D. 1998. Optical immunoprobe development for multiresidue monitoring in water. Anal. Chim. Acta 362, 69-79.

Brennan, J.D., Brown, R.S., Della Manna, A., Kallury, K.M.R., Piunno, P.A., Krull, U.J. 1993. Covalent immobilization of amphiphilic monolayers containing urease onto optical fibers for fluorometric detection of urea. Sens. Actuators, B11, 109-19.

Busse, S., Kashammer, J., Kramer, S., Mittler, S. 1999. Gold and thiol surface functionalized integrated optical Mach-Zehnder interferometer for sensing purposes. Sens. Actuators, B60, 148-154.

Carpenter, J.F., Prestrelski, S.J., Arakawa, T. 1993. Separation of freezing- and drying-induced denaturation of lyophilized proteins using stress-specific stabilization. I. Enzyme activity and calorimetric studies. Arch. Biochem. Biophys. 303, 456-64.

Cass, T., Ligler, F.S. 1998. Immobilized Biomolecules in Analysis: a Practical Approach, Oxford University Press, Oxford, UK.

Castanho, S., Moreno, R., Fierro, J.L. 1997. Influence of process conditions on the surface oxidation of silicon nitride green compacts. J. Mater. Sci. 32, 157-162.

Chelnokov, A.V., Lourtioz, J.M., Boucaud, P., Bernas, H., Chaumont, J., Plowman, T. 1994. Deep high-dose erbium implantation of low-loss silicon oxynitride waveguides. Electron. Lett. 30, 1850-2.

Choi, W.-K., Koh, S.-K., Jung, H.-J. 1999. X-ray photoelectron spectroscopy studies of modified surfaces of a-Al_2O_3, SiO_2, and Si_3N_4 by low energy reactive ion beam irradiation. J. Vac. Sci. Technol., A17, 3362-3367.

Clerc, D., Lukosz, W. 1997. Direct immunosensing with an integrated-optical output grating coupler. Sens. Actuators, B40, 53-58.

Ekins, R.P., Chu, F.W. 1991. Multianalyte microspot immunoassay-microanalytical "compact disk" of the future. Clin.Chem. 37, 1955-67.

Ganapathy, R., Manolache, S., Sarmadi, M., Denes, F. 2001. Immobilization of papain on cold-plasma functionalized polyethylene and glass surfaces. J. Biomater. Sci., Polym. Ed. 12, 1027-1049.

Gao, H., Saenger, M., Luginbuehl, R., Sigrist, H. 1995. Immunosensing with photoimmobilized immunoreagents on planar optical wave guides. Biosens. Bioeletron. 10, 317-28.

Gong, P., Grainger, D.W. 2004. Comparison of DNA immobilization efficiency on new and regenerated commercial amine-reactive polymer microarray surfaces. Surf. Sci. 570, 67-77.

Haron, S., Nabok, A.V., Ray, A.K. 2003. Optical biosensing transducer based on silicon waveguide structure coated with polyelectrolyte nano layers. Proc. SPIE 5119, 100-108.

Harris, M.J. 1992. Poly(ethylene glycol) chemistry: Biotechnical and biomedical applications Plenum, New York.

Henke, L., Piunno, P.A.E., McClure, A.C., Krull, U.J. 1997. Covalent immobilization of single-stranded DNA onto optical fibers using various linkers. Anal. Chim. Acta. 344, 201-213.

Hermanson, G.T., editor. 1995. Bioconjugate Techniques, Academic Press, San Diego, CA.

Hitchcock, A.P., Morin, C., Heng, Y.M., Cornelius, R.M., Brash, J.L. 2002. Towards practical soft X-ray spectromicroscopy of biomaterials. J. Biomater. Sci., Polym. Ed. 13, 919-937.

Hofmann, O., Voirin, G., Niedermann, P., Manz, A. 2002. Three-dimensional microfluidic confinement for efficient sample delivery to biosensor surfaces. Application to immunoassays on planar optical waveguides. Anal. Chem. 74, 5243-5250.

http://www.phy.cuhk.edu.hk/~surface/XPSPEAK/.

Jin, L., Horgan, A., Levicky, R. 2003. Preparation of end-tethered DNA monolayers on siliceous surfaces using heterobifunctional cross-linkers. Langmuir 19, 6968-6975.

Klainer, S.M., Coulter, S.L., Pollina, R.J., Saini, D. 1997. Advances in miniature optical waveguide sensors. Sens. Actuators, B38, 176-182.

Lateef, S.S., Boateng, S., Hartman, T.J., Crot, C.A., Russell, B., Hanley, L. 2002. GRGDSP peptide-bound silicone membranes withstand mechanical flexing in vitro and display enhanced fibroblast adhesion. Biomaterials 23, 3159-3168.

Li, Y., Nath, N., Reichert, W.M. 2003. Parallel comparison of sandwich and direct label assay protocols on cytokine detection protein arrays. Anal. Chem. 75, 5274-5281.

Ligler, F.S., Taitt, C.A.R., editors. 2002a. Optical Biosensors: Present and Future.

Ligler, F.S., Breimer, M., Golden, J.P., Nivens, D.A., Dodson, J.P., Green, T.M., Haders, D.P., Sadik, O.A. 2002b. Integrating waveguide biosensor. Anal. Chem. 74, 713-719.

Lin, C.-W., Lin, J.-C. 2001. Surface characterization and platelet compatibility evaluation of surface-sulfonated chitosan membrane. J. Biomater. Sci., Polym. Ed. 12, 543-557.

Manning, M., Harvey, S., Galvin, P., Redmond, G. 2003. A versatile multi-platform biochip surface attachment chemistry. Mat. Sci. & Eng., C: C23, 347-351.

Manning, M., Redmond, G. 2005. Formation and characterization of DNA microarrays at silicon nitride substrates. Langmuir 21, 395-402.

Marcuse, D. 1974. Theory of dielectric optical waveguides Academic Press, New York.

Matinlinna, J.P., Laajalehto, K., Laiho, T., Kangasniemi, I., Lassila, L.V.J., Vallittu, P.K. 2004. Surface analysis of Co-Cr-Mo alloy and Ti substrates silanized with trialkoxysilanes and silane mixtures. Surf. Interface Anal. 36, 246-253.

May, C.J., Canavan, H.E., Castner, D.G. 2004. Quantitative X-ray Photoelectron Spectroscopy and Time-of-Flight Secondary Ion Mass Spectrometry Characterization of the Components in DNA. Anal. Chem. 76, 1114-1122.

Metzger, S.W., Lochhead, M.J., Grainger, D.W. 2002. Improving performance in protein-based microarrays. IVD Technol. 8, 36-43.

Misiakos, K., Kakabakos, S.E. 1998. A multi-band capillary immunosensor. Biosens. Bioeletron. 13, 825-30.

Nabok, A.V., Starodub, N.F., Ray, A.K., Hassan, A.K. 2000. Registration of immunoglobulin AB/AG reaction with planar polarization interferometer. Proc. SPIE 4200, 1-9.

Plowman, T.E., Saavedra, S.S., Reichert, W.M. 1998. Planar integrated optical methods for examining thin films and their surface adlayers. Biomaterials 19, 341-355.

Plowman, T.E., Durstchi, J.D., Wang, H.K., Christensen, D.A., Herron, J.N., Reichert, W.M. 1999. Multiple-Analyte Fluoroimmunoassay Using an Integrated Optical Waveguide Sensor. Anal. Chem. 71, 4344-4352.

Plueddemann, E.P. 1982. Silane Coupling Agents.

Prieto, F., Sepulveda, B., Calle, A., Llobera, A., Dominguez, C., Abad, A., Montoya, A., Lechuga, L.M. 2003. An integrated optical interferometric nanodevice based on silicon technology for biosensor applications. Nanotechnol. 14, 907-912.

Rezania, A., Johnson, R., Lefkow, A.R., Healy, K.E. 1999. Bioactivation of Metal Oxide Surfaces. 1. Surface Characterization and Cell Response. Langmuir 15, 6931-6939.

Sahu, B.S., Agnihotri, O.P., Jain, S.C., Mertens, R., Kato, I. 2000. Influence of hydrogen on losses in silicon oxynitride planar optical waveguides. Semicon. Sci. Technol. 15, L11-L14.

Seah, M.P., Dench, W.A. 1979. Quantitative electron spectroscopy of surfaces: a standard data base for electron inelastic mean free paths in solids. Surf. Interface Anal. 1, 2-11.

Shibata, Y., Miyazaki, T. 2002. Anode glow discharge plasma treatment enhances calcium phosphate adsorption onto titanium plates. J. Dent. Res. 81, 841-844.

Shriver-Lake, L.C., Donner, B., Edelstein, R., Breslin, K., Bhatia, S.K., Ligler, F.S. 1997. Antibody immobilization using heterobifunctional crosslinkers. Biosens. Bioeletron. 12, 1101-1106.

Tilstone, C. 2003. DNA microarrays: Vital statistics. Nature (London) 424, 610-612.

Trummer, N., Adanyi, N., Varadi, M., Szendroe, I. 2001. Modification of the surface of integrated optical wave-guide sensors for immunosensor applications. Fresn.. J. Anal. Chem. 371, 21-24.

Valette, S. 1988. State of the art of integrated optics technology at LETI for achieving passive optical components. J. Mod. Opt. 35, 993-1005.

Weng, L.T., Poleunis, C., Bertrand, P., Carlier, V., Sclavons, M., Franquinet, P., Legras, R. 1995. Sizing removal and functionalization of the carbon fiber surface studied by combined TOF SIMS and XPS. J. Adhes. Sci. Technol. 9, 859-87.

CHAPTER III

COMPARISON OF HYDROXYLATED PRINT ADDITIVES ON ANTIBODY MICROARRAY PERFORMANCE

This chapter contains the manuscript of a full paper submitted to *Journal of Proteome Research*, formatted according to requirement of *Journal of Proteome Research*. References are formatted in the style set by the American Chemical Society. This manuscript was written by Peng Wu, and edited by David W. Grainger. This chapter describes a study that investigates influences of various hydroxylated printing additives in antibody (anti-human IL-1β, IL-4 and TNFα) microarray performance.

Comparison of hydroxylated print additives on antibody microarray performance

Peng Wu, David W. Grainger

Abstract

Various hydroxylated additives were added to antibody print buffers at different concentrations to stabilize printed antibodies during normal array spot desiccation on commercial polymer-coated microarray slides. Polyvinyl alcohol addition to print buffers produced the most regular spot morphologies, homogenous intra-spot antibody distribution, uniform fluorescence intensity, and improved analyte capture activity, maintained up to 1 month at 4°C for capturing model analytes, anti-human IL-1β, IL-4 and TNFα, on these microarraying slides.

Introduction

Antibody microarrays exploit the surface immobilization of different antibodies into isolated micro-domains as capture reagents for immunoassay [1, 2]. These formats remain of considerable interest to in the fields of proteomics, diagnostics and therapeutics [3]. Many technological issues remain for antibody microarrays to become a quantifiable, reliable technology validated for both diagnostic assay and proteomics use. These include challenges with absolute quantitation, analyte detection limits, assay reliability and reproducibility, antibody batch-batch variance, print conditions, and assay storage variables [4, 5]. Antibody microarrays have the potential to become a new, attractive

characterization method for molecular mixtures at the protein level that DNA microarrays already make possible at the RNA and DNA level [6]. However, as the diagnostic, bioreactor and biosensor fields have shown for decades [7, 8] surface-immobilized globular proteins (e.g., antibodies) have much more complex requirements for stabilizing intrinsically less robust native structures to provide their exquisite assay capture selectivity compared to immobilized nucleic acids (e.g., RNAs and DNAs). Hence, protein-surface interactions remain much more of a critical issue for antibody array performance. Print buffers, print conditions, protocols for antibody surface immobilization, storage routines and assay formats still require optimization and improvements to facilitate acceptance of this technology as a standard quantitative assay [3].

Many possible stresses influence immobilized antibody activity after microarray printing onto solid supports. Evaporation of printing solution (typically droplets originally containing antibody in aqueous media at sub-milligram per milliliter concentrations, dispensed as nanoliter volumes onto surfaces) during and after the printing process causes rapid increases in solute concentrations, ionic strengths, hydration changes of antibodies, pH shifts, and modification of surface energetics as the three-phase (e.g., solid-liquid-air) line moves across the drying proteins spots upon water evaporation. Since the surface energy of pure water is ~72 mN/m at room temperature and only slightly less for salt-containing buffers [9], the immobilized protein species is subject to enormous local forces that can readily dismantle native globular protein structure, reducing antibody bioactivity. Even hydrogel "protein friendly" surfaces do

not appear to be a complete solution for providing the necessary capability to preserve bioactivity and structure of desiccated immobilized proteins [7].

By comparison, bulk proteins are typically carefully lyophilized in attempts to maintain stability over storage periods of many months. However, many analogous stability and reliability problems remain unsolved for these materials as pharmaceuticals [10]. Problems are compounded when globular proteins are printed as thin films on surfaces and then subjected to the same destabilizing drying and interfacial conditions. This scenario really constitutes a 'return to the past' for many protein-surface biophysical chemistry issues that have been well-studied (but nonetheless remain unsolved) in the areas of soluble protein surface adsorption, protein-surface stabilization, and protein denaturation on surfaces. Despite problems, the advantages of surface printing of protein microarray formats include the capability to print many more protein molecules onto a surface than can possibly bind by solution adsorption into that footprint, and the use of surface sorption and rapid evaporation of printed droplet to "force" protein-surface immobilization during spot drying. Evidence is lacking to confirm roles of microarray surface chemistry and its functional reactive group densities in this reaction in the few seconds between liquid spot deposition and drying. Certainly, the non-equilibrium drying dynamics occurring in protein microarray fabrication present unique protein-surface conditions that are not duplicated or studied in previous protein interfacial studies.

Recently, several studies using contact microarray printing for optimizing protein and antibody microarray immobilization, protein assay and storage conditions have been published [11-13]. In one case, five different antibodies were immobilized onto eleven

different array surfaces. Direct label assay using Cy3 or Cy5 fluorescent dye-labeled antigen was used to show that some antibodies are intrinsically more suited for use on antibody arrays than others. Furthermore, it was suggested that antibodies for array use be screened for their suitability in this specific capture application. Importantly, no significant performance or stability differences were shown between immobilized antibody microarrays on non-hydrogel-coated surfaces stored dry at 4°C compared to those stored wet in blocking solution at 4°C. However, hydrogel-coated slides exhibited higher signal intensities in dry conditions, due to loss of coated antibodies into the blocking storage solution under wet storage [11]. Another study systematically compared protein microarrays using direct label versus sandwich immunoassay for parallel detection of five cytokines and growth factors on four different array printing slides. Sandwich format outperformed the corresponding direct label assays in terms of background-subtracted fluorescent intensity, although the extent varied for different slides examined and antibodies capturing cytokines and growth factors [4]. Antibody sourcing and batch-batch variations, intrinsically different affinities against different antigens, and differential effects of surface immobilization on antibody surface capture affinities and stabilities in arrays all present a complex scenario for understanding signal generation in this format.

Hydroxylated additives including trehalose, sucrose, glucose, polyethylene glycol (PEG), and glycerol have all been commonly used as bulk protein cryo- and lyo-protectants, preserving bioactivity during bulk lyophilization processes [14]. Different hypotheses have been proposed to explain the mechanisms of protection by such excipients during the lyophilization cycle, including the (a) vitrification hypothesis [15, 16]

proposing that amorphous protein stabilization can only be achieved if another amorphous compound provides immobilization and spatial separation in a glassy, solid matrix during dehydration; (b) "water replacement hypothesis" [17, 18 19] wherein hydroxylated additives stabilize proteins by hydrogen bonding and other weak forces of attraction to protein polar and charged groups of proteins, replacing the water loss, thus preventing drying-induced protein denaturation; and (c) "preferential hydration" or "preferential binding" concept wherein stabilizing additives are preferentially excluded from the protein surface, leading to an apparent increased protein hydration and improved stability [20, 21]. Different mechanisms may account for specific protein stabilization systems depending on the type of protected proteins, stabilizing additives, and lyophilization conditions. Moreover, a consensus has recently emerged that these mechanisms are not necessarily mutually exclusive [22-24].

Little is yet published that thoroughly investigates effects of additives in applications to antibody microarray performance. One study using direct label assay with Cy3- or Cy5- labeled antigen investigated various factors in the production of antibody microarrays on home-made and commercially available slides [12]. Addition of trehalose into the PBS buffer increased antibody capture activity coupled to several home-made silane glass slides with cross-linkers. Surprisingly, no substantial differences were observed using several different print buffers (carbonate buffer, pH 8.5; PBS buffer, pH 7.4; acetate buffer, pH 5.5; and citrate buffer, pH 4.5) [12]. In another study seeking to improve protein stability in microarrays on commercial aldehyde-coated glass slides [13], additives including trehalose, sucrose, glycerol and PEG (mol. wt. 200) were added to PBS print buffer. PEG (mol. wt. 200, 30% w/v) greatly improved printed streptavidin

stability and activity, whereas trehalose, sucrose and glycerol showed no improvement or even decreased activity compared to PBS buffer without any additive. Improved capture performance using PEG (mol. wt. 200) was explained by reduced water evaporation rates of printed microarray spots and preferential hydration and hydrophobic interactions between PEG and streptavidin in spots on surfaces [13]. In several other microarray contact printing studies, relatively high percent (20 ~ 50%) glycerol has been added to protein microarray print buffers to inhibit nanoliter droplet evaporation [25, 26]. However, printing with such high concentrations of additives produces print problems including pin clogging during protein spotting, high spot background and spot smearing, especially in high viscosity solutions (e.g., with 20~ 50% glycerol additives). Additive adsorption on the interior walls of contact print pins increases the well-known "carry-over effect" (e.g., residual print solution carried into the next print sample reservoir, even if these pins are repeatedly rinsed and dried between prints).

Mechanisms of protein stabilization by hydroxylated additives in microarray printing/drying cannot be simply extrapolated from bulk protein stabilizing hypotheses invoked for bulk protein lyophilization or spray drying process due to numerous, complex interactions between proteins and array surfaces. Microarray printing process variables, including substrate surface characteristics (e.g., surface hydrophilicity, surface chemistry, polymer layer thickness, density), different print conditions (e.g., antibody sources, print buffers, print chamber humidity, non-contact versus contact printing, contact pressure between spotting pins and slide surfaces) will produce different spot morphologies, homogeneities and immobilized protein densities, and, therefore, different

distributions of protein and stabilizing additives in spots on surfaces, leading to different local stabilizing environments.

In this study, several soluble hydroxylated additives were analyzed in contact-printed protein microarrays. Three common cytokines were selected as model analytes and assayed using a sandwich assay format on two commercially available amine-reactive microarraying slides. Over the past decade, cytokine detection has been an increasing bioassay focus. Regulation of cytokine production is involved in the pathogenesis of various diseases, and in trauma and healing. Rapid, reliable, multi-plexed determination of cytokine levels is therefore of increasing diagnostic importance [27, 28]. Print-immobilized microarrays were stored dry at 4°C to investigate antibody activity after 1 month. Effects of covalent binding and physisorption upon spot drying between printed antibodies and reactive groups on microarraying slide surfaces were also studied.

Experimental Methods

Commercially sourced, printed capture antibodies and secondary biotinylated sandwich antibodies used in all experiments are listed in Table 1. Antibodies, recombinant human IL-1β (mol. wt. 17 kDa), TNFα (mol. wt. 17.4 kDa) and IL-4 (mol. wt. 14 kDa) cytokine analytes (Pierce, Rockford, IL), streptavidin-Alexa Fluor® 647 conjugate, Alexa Fluor® 555-goat anti-mouse IgG and biotinylated goat anti-mouse IgG (Molecular Probes, Eugene, OR) were aliquoted immediately after receipt according to manufacture's recommendations and stored frozen at -70°C.

Table 1. Vendors and sources of assay capture antibodies

	Supplier	Source
Anti-human IL-4 (1° capture)	R&D Systems (Minneapolis, MN)	Monoclonal, Mouse
Anti-human IL-4 (2° biotinylated)	R&D Systems (Minneapolis, MN)	Polyclonal, Goat
Anti-human IL-1β (1° capture)	R&D Systems (Minneapolis, MN)	Monoclonal, Mouse
	Pierce (Rockford, IL)	Monoclonal, Mouse
Anti-human IL-1β (2° biotinylated)	R&D Systems (Minneapolis, MN)	Polyclonal, Goat
	Pierce (Rockford, IL)	Monoclonal, Mouse
Anti-human TNFα (1° capture)	R&D Systems (Minneapolis, MN)	Monoclonal, Mouse
	Pierce (Rockford, IL)	Monoclonal, Mouse
Anti-human TNFα (2° biotinylated)	R&D Systems (Minneapolis, MN)	Polyclonal, Goat
	Pierce (Rockford, IL)	Monoclonal, Mouse

Antibody Array Printing

Antibodies were printed onto two commercial arraying slide surfaces, Optarray™ (Accelr8 Technologies, Denver, CO) and Codelink™ (Amersham, Piscataway, NJ). Both slides are amine-reactive, three-dimensional hydrogel-type coated glass slides[29] (not monolayer silane chemistries) according to their respective product literature. Additives including polyethylene glycol (PEG, mol.wt. of 150, 750, 2000 and 6000, J.T.Baker Chemical Co., Phillipsburg, NJ), polyvinyl alcohol (PVA, mol.wt. 9000-10000, Aldrich, Milwaukee, WI) trehalose (Sigma, St Louis, MO), D-glucose and sucrose (Fisher

Scientific, Fair Lawn, NJ) are added in different concentrations to base print buffer containing 0.25M Na_3PO_4, 0.005% Tween 20, and 0.05M NaCl (pH = 7.5). Capture antibody concentration is 100 ~ 200 μg/ml. A SpotBot® Personal Microarrayer (TeleChem International, Inc., Sunnyvale, CA) and quill pins SMP6 (spot diameter 200 μm, delivery volume 1.8 nl, TeleChem International, Inc., Sunnyvale, CA) are used in this experiment to contact-print antibodies onto both commercial slide formats. Relative humidity of 65 ~70 % is maintained throughout the printing process. Printed biotinylated goat anti-mouse IgG was chosen as a printed capture positive control because of its direct interactions with the streptavidin-Alexa Fluor® 647 sandwich fluorescent label without significant concern about lost printed antibody bioactivity influencing fluorescence signal in the Cy5 channel (e.g., capture is only biotin-streptavidin, not antibody binding site mediated). Buffer lacking any capture antibody served as a negative printed control. Stable surface immobilization was attempted by storing printed microarray slides under nitrogen overnight at 4°C. Thereafter, residual amine-reactive groups on printed microarray slides were blocked using ethanolamine (1:500 v/v) in 50 mM sodium borate buffer (pH = 9.1). Slides were then rinsed with PBS and Millipore water, and finally dried under nitrogen. These microarray slides were then applied to anti-human cytokine sandwich immunoassay. For longer period storage periods, slides were stored sealed under nitrogen at 4°C after blocking, rinse and drying with nitrogen.

To investigate the importance of covalent binding in printed antibody microarray immobilization, both amine-reactive microarraying polymer surfaces (OptArray™ and Codelink™ slides) were first blocked using ethanolamine (1:500 v/v) in 50 mM sodium borate buffer (pH=9.1) before identical microarray printing. These pre-blocked slides

were then compared with slides printed without pre-blocking using anti-human cytokine sandwich assays.

Microscope imaging of printed microarray spot morphology

A Nikon Eclipse TE 2000-U microscope (equipped with Plan Fluor ELWD 40 X Nikon objective) is used to observe printed microarray spots on commercial microarraying slides. Differential interference contrast (DIC) mode is used to observe printed, dried microarray spots. Images were taken on printed microarray slides stored under nitrogen overnight at 4°C before blocking and rinsing.

Anti-human cytokine sandwich immunoassay

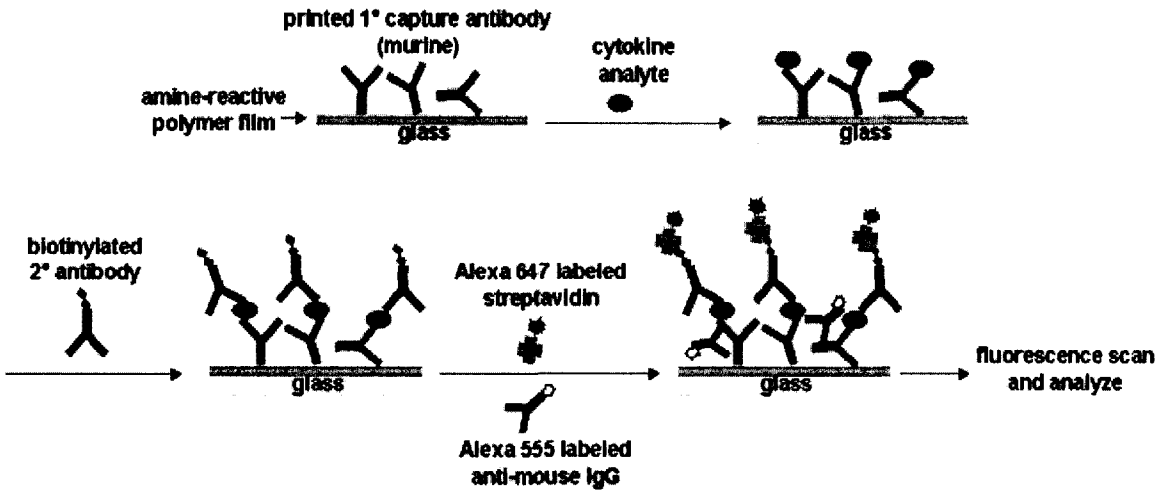

Figure 1. Anti-human cytokine sandwich immunoassay scheme

Human IL-1β, a clinically relevant inflammatory cytokine, was assayed using a sandwich immunoassay format with array-printed anti-human IL-1β antibodies on solid supports [4, 30] (Figure 1). Recombinant human IL-1β model analyte was diluted in incubation buffer (PBS buffer, pH =7.5 + 0.05 % (v/v) Tween20 + 0.1 % (w/v) BSA) at

20 pg/ml to 20 ng/ml and incubated on-array for 1.5 ~ 2 hours using CoverWell™ perfusion chambers (Grace Bio-Labs, Inc., Bend, OR) under 100% humidity. Slides were then rinsed with PBST (PBS buffer + 0.01% (v/v) Tween20, pH = 7.5) and water, then dried with nitrogen. Biotinylated secondary anti-human IL-1β (biotin) was diluted to ~6.6 μg/ml in incubation buffer solution from 1 mg/ml frozen stock and incubated on-array for 1 hour. After repeated rinsing with PBST /water and drying with nitrogen, arrays were finally incubated for 30 minutes with streptavidin-Alexa Fluor® 647 conjugate (5 μg/ml) and Alexa Fluor® 555-goat anti-mouse IgG (5 μg/ml) together in incubation buffer. Alexa Fluor® 555-conjugated goat anti-mouse IgG was used to verify surface loading of printed capture antibody, whereas Alexa Fluor® 647-conjugated streptavidin was used to verify bioactivity of printed capture antibody for sandwich assay capture of cytokine analyte. Human TNFα and IL-4 analytes were assayed in the same format with corresponding array-printed capture antibodies and biotinylated secondary antibodies. To investigate assay specificity, anti-human TNFα was used as a negative printed control for human IL-1β assay, whereas anti-human IL-1β was used as a negative control for human TNFα and human IL-4 assays.

Microarray fluorescence detection and image processing

All substrates were imaged using a Perkin Elmer ScanArray Express™ Microarray Scanner with two selectable lasers with wavelengths 543 nm (Cy3 channel) and 633 nm (Cy5 channel). Resolution was set to 5 microns, and power and gain settings were fixed for all scanning measurements. All microarray scanned fluorescence images were processed with ScanArray Express™ software. Intensities (mean intensity of the

spot minus off-spot background) from spotted replicates (n = 5) were averaged and standard deviations calculated. Altogether, data from more than 100 microarrays and 30 individual experiments were considered. Although fluorescence intensity varies between individual experiments, and different batches of printed slides, the data trends are all very similar, with representative data shown.

Results and Discussion

Antibody microarray spot morphology

During microarray printing, nanoliter droplets were delivered from pins onto microarraying slides. Even in the 65%~70% relative humidity chamber, evaporation of this droplet occurs within a few seconds, rapidly depositing an aggregated protein film on the substrate surface. Microscope images were compared in parallel with fluorescence-scanned images of antibody microarray spots (Figure 2). For each sample, the left image in Fig. 2 is the CCD image from DIC microscopy mode before blocking and rinse, and the right image is the fluorescence scan (Cy3 channel after capture assay). This Cy3 channel signal shows fluorescence from the Alexa Fluor® 555 goat anti-mouse IgG, which directly binds to all printed murine capture antibodies, allowing direct examination of capture antibody printing loads. Phase contrast microscopy was also used to capture high contrast spot images, producing similar images on these microarray spots as DIC but with slightly higher contrast in DIC modes (hence, these images are not shown in Figure 2). Direct comparison of these images side by side provides important new information about distributions of printed antibodies, hydroxylated additives, and salt contents in the print buffer remaining after rapid evaporation. These dry spots are about 100 - 200

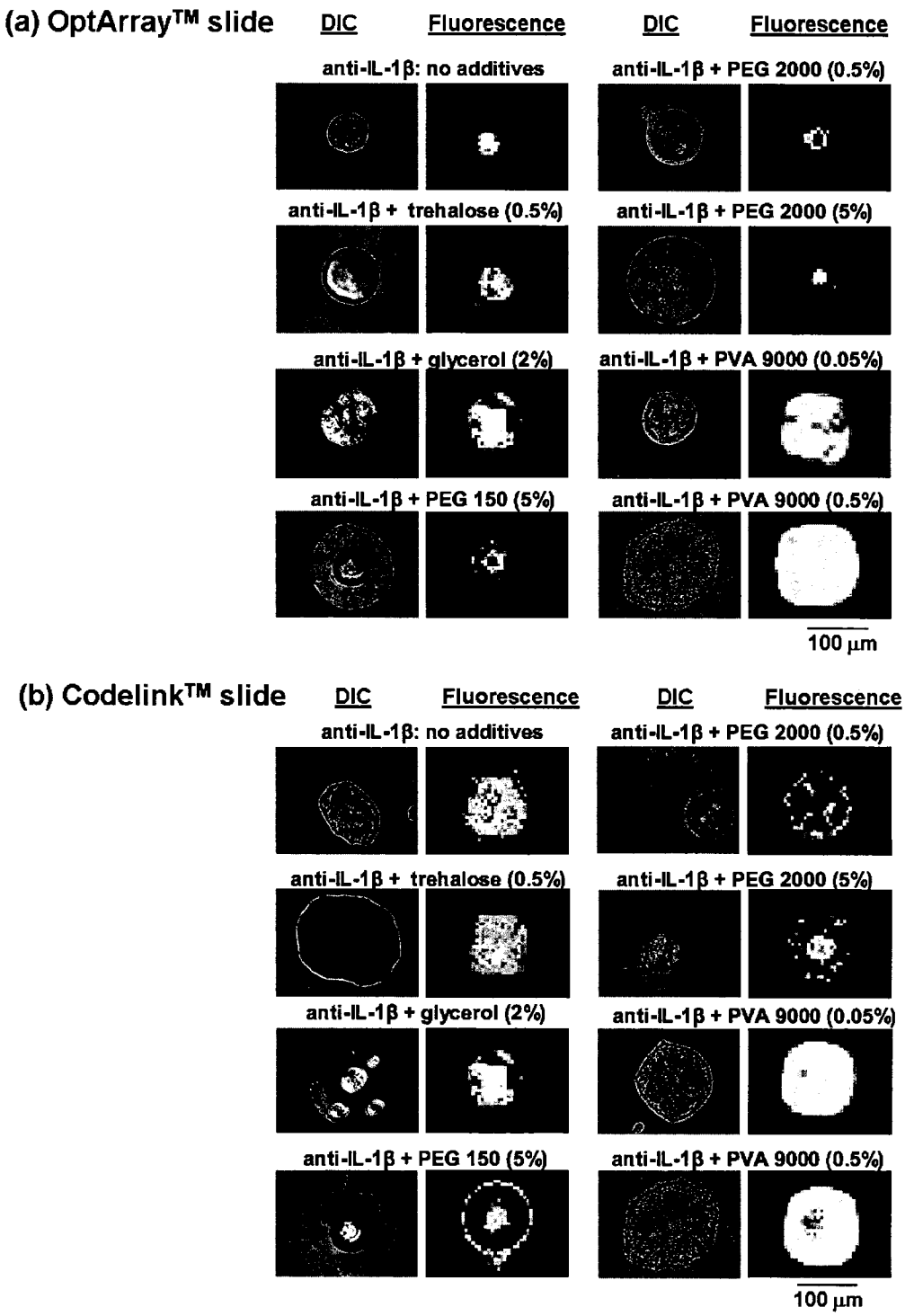

Figure 2. Digital microscope images of printed microarray spots (before blocking, rinse and protein analyte assay) under differential interference contrast (DIC) microscopy, and fluorescence scanned images of printed microarray spots after rinse and sandwich assays. For each sample, two images were taken (left: DIC image; right: fluorescence image). Images for the same sample were not taken on the same spot, but these images were representative of antibody samples printed with different additives.

microns in diameter, while the resolution of the fluorescence scan is 5 microns. Fluorescence signal in Figure 2 represents presence of capture antibodies on the surface. Although little quantitative information about thickness, or surface density of capture antibodies can be derived from these fluorescence images, rough distributions of capture antibodies within spots are clearly observable. As assessed from fluorescence images in Fig. 2, adding PVA (mol.wt. 9000, 0.5% and 0.05% w/v) to print buffer produces the most homogenous capture antibody distribution, with regular round spot morphologies and smallest variance from spot to spot. Figure 2 DIC images show that PVA facilitates evenly spread films on the surface with homogenous capture antibody mass within this film. By contrast, adding PEG (mol. wt. 150 and 2000, 5% w/v and 0.5% w/v) to print buffer produced double–ring (donut) fluorescence images on Codelink™ slides (bright fluorescence signal at both spot center and outer edge, but very low signals in other areas), and only bright fluorescence signals at the very spot center on OptArray™ slides. This fluorescence distribution pattern is also related to the drying patterns observed in corresponding DIC microscope images. At the outer edges of spots on OptArray™ slides, most visible are salt particles from the print buffer: no signal is observed at these outer edges in the corresponding fluorescence images. On Codelink™ slides, fluorescence signals concentrated at outer edges of microarray spots are attributed to antibodies at the outer edge of the spot usually caused by common "coffee-spot" drying effects [31]– rapid drying causing spotting solution (including antibodies) to wick and dry to the outer edge of the spot during the printing process. This typically occurs when the humidity in the microarray printing chamber is relatively low [32]. However, here, microarray printing is controlled to 65 ~70% humidity, so "donut shapes" are not

observed when printing with print buffer lacking hydroxylation additives. Fluorescence signals at the outer edges of PEG/antibody printed spots exhibited only on Codelink™ but not on OptArray™ slides are partially due to PEG additives, and partially due to higher hydrophilicity of Codelink™ polymer surface [29], causing the spotting solution to spread to outer spot edges faster, producing double-ring patterned fluorescence images. Generally, larger diameter spots are observed on Codelink™ than on OptArray™ slides. On both slides, PEG addition confines antibody molecules near the spot center, producing high spot-spot and array-array spot morphology and fluorescence intensity variations (Figure 2). Adding trehalose and glycerol to print buffer seems to induce formation of glassy amorphous spots (adding glucose or sucrose produced similar images as adding trehalose, images not shown). However, from corresponding fluorescence images (Figure 2) antibody distributions in these spots are not as homogeneous as in spots printed with PVA additives.

Comparison of hydroxylated additives on capture activity

Quantified fluorescence intensity from streptavidin-Alexa Fluor® 647 (Cy5 channel) indicated a relative analyte capture bioactivity in sandwich assays of capture antibodies printed with different hydroxylated additives. As shown in Figure 3, adding PVA (0.5% and 5%) to print buffer produced the highest capture antibody bioactivity observed (anti-human IL-1β, TNFα and IL-4) on both OptArray™ and Codelink™ slides. Adding glycerol (2% v/v) also improved antibody capture activity, especially on OptArray™ slides. Further experiments (see below) showed that adding glycerol (2% v/v) to print buffer produces false positive signals on OptArray™ slides (Figure 4).

(a)

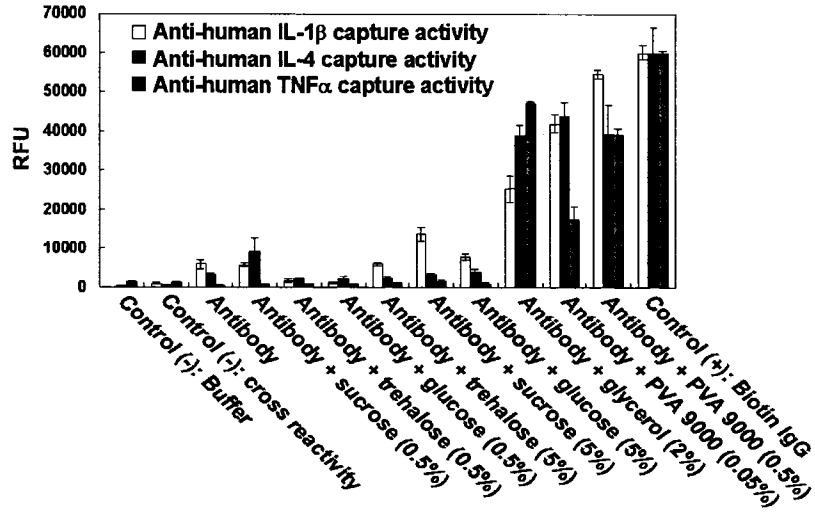

(b)

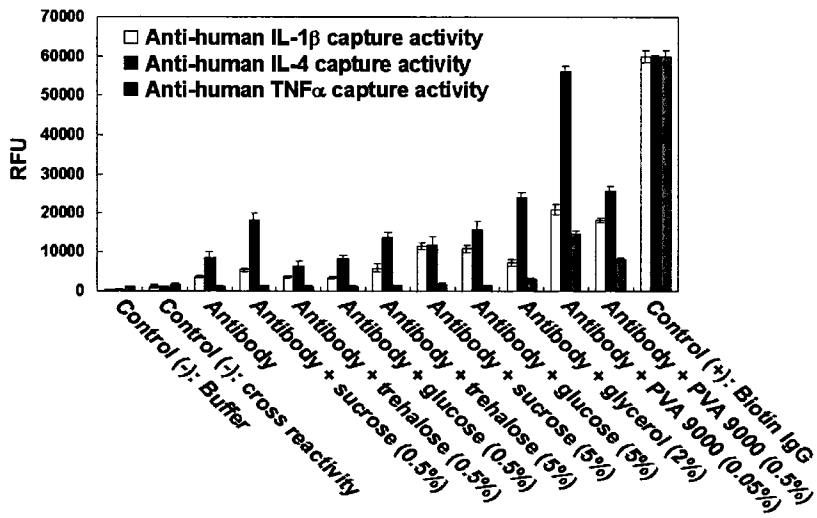

Figure 3. Quantified streptavidin-Alexa Fluor® 647 fluorescence intensity (Cy5 scanner channel) representing activity of printed anti-human cytokine antibodies in sandwich assay. Anti-human IL-1β (100 μg/ml printed concentration), anti-human IL-4 (200 μg/ml printed conc.) and anti-human TNFα (200 μg/ml printed conc.) were printed into three individual microarrays on **(a)** OptArray™ and **(b)** Codelink™ polymer microarray surfaces with different print buffer additives. Relative fluorescence intensities (RFU) of positive control (printed biotinylated non-specific IgG) in each microarray were normalized to the same RFU value (60,000). RFU signals of anti-human cytokine samples were then normalized to positive controls, marked (+), in each microarray. Two negative controls, marked (-) were used in these experiments: (1) pure buffer, and (2) cross reactivity controls: anti-human IL-1β secondary antibody applied to anti-human IL-4 and anti-human TNFα primary microarrays; and anti-human TNFα secondary antibody applied to anti-human IL-1β primary microarrays (n = 5 spots). (+) = positive control; (-) = negative control.

Surprisingly, trehalose, with its reputation as an exceptional protein stabilizer [33-35], did not exhibit much improved antibody capture activity compared to antibodies printed without any additive. Similar performance was observed for glucose and sucrose. These observations are consistent with the study by Lee et al. [13] but differ with results from Kusnezow et al. [12]. However, even in the latter study, increases in bioactivity (from ~ 30% to ~ 150% increases) using trehalose are different on different microarray substrates. The printing surface plays an important role in microarray spotting and immobilization, producing different spot morphologies, sizes, immobilized densities and stabilizing effects from hydroxylated additives.

Amounts of antibodies or proteins in printed nanoliter droplets for microarray spots (~ 10^{-15} mole) are much more than that required for an immobilized antibody/protein monolayer. After complete evaporation in a few seconds following spotting, stacked, aggregated multi-layers of antibody/protein form into each microarray spot. The drying is a non-equilibrium event: antibody concentration rapidly increases from μg/ml ~ mg/ml to saturation in seconds, producing irreversible protein aggregation. There is no control over either deposited thickness or antibody immobilization orientation. Dried antibodies adsorb onto surfaces in any orientation through multi-point contacts by mixtures of covalent bonds, hydrogen bonds, electrostatic or other physical interactions. Rapid spot drying onto the surface promotes irreversible surface adhesion of printed proteins,[36], resulting from protein denaturation, aggregation and conformational changes in drying proteins on all surfaces. During blocking steps, loosely attached proteins are washed away from the surface, with only strongly adsorbed antibody multilayers remaining both in the presence and absence of covalently reactive

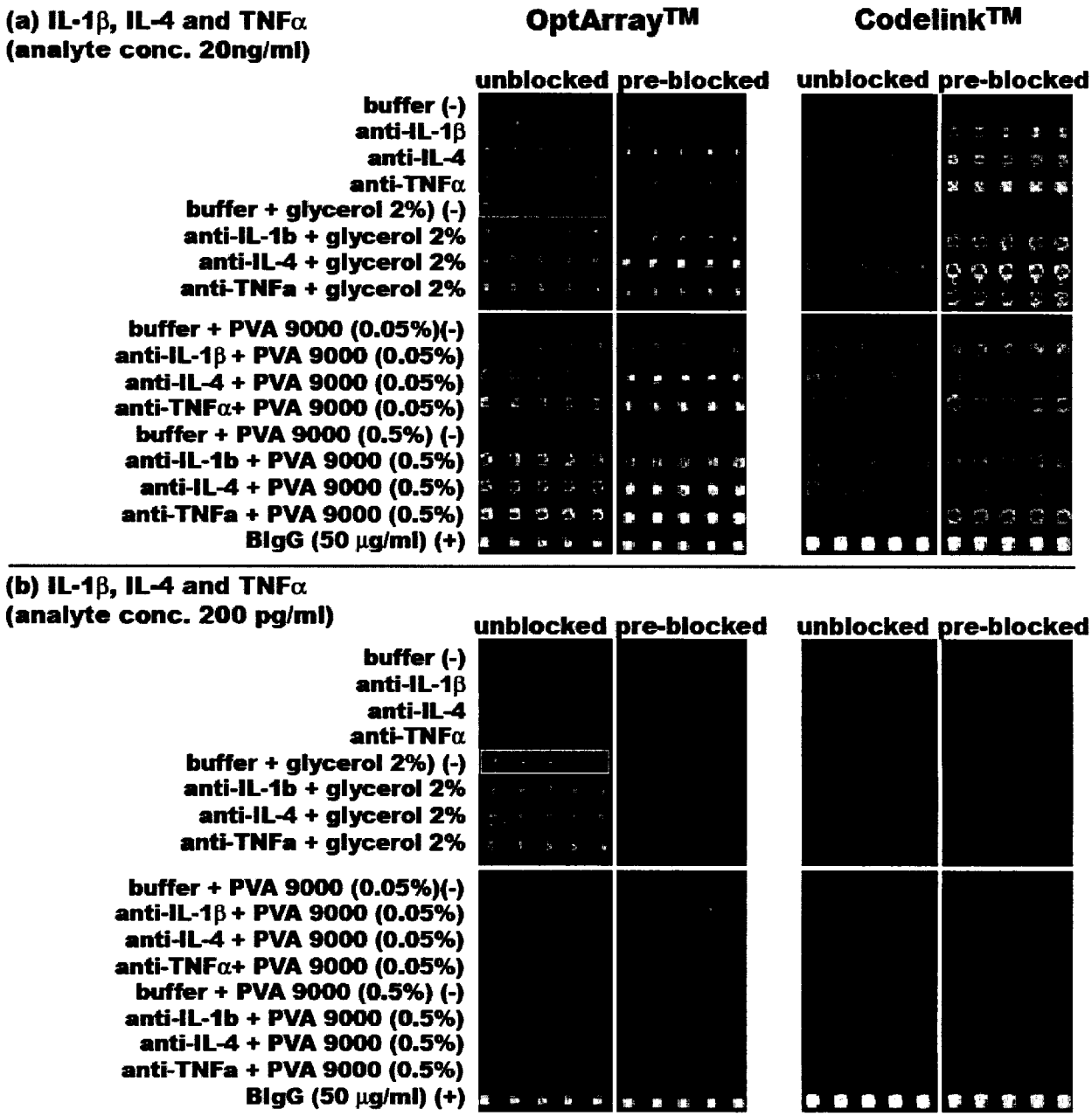

Figure 4. Array fluorescence scanned images (Cy5 scanner channel) showing analyte capture activity for anti-human IL-1β (100 μg/ml printed concentration), anti-human IL-4 (200 μg/ml printed conc.) and anti-human TNFα (200 μg/ml printed conc.) printed with glycerol, PVA , and without any additives on both amine-reactive OptArray™ and Codelink™ array slides (both unblocked and pre-blocked with ethanolamine) in cytokine analyte sandwich assays. Serial cytokine analyte concentrations 20 ng/ml, 2 ng/ml, 200 pg/ml and 20 pg/ml concentrations (descending order) were used in sandwich assays. For clarity, fluorescence scanned images of only **(a)** 20 ng/ml and **(b)** 200 pg/ml are shown. (+) = positive control; (-) = negative control.

surface groups [36]. Final antibody print densities, amounts, and fractional bioactivities post-print are largely unreported.

Adding PVA produced the most homogenous antibody printed distribution, and largest diameter spots on both OptArray™ and Codelink™ slides. Antibody/PVA mixtures are evenly distributed across microarray spots, meaning less antibody aggregation, and improved availability of antibody binding domains for analyte capture in sandwich assays. These effects are attributed to several properties, including PVA surfactancy that promotes droplet-surface spreading, uniform wetting and contribution to protein drying [37-39]. Several studies have shown that freeze-drying processes produce more extensive protein structural changes than that of dehydration at ambient temperature [40-43]. The latter does not necessarily result in large changes in protein structure, such as unfolding, although some secondary structural or conformational distortions can occur [40, 44, 45]. Beyond just the removal of water directly associated with the protein, freeze-drying provides extra mechanisms for denaturation or large distortions of protein structure. These mechanisms including "cold denaturation" processes (the temperature of a protein sample during freeze-drying might approach the cold denaturation temperature, see review [40]), and pH or ionic strength changes as the solution components are concentrated.

It seems reasonable to suggest, therefore, that protein/antibody unfolding and large structural or conformational changes, if any, in microarray printing process are not due to dehydration, but to other extra stresses/mechanisms such as sudden ionic strength and pH shifts, and interplay with surface energetics (*vida infra*). So, thermodynamic (water replacement) or dynamic protecting mechanisms (e.g., vitrification hypothesis) [46] of traditional freeze-drying lyoprotectants such as trehalose, sucrose and other sugar

molecules do not likely apply in microarray printing processes at ambient temperature. In contrast, if proteins/antibodies do not unfold or exhibit structural changes from the microarray printing process, the observed low bioactivities of capture antibodies are probably contributed by protein aggregation and misoriented binding domains that are unable to bind target analytes in solutions. PVA apparently can improve antibody capture activity through improved distribution of antibodies/PVA mixtures in microarray spots. Additionally, unlike sugar additives, PVA decreases aqueous surface tension and is well-known as both a colloid protective agent [37, 39] and stabilizing agent in spray-dried protein particles [38]. It is possible that the PVA, as a polymeric surfactant, preferentially adsorbs to droplet surfaces, displacing protein from the surface [38], and reducing local stress on proteins from surface energetics during solution evaporation. In summary, no additives are as effective as PVA in promoting preferential antibody distribution and immobilization on these surfaces. Beyond PVA and glycerol, none significantly improve antibody binding activity in analyte capture assays.

Covalent antibody immobilization in microarray printing

The role of covalent binding in antibody spotting and immobilization in microarray contact printing was assessed by comparing capture antibody activities printed on both normally amine-reactive and non-reactive slides (slides pre-blocked with ethanolamine). Capture antibodies were printed using print buffer lacking any additive, or with either PVA or glycerol. As shown in Figure 3, these two additives provided the best performance among all hydroxylated additives tested in stabilizing dried spotted antibodies and maintaining their bioactivity in sandwich assays. Background fluorescence intensity from additives was assessed using corresponding print buffers

lacking antibody as negative controls: buffer, buffer + glycerol (2%), buffer + PVA (0.5%), buffer + PVA (0.05%). Serial dilutions (20 ng/ml, 2 ng/ml, 200 pg/ml, 20 pg/ml) of cytokine analytes (recombinant human IL-1β, TNFα and IL-4) were probed in sandwich assays and scanned images for 20 ng/ml and 200 pg/ml are shown in Figure 4 (complete scanned images were shown in supplemental data). Negative controls containing buffer + glycerol (2%) shown in Figure 4's white box exhibit a strong false positive fluorescence signal (Cy5 channel) on amine-reactive OptArray™ slides. Unlabeled capture antibodies printed with glycerol (2%) additives showed similar fluorescence intensities in sandwich assays for both 20 ng/ml and 200 pg/ml cytokine analyte concentrations, whereas fluorescence intensity signals (Cy5 channel) for assays using antibodies printed with PVA (0.5% and 0.05%) additives, or printed without any additive, correspond to respective analyte concentrations. High fluorescence intensities (Cy5 channel) on OptArray™ slides are attributed to glycerol autofluorescence after drying on this chemistry, not from printed capture antibodies. Buffer control and antibodies printed with glycerol (2%) additives on pre-blocked deactivated OptArray™, amine-reactive Codelink™, and pre-blocked Codelink™ slides showed no such false positive signals.

Interestingly, as shown in Figures 4 and 5, deactivating amine-reactive groups on both OptArray™ and Codelink™ surface with ethanolamine before microarray printing did not substantially alter fluorescence intensities in Cy3 and Cy5 detection channels on pre-blocked slides compared to unblocked amine-reactive slides (Cy3 fluorescence images shown in supplement data). Even stronger analyte fluorescence signal was observed on pre-blocked antibody-printed slides, representing similar or even improved

antibody printing/immobilization and analyte capture activity without surface covalent reaction. Amine-reactive covalent binding is therefore not a distinguishing performance feature in this particular microarray contact printing system. Antibodies are seemingly immobilized onto these commercial array surfaces primarily through drying, by antibody-antibody aggregation and physisorption interactions including hydrogen bonding, electrostatic interactions and van der Waals forces. This result is consistent with that with proteins printed on Codelink™ slides in a previous study [36]. Antibodies are basically dried down onto substrate surfaces. Many possible forces can be involved in this immobilization process. Small contributions from covalent binding between antibody lysine amine groups and amine-reactive commercial slide chemistries are masked by many physical interactions produced by rapid spot drying.

In Figure 5, fluorescence intensities (Cy5 channel) were quantified for capture antibodies printed without any print additive versus with PVA (5%), and plotted against cytokine analyte concentration. On unblocked amine-reactive OptArray™ and Codelink™ slides, adding PVA (5%) to print buffer outperformed print buffer without any additive in capture activity for all three tested capture antibodies. This is consistent with capture activity data in Figure 3. For the identical sample (same antibody printed with same additive), capture antibodies printed on deactivated pre-blocked slides show improved analyte capture activities over those printed on unblocked activated slides. This is more apparent on Codelink™ slides, with the highest analyte capture signal obtained from antibodies printed without any additive on deactivated pre-blocked slides. For antibodies printed with the same additive, this improved bioactivity is directly related to increased capture antibody immobilization density witnessed on pre-blocked slides, as

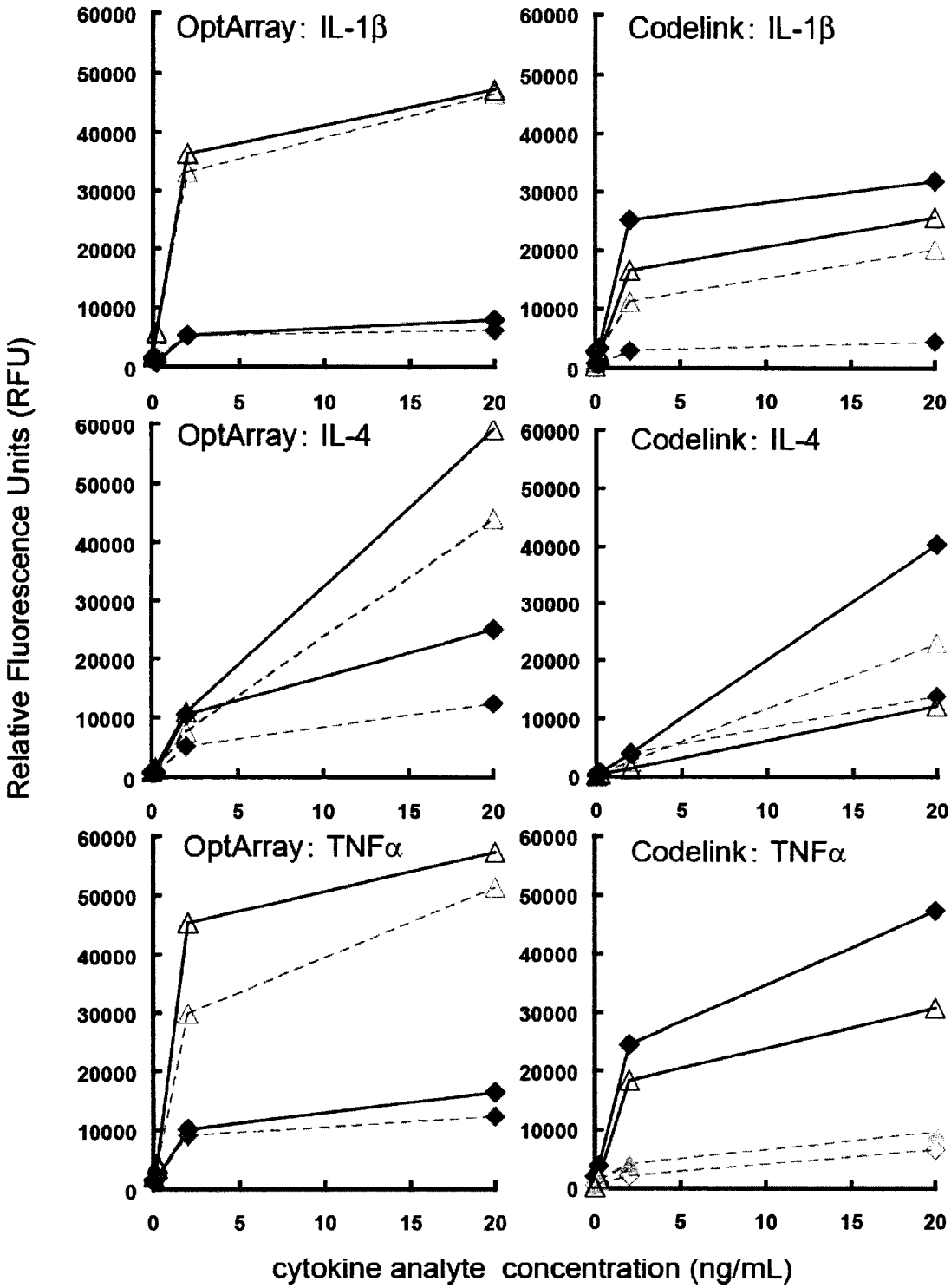

Figure 5. Quantified streptavidin-Alexa Fluor® 647 fluorescence intensities (Cy5 scanner channel) for cytokine analyte capture in antibody sandwich assays shown in Figure 4, showing activity of anti-human cytokines printed without any additive, or with PVA (M.W. 9000, 0.5%) on both OptArray™ and Codelink™ array slides as a function of cytokine analyte concentration. (Δ: antibody + PVA(0.5%) on pre-blocked slides; △: antibody + PVA (0.5) on amine-reactive slides; ◆: antibody on pre-blocked slides; ◆: antibody on amine-reactive slides. n = 5 spots; error bars/standard variation smaller than graph symbols.

exhibited by antibody printed fluorescence intensity (Cy3 fluorescence images shown in supplementary data). Covalent ethanolamine blocking prior to microarray printing not only consumes amine-reactive chemistry on slide substrate surfaces, but also produces hydroxyl groups (i.e., primary amine nucleophilicity is several orders higher than hydroxyl reactivity). This change in surface chemistry produces new interactions between surfaces and capture antibodies, resulting in increased capture antibody immobilization and binding activity on pre-blocked slides versus unblocked slides. Furthermore, different surface chemistry also results in different influences on PVA-surface and PVA-protein interactions.

Assay detection limits (defined as 3 times the fluorescence intensity of corresponding print buffer background) are approximately 200 pg/ml for IL-4, and near 20 ng/ml for IL-1β and TNFα. Linear response ranges for the assays are 200 pg/ml ~ 20 ng/ml for IL-4, and 20 pg/ml ~ 2 ng/ml for IL-1β and TNFα (Figure 5). Different capture antibodies and secondary antibodies have widely varying binding efficiencies to respective analytes, producing different response ranges and detection limits in microarray formats. These differences are manifested in differential signals characteristic of each printed antibody, where assay signals do not represent absolute analyte abundance, but a combination of relative abundance, printed, dried antibody density, dried antibody efficiency, and resulting affinity for analyte capture.

Printed antibody microarray shelf life

Storing printed antibody microarray slides is an important and necessary process in practical microarray utilization. The ability to reliably maintain antibody activity on

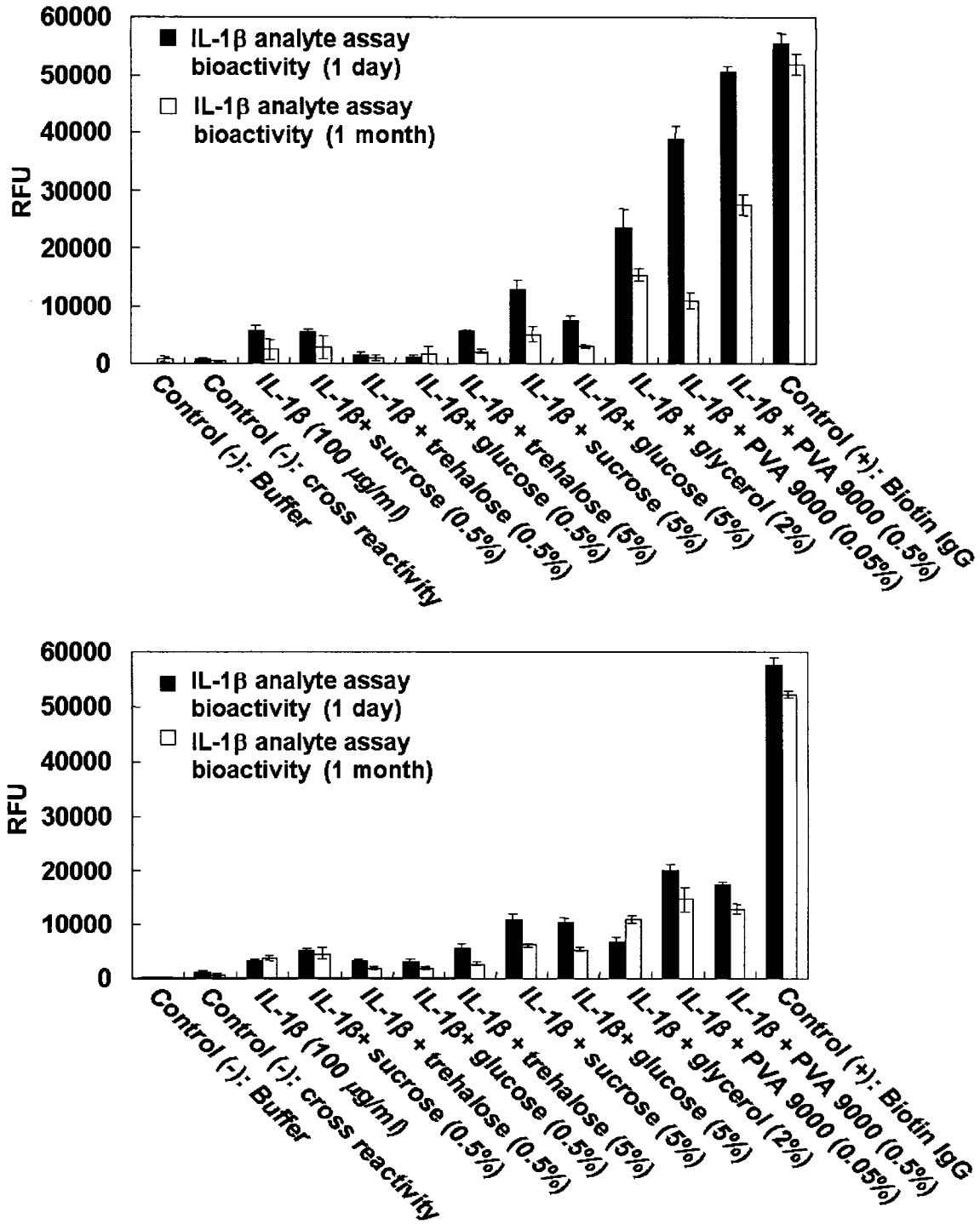

Figure 6. Quantified streptavidin-Alexa Fluor® 647 fluorescence intensity showing activity of printed anti-human IL-1β on **(a)** OptArray™ and **(b)** Codelink™ array slides after 1 day and 1 month storage dry under nitrogen at 4°C, with different print buffer additives (labeled as IL-1β + different additives) in cytokine sandwich assays (n = 5 spots). (+) = positive control; (-) = negative control.

microarray slides under storage is therefore an essential performance element for both microarray manufacturer and user. Pre-printed commercial formats are generally stored dry until shipped and used; wet storage presents numerous practical issues. Printed antibody microarray slides stored in wet conditions (blocking solutions, protein stabilizing additives) could compromise antibody immobilization. Antibodies adsorbed only through physical interaction (shown here to be significant) could desorb and diffuse into storage solutions over time [11]. Dry storage conditions at 4°C have been reported by several previous studies [11, 12]. Printed antibody microarrays (anti-human IL-1β microarray data shown in Figure 6) were therefore stored at 4°C, and sealed under nitrogen for 1 month. After this period, slides were brought to room temperature and assayed. Quantified fluorescence signal (Cy5 channel data) was compared to microarray slides printed at the same time, but assayed after only overnight storage under the same conditions. Figure 6 shows that capture activities for antibodies printed both with all hydroxylated additives and without any additives all decreased after 1-month storage. With PVA additives, capture activity after storage remains at reasonable levels, higher than capture activities of antibodies printed with most other additives or without any additive at day 1.

Conclusions

Analyte capture capabilities for printed, desiccated anti-human IL-1β, IL-4 and TNFα antibody microarrays on two commercial amine-reactive polymer slides were improved by addition of PVA (mol. wt. 9000, 0.05 ~ 0.5%) to the print buffer. PVA demonstrated the best performance among several hydroxylated additives in terms of

spotted antibody distribution homogeneity, uniform microspot morphology, immobilized antibody bioactivity, and spot-to-spot variance. PVA also maintained antibody capture activity reasonably well after 1-month storage under dry conditions at 4°C. Ideally, the capture antibody should form a bound, bioactive monolayer in each microarray spot, with retention of full analyte selectivity, capture bioactivity and lack of cross-reactivity. However, the influence of multiple factors including varying surface chemistry, printing conditions, different antibody sources and analyte affinities, assay conditions and printing durability, makes realization of universal optimized printing and assay parameters applicable to all capture antibodies on all arraying surfaces likely impossible.

Antibody microarray assays have significant reliability and metric challenges. Considerable variability in antibody sourcing and intrinsic array stability, variable printing behavior including surface loading, intra-spot antibody distribution in microarray spots, spot homogeneity, immobilized antibody reproducibility, fiduciary markers or on-array calibrating standards, low print variance, and antibody desiccation issues all require resolution for improved array performance. Without improved antibody printing/immobilization strategies on surfaces, hydroxylated print additives contribute only marginally to improve analyte capture activities of printed antibodies. Physisorption, not covalent immobilization, dominates antibody-surface printing interactions on two commercial polymer arraying slides, forced by rapid array spot desiccation. Under these common print conditions and storage, antibody covalent attachment is not a reliable parameter in contact microarray print stability and array performance.

Acknowledgements

The authors acknowledge support from NIH grant EB00726. Gift of OptArray™ slides from Accelr8 (Denver, CO), and technical guidance and reproducible spotting protocols from Dr. C. Greef (Accelr8) are gratefully acknowledged.

References

(1) Haab, B. B. *Proteomics* **2003**, *3*, 2116-2122.

(2) Templin, M. F.; Stoll, D.; Schwenk, J. M.; Potz, O.; Kramer, S.; Joos, T. O. *Proteomics* **2003**, *3*, 2155-2166.

(3) Glokler, J.; Angenendt, P. *J Chromatogr B Analyt Technol Biomed Life Sci* **2003**, *797*, 229-240.

(4) Li, Y.; Nath, N.; Reichert, W. M. *Anal. Chem.* **2003**, *75*, 5274-5281.

(5) McQuain Mark, K.; Seale, K.; Peek, J.; Levy, S.; Haselton Frederick, R. *Anal. Biochem.*, *320*, 281-291.

(6) Kusnezow, W.; Hoheisel Jorg, D. *BioTechniques* **2002**, *Suppl*, 14-23.

(7) Reichert, W. M.; Blawas, A. S. *Biomaterials* **1998**, *19*, 595-609.

(8) Zhu, H.; Snyder, M. *Curr Opin Chem Biol* **2001**, *5*, 40-45.

(9) Adamson, A. *Physical Chemistry of Surfaces*, 5 ed.; Wiley: New York, 1990.

(10) Rey, L.; May, J. C. *Freeze-Drying/Lyophilization of Pharmaceutical and Biological Products.* ; Marcel Dekker, Inc.: New York, 1999.

(11) Angenendt, P.; Glokler, J.; Murphy, D.; Lehrach, H.; Cahill Dolores, J. *Anal. Biochem.*, *309*, 253-260.

(12) Kusnezow, W.; Jacob, A.; Walijew, A.; Diehl, F.; Hoheisel, J. D. *Proteomics* **2003**, *3*, 254-264.

(13) Lee, C.-S.; Kim, B.-G. *Biotechnol. Lett.* **2002**, *24*, 839-844.

(14) Pikal, M. J. In *Drugs and the Pharmaceutical Sciences*; Rey, L., May, J. C., Eds.; Marcel Dekker, Inc.: New York, 1999; Vol. 96, pp 161-198.

(15) Crowe, J. H.; Carpenter, J. F.; Crowe, L. M. *Annu Rev Physiol* **1998**, *60*, 73-103.

(16) Pereira, C. S.; Lins, R. D.; Chandrasekhar, I.; Freitas, L. C. G.; Huenenberger, P. H. *Biophys. J.* **2004**, *86*, 2273-2285.

(17) Crowe, J. H.; Crowe, L. M.; Carpenter, J. F. *BioPharm (Duluth, MN, United States)* **1993**, *6*, 28-29, 32-23.

(18) Crowe, J. H.; Crowe, L. M.; Carpenter, J. F. *BioPharm (Duluth, MN, United States)* **1993**, *6*, 40-43.

(19) Remmele, R. L., Jr.; Stushnoff, C.; Carpenter, J. F. *Pharm. Res.* **1997**, *14*, 1548-1555.

(20) Arakawa, T.; Timasheff, S. N. *Biophys. J.* **1985**, *47*, 411-414.

(21) Timasheff, S. N. *Annu Rev Biophys Biomol Struct* **1993**, *22*, 67-97.

(22) Clegg, J. S. *Comp Biochem Physiol B Biochem Mol Biol* **2001**, *128*, 613-624.

(23) Crowe, L. M. *Comp Biochem Physiol A Mol Integr Physiol* **2002**, *131*, 505-513.

(24) Sun, W. Q.; Leopold, A. C. *Comp Biochem Physiol A Mol Integr Physiol* **1997**, *117A*, 327-333.

(25) MacBeath, G.; Schreiber, S. L. *Science* **2000**, *289*, 1760-1763.

(26) Levit-Binnun, N.; Lindner, A. B.; Zik, O.; Eshhar, Z.; Moses, E. *Anal. Chem.* **2003**, *75*, 1436-1441.

(27) Huang, R. P.; Yang, W.; Yang, D.; Flowers, L.; Horowitz, I. R.; Cao, X.; Huang, R. *Expert Opin Ther Targets* **2005**, *9*, 601-615.

(28) Satwani, P.; Morris, E.; van de Ven, C.; Cairo, M. S. *Biol Neonate* **2005**, *88*, 214-227.

(29) Gong, P.; Grainger, D. W. *Biomed Sci Instrum* **2004**, *40*, 18-23.

(30) Blawas, A. S.; Reichert, W. M. *Biomaterials* **1998**, *19*, 595-609.

(31) Deegan, R. D.; Bakajin, O.; Dupont, T. F.; Huber, G.; Nagel, S. R.; Witten, T. A. *Nature (London)* **1997**, *389*, 827-829.

(32) Pirrung, M. C. *Angew. Chem., Int. Ed.* **2002**, *41*, 1276-1289.

(33) Kaushik, J. K.; Bhat, R. *J Biol Chem* **2003**, *278*, 26458-26465.

(34) Chang, L. L.; Shepherd, D.; Sun, J.; Ouellette, D.; Grant, K. L.; Tang, X. C.; Pikal, M. J. *J. Pharm. Sci.* **2005**, *94*, 1427-1444.

(35) Sola-Penna, M.; Meyer-Fernandes, J. R. *Arch. Biochem. Biophys.* **1998**, *360*, 10-14.

(36) Wu, P.; Hogrebe, P.; Grainger, D. W. *Biosens. Bioelectron.* **2006**, *21*, 1252-1263.

(37) Boyd, S.; Yamazaki, H. *Immunol Invest* **1995**, *24*, 795-803.

(38) Liao, Y.-H.; Brown, M. B.; Jones, S. A.; Nazir, T.; Martin, G. P. *Int. J. Pharm.* **2005**, *304*, 29-39.

(39) Sakai, Y.; Yasueda, S.; Ohtori, A. *Int. J. Pharm.* **2005**, *305*, 176-179.

(40) Hill, J. J.; Shalaev, E. Y.; Zografi, G. *J. Pharm. Sci.* **2005**, *94*, 1636-1667.

(41) Heller, M. C.; Carpenter, J. F.; Randolph, T. W. *Biotechnol Prog* **1997**, *13*, 590-596.

(42) Liao, Y. H.; Brown, M. B.; Quader, A.; Martin, G. P. *Pharm. Res.* **2002**, *19*, 1854-1861.

(43) Griebenow, K.; Klibanov, A. M. *Proc Natl Acad Sci U S A* **1995**, *92*, 10969-10976.

(44) Kachalova, G. S.; Morozov, V. N.; Morozova, T.; Myachin, E. T.; Vagin, A. A.; Strokopytov, B. V.; Nekrasov Yu, V. *FEBS Lett.* **1991**, *284*, 91-94.

(45) Rupley, J. A.; Careri, G. *Adv Protein Chem* **1991**, *41*, 37-172.

(46) Cicerone, M. T.; Soles, C. L.; Chowdhuri, Z.; Pikal, M. J.; Chang, L. *Am. Pharm. Rev.* **2005**, *8*, 22, 24-27.

Supplemental Data

Fluorescence scanned images (Cy3 and Cy5 channel) showing capture antibody loading and capture activity for anti-human IL-1β (100 μg/ml printed concentration), anti-human IL-4 (200 μg/ml printed conc.) and anti-human TNFα (200 μg/ml printed conc.) printed with glycerol, PVA, and without any additive. Microarray sample layout were shown in the white box. Identical microarrays were printed on OptArray™ and Codelink™ slides (unblocked and pre-blocked with ethanolamine), then incubated with serial cytokine analyte concentrations (20 ng/ml, 2 ng/ml, 200 pg/ml and 20 pg/ml) in sandwich assays (shown in descending orders). (+) = positive control; (-) = negative control.

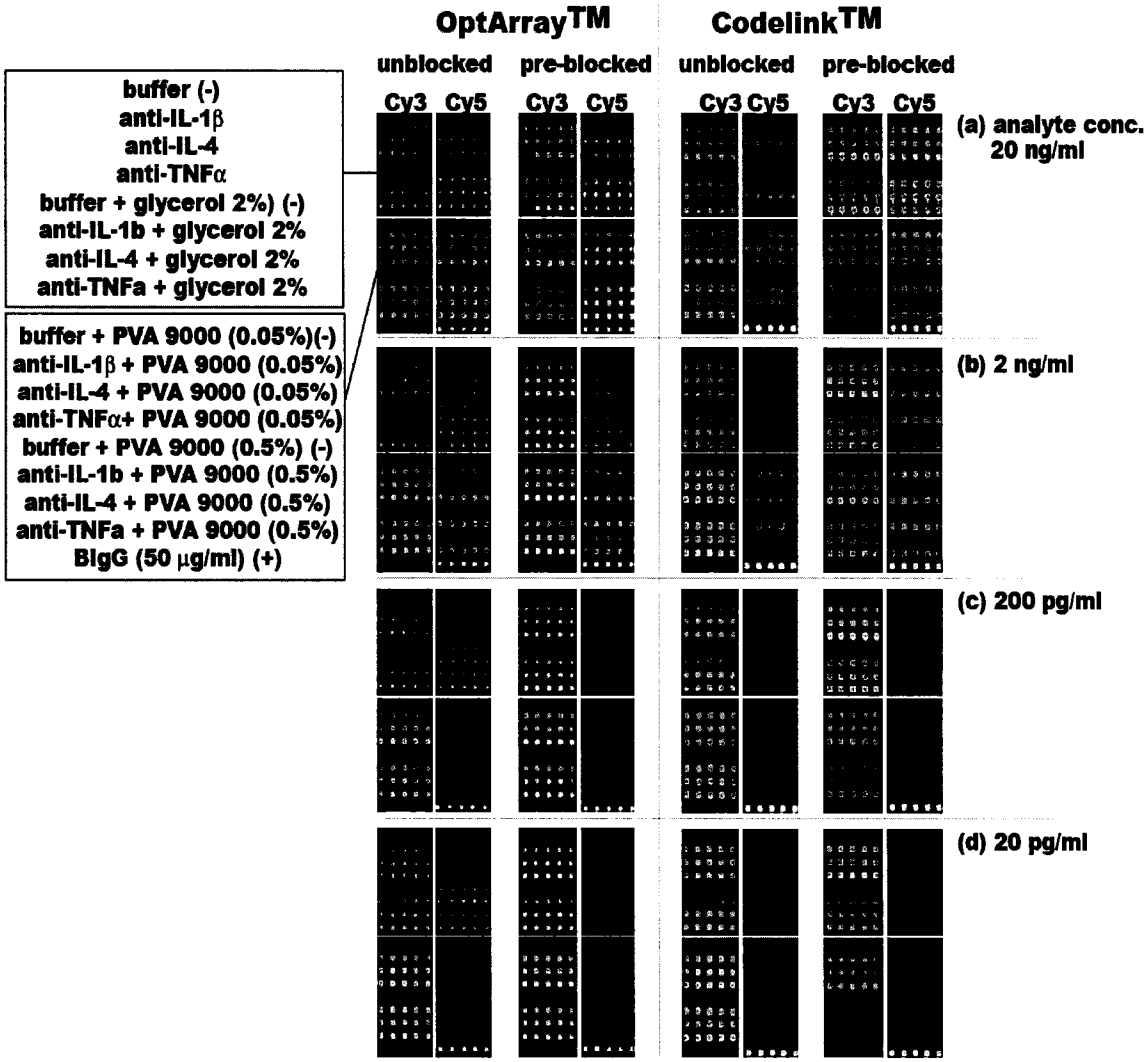

CHAPTER IV

ARRAY FEATURE SIZE INFLUENCES NUCLEIC ACID SURFACE CAPTURE IN DNA MICROARRAYS

This chapter contains the manuscript of a full paper submitted to *Proceedings of the National Academy of Sciences (PNAS)*, formatted according to requirement of *PNAS*. References are formatted in *PNAS* style. This manuscript was written by David S. Dandy, Peng Wu, and David W. Grainger, and edited by David S. Dandy and David W. Grainger. This chapter examines the relationship between surface capture efficiency and capture feature size by combination of a full reaction-diffusion numerical model and a DNA oligomer/gold experiment system. Both radiometric and fluorescence detection methods were used for validating the inverse relationship between analyte flux /surface capture efficiency and capture feature size under mass transfer limiting capture conditions that characterize many such assay formats. The full reaction-diffusion model was established by David S. Dandy, and experiments were carried out by Peng Wu.

Array feature size influences nucleic acid surface capture in DNA microarrays

David S. Dandy, Peng Wu, David W. Grainger

Abstract

Analyte affinity capture by surface-immobilized agents is a routinely employed assay format for profiling numerous medically and technologically important target analyte species. These assays suffer from numerous performance limitations, including, sensitivity and rapidity. Assay miniaturization is advocated as a strategy to improve surface-capture performance, specifically exploiting the inverse relationship between analyte flux and capture feature size under mass transfer limiting capture conditions that characterize many such assay formats. Reduced capture feature sizes, e.g., microarrays, are proposed to overcome mass transfer limitations, yet this is difficult to achieve across several size scales. This study validates the advantages advocated for capture spot miniaturization using a rationale to understand surface capture miniaturization strategies. Experimentally derived immobilized ligand and target capture densities as a function of microspot size for DNA oligomers on model gold substrates are compared directly with theoretical analysis, validating the hypothesis that miniaturization will yield many practical assay advantages. Specifically, results show that the transitions from assay mass transfer limiting to kinetic limiting conditions as feature size decreases identify an optimal microspot size range for a specific bioassay system. The analytical advantages realized from this assay miniaturization are more uniform target-spot coverage and

substantially increased rate of binding (hybridization), providing increased assay signal and assay rapidity.

Introduction

New strategies to improve bio-analytical methods, clinical assay designs, diagnostic devices, and rapid screening tools for disease biomarkers, biosecurity threats, and food pathogens have nearly universally emphasized miniaturization as a route to improve performance, cost, convenience, speed-to-answer, and portability. Reducing size scales for these applications has many practical implications to measurement of biological analytes and such assay designs. One key design feature surrounds optimal device sizing for assays that commonly involve affinity binding of analytes to surfaces. Surface capture microassays employ diverse affinity reagents (e.g., antibodies, aptamers, DNA) to capture broad varieties of analytes (e.g., small molecules, peptides, proteins, pathogens). Without active transport (e.g., stirring, field-induced), all current microassay platforms suffer from severe mass transfer limitations, that is, the rate of analyte transport to the assay capture surface significantly lags the rate of analyte binding. This is particularly problematic in producing rapid results in DNA microassays where resulting DNA-DNA charge-charge interactions produce complications. A long-standing yet experimentally tentative assertion is that surface capture assays benefit significantly from reduced capture feature (i.e., microarray spot) size; specifically, that these assay systems capitalize on the inverse relationship between analyte flux and capture feature size under mass transfer limiting conditions [1, 2]. It is demonstrated here that the assertion is correct, but not as a result of this flux behavior associated with the mass transfer limit. Instead, a

tremendous enhancement in nucleic acid hybridization rate and capture yield may be realized as assay feature size decreases through mitigation of mass transfer limitations. Additionally, fractional feature capture capacity and coverage uniformity for analyte capture are both also predicted to increase with decreasing spot size. While this offers rational design improvements to guide current microassays, actual performance advantages based on such scaling are not fully experimentally exploited. Despite its promise, the microarray assay format remains largely a research tool, with several clinical, biothreat, and food safety applications lacking sufficient chemometric reliability or analytical sensitivity for widespread applications.

The Ekins hypothesis [3] is intriguing as a motivation for assay miniaturization, claiming that surface-capture assay signal increases as the dimension of the immobilized surface-capture affinity ligand area decreases, reaching a signal:noise maximum of approximately 60 as immobilized capture antibody density approaches zero (i.e., immobilized spot size approaches zero). While details of this largely theoretical proposal are deferred to a substantial precedent literature, the experimental validation of this prediction is not yet clear. One reason is that the Ekins model assumes scale-dependent microspot assay sensitivity using a uniform and known surface immobilization density of surface-capture ligand. This uniform surface immobilization density required for validating the hypothesis is difficult to reliably experimentally control across several orders of magnitude of surface feature dimensional changes. We now present such a validation using a size-scaling for immobilized DNA probe oligomers on planar gold surfaces as a model. Experimentally derived immobilized ligand and target capture densities as a function of microspot size are compared directly with theoretical analysis

that validates the hypothesis that miniaturization will yield many practical assay advantages. Specifically, it is demonstrated that the transition from mass transfer limiting to kinetic limiting conditions as feature size decreases may be applied to identify an optimal microspot size range for a specific system. The advantages realized from this miniaturization are more uniform target coverage on the feature and substantially increased rate of binding or hybridization, leading to more signal.

Results

Spot size dependence

Terminally thiolated 20-mer DNA oligonucleotide probes were immobilized on fabricated gold surface structures of different diameters, followed by hybridization with complimentary target DNA. Tethering of thiolated nucleic acids to gold surfaces has been widely reported [4-13], providing a well-characterized, readily scaled, quasi-two dimensional surface capture model to study DNA hybridization efficiency. As DNA thiols form surface adlayers with reliable thermodynamic stability and reproducible density, fabricated gold feature size scaling can be used to produce different surface-capture feature sizes with relatively uniform DNA probe density. Both ^{32}P- and fluorescent dye-labeled oligonucleotides were used to investigate DNA immobilization and hybridization. ^{32}P-DNA experiments provide an absolute surface density of immobilized DNA probes and captured targets. Fluorescence analysis provides relative intensities for molecules tethered and captured on these surface, with a ready capability to compare relative immobilization and hybridization efficiencies across different spots. Different gold spot sizes (diameters: 2 mm, 600 μm and 100 μm) were created to

compare DNA immobilization and hybridization across a range of gold spot sizes amenable to DNA density analysis.

^{32}P-labeled 20-mer oligonucleotide probe and target were used to quantify immobilization and hybridization of DNA on fabricated gold features using phosphor imaging [6, 10]. As shown in Figure 1, surface density of hybridized DNA target increases substantially as gold spot diameter decreases from 2 mm to 100 μm, despite the reduced surface density of immobilized DNA probes as gold spot size decreases.

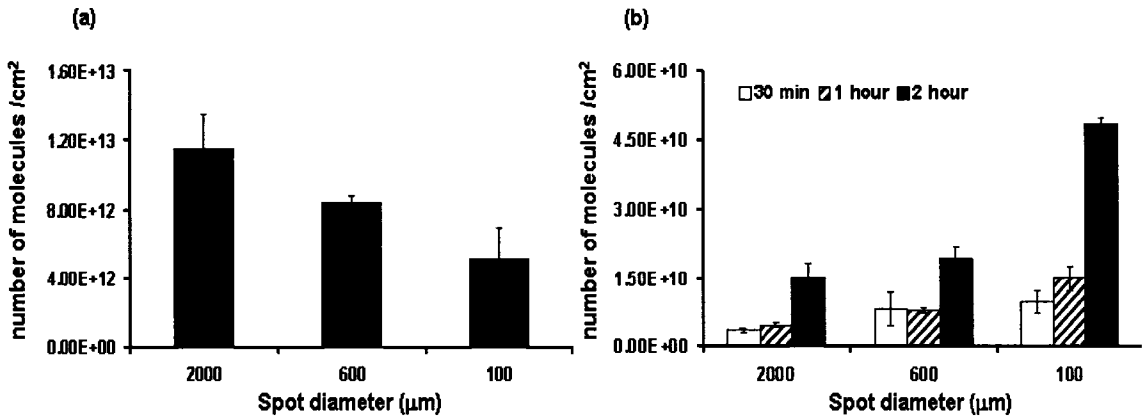

Figure 1. Surface density of DNA (a) probe immobilized on gold features of different sizes, and (b) hybridized complementary target ($n \geq 3$ spots) calculated from ^{32}P-labeled 20-mer oligonucleotide probes and complimentary targets.

Results for analogous fluorescence intensity imaging of gold features using thiolated DNA probes labeled with Cy3 dye and complimentary target labeled with Cy5 dye [10] are shown in Figure 2. Both probe and target fluorescent signals are scanned simultaneously, and the Cy5:Cy3 signal ratio on each spot used to compare hybridization efficiencies across different feature sizes. Unlike more spatially resolved ^{32}P imaging results, quantified fluorescence surface densities for probes and targets represent the

integrated average of spots of the same size over each gold feature containing DNA. Fluorescence experiments typically produced higher background signals and larger data variances from spot to spot due to light scattering from gold surface defects (i.e., scratches from handling and trace residual salt crystals on the surface). Fluorescent dye DNA labeling also introduces some minor non-specific binding influence (i.e., hydrophobic surface adsorption) during DNA probe immobilization and target hybridization (data not shown). However, fluorescence imaging provides improved resolution (5 μm) compared to that of phosphor imaging (50 μm), allowing imaging of even smaller diameter spots (e.g., to 42 μm diameter). Despite different DNA probe and target labels, distinct data processing and different experimental limitations in these two approaches, observed relationships between feature size and DNA hybridization efficiency exhibited similar trends with both methods (compare Figures 1 and 2).

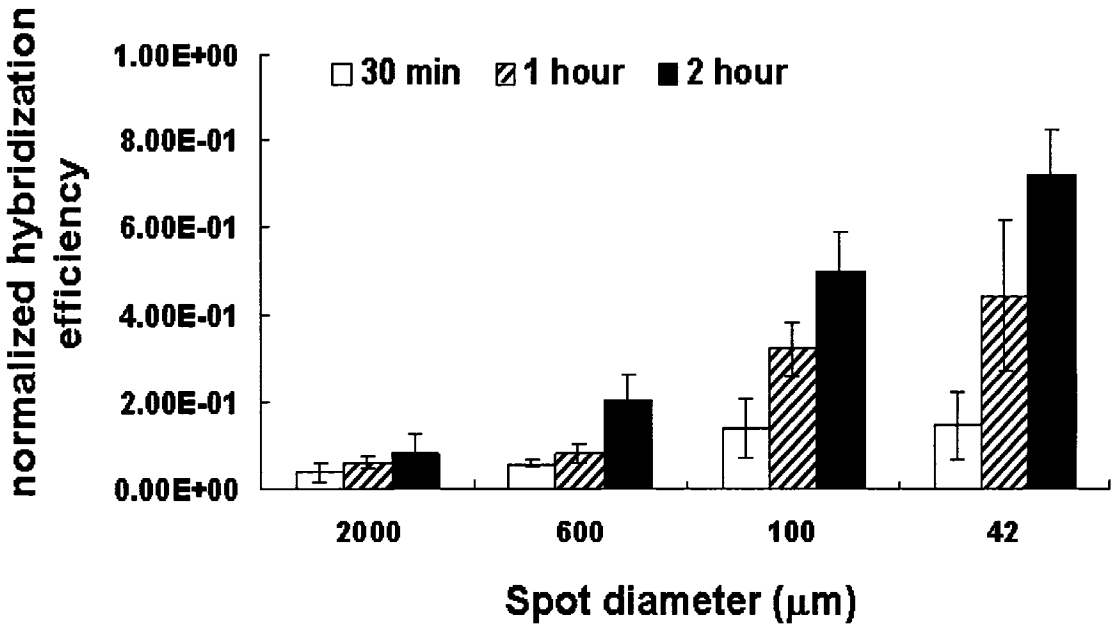

Figure 2. Normalized fractional coverage of complimentary target DNA to immobilized DNA probe on gold surface features of varying diameters ($n \geq 3$ spots) taken from fluorescence imaging results. Cy3-labeled 20-mer oligonucleotide probe and Cy5-labeled complementary target were used to compare hybridization efficiency ($n \geq 3$ spots).

The most significant result of this study is represented by the quantitative data in Figure 1(b), which is further supported qualitatively by the fluorescence data in Figure 2. The assertion that capture efficiency (fractional occupancy) depends inversely on capture feature size [14] is indeed borne out by these results. Although data in Figure 1(b) correspond to absolute target densities, results shown in Figure 3 definitively demonstrate that average hybridization efficiency increases as capture spot size decreases. After 2 h of incubating target with immobilized probe, the largest features have reached 10 to 20% of equilibrium coverage, while the smallest spots have achieved 60 to 80% of equilibrium hybridization efficiency, which in this system is approximately 1% of available probes.

The particular values reported here are specific to the system (e.g., DNA 20-mers on gold) and assay conditions employed in this study, but the general trends in Figure 3 are the same as predicted by the model for a wide range of dissociation constants, diffusion coefficients, initial target concentrations, and probe-target combinations.

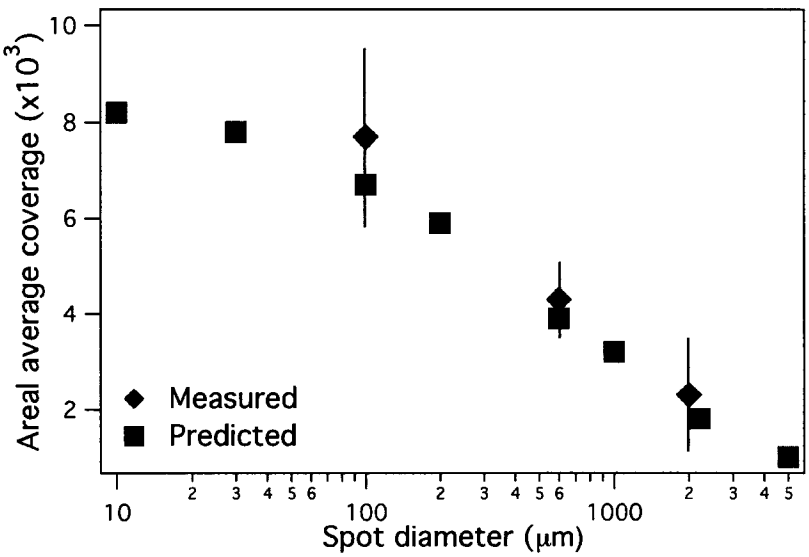

Figure 3. Average hybridization efficiency (fractional coverage) after 2 h of incubating target with immobilized probe, as a function of spot size. The diamonds represent data collected via ^{32}P DNA signal of probe and target, while the squares are the results of the reaction-diffusion model.

Intra-spot variability

Figure 1(a) represents average probe densities for each of the three spot sizes. The 50μm resolution of the phosphor imager allows quantitation of probe coverage as a function of position on the 2 mm spots. ^{32}P DNA signals from immobilized probes were collected along multiple radial lines across these spots and averaged. It is determined in this system that probe coverage is not uniform across the 2 mm spot surface, as indicated by the symbols in Figure 3. To rigorously model target hybridization through application of Equations (2) and (3) it is therefore necessary to capture this radial dependence in mathematical form; to that end a simple nonlinear least squares fit is applied to the data, resulting in the curve in Figure 3.

As with the probe data in Figure 1(a), the results in Figures 1(b) and 2 represent average hybridization efficiencies for each spot size at three time points. Collecting ^{32}P-labeled DNA signals from hybridized target along multiple radial lines on the 2-mm spots, and ratioing this result with the data in Figure 4, it is possible to determine variations in hybridization efficiency across the spot surface. As indicated by the symbols

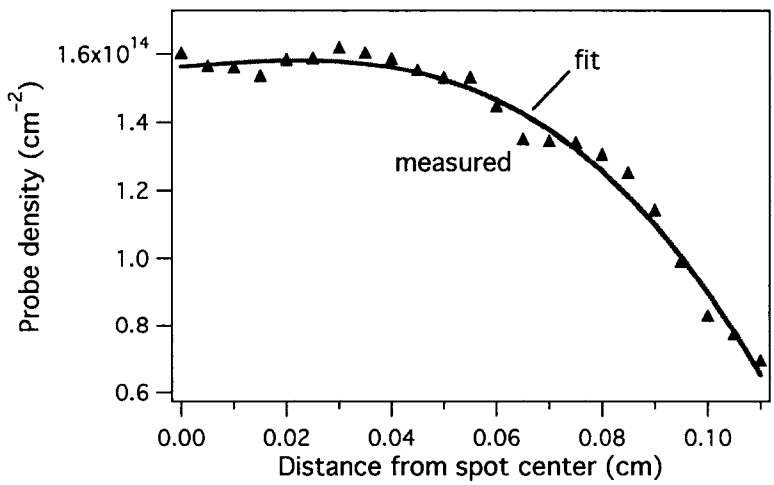

Figure 4. Surface density profile of immobilized DNA probe on 2 mm spot as a function of distance from spot center (symbols), and an accompanying polynomial fit used in the reaction-diffusion model (curve).

in Figure 5 at two different time points, hybridization efficiency monotonically increases from the spot center to the outer edge. Thus, while probe (Figure 4) and target (data not shown) densities both decrease monotonically from the spot center to outer edge, the ratio of these two quantities manifests an inverse trend. To investigate this phenomenon, the probe coverage dependence in Figure 4 is incorporated into the reaction-diffusion model described in the next section, and represented by Equations (1) – (3). The curves shown in Figure 5 were obtained via numerical solution of the reaction-diffusion equation and boundary conditions, using the parameters specified in the Materials and Methods section.

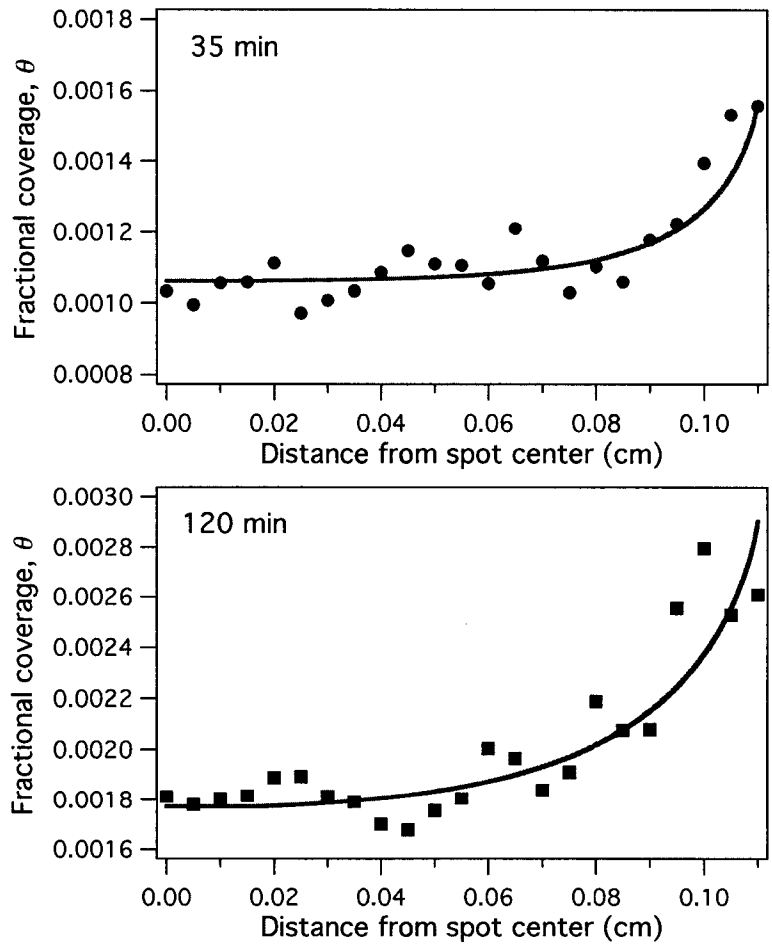

Figure 5. Hybridization efficiency as a function of radial position on the spot surface, for 35- and 120-minute DNA target incubations on the 2 mm spots. Symbols represent averages of replicate data collected from ^{32}P signals, and curves are predictions from the reaction-diffusion model.

Discussion

By combination of a full reaction-diffusion numerical model and a DNA oligomer/gold experiment system, our results (Figure 3) directly demonstrated that the surface fractional occupancy rate increases when the microspot surface area decreases [14]. Also, the radial occupancy gradient from center to edge of microspot is predicted to decrease as feature surface area decreases, producing more uniform probe/analyte binding within the microspot. The monotonic increase in fractional coverage with radial position, such as that shown in Figure 5, is a consequence of the mass transfer limited conditions associated with the larger spots used in this study. Across the entire feature the numerical model predicts that target concentration remains low—approximately 1% of the bulk concentration—in the vicinity of the spot's surface, even after 2 h of hybridization. This $C_T \to 0$ behavior at the surface, that is, the formation of an analyte depletion layer, is consistent with mass transfer limiting conditions. Near the center of the spot, target is delivered to the surface solely through the linear diffusive component, while toward the outer edge a lateral (radial) component of diffusive flux augments the linear component, producing hemispherical diffusion, resulting in a net increase in the rate that target can be transported to the feature. This scale-dependent mass transfer limiting behavior is analogous to that recognized by the microelectrode community [15], and was first characterized by Saito [16]. Put another way, the region on the feature near the outer edge samples more target through greater proximate fluid volume than does the region near the center. This radial occupancy gradient diminishes as the feature size diminishes, eventually becoming flat (uniform) over the surface (data not shown). The specific reasons for this behavior center on the transition from mass transfer limiting to

kinetic limiting conditions as the feature size decreases. The transition from one limit to the other is discussed in more detail below; here the effect manifests itself as a gradual disappearance of the target depletion layer, to the point where the solution target concentration is uniform across the feature surface and close to its concentration away from the surface. Physically, the region near the spot center dependent on linear diffusion decreases with spot size to the point where transport is essentially hemispherical (i.e., linear and radial, where linear ~ radial contributions) when the feature is small enough. Thus, purely from the perspective of enhancing hybridization efficiency uniformity across the feature it is desirable to decrease its size toward this transition point in rate mechanisms.

In general, the smaller the values of K_D or C_{To}, the higher the assay sensitivity to feature size; that is, the degree of mass transfer limitation impacts the degree to which a spot size dependence is exhibited. At one extreme, for very efficient hybridization and vanishingly small target concentrations, even nanometer-scale spots may be subjected to mass transfer limitations. At the other end of the spectrum, if binding or hybridization rates are low and target concentrations are large, all capture features, regardless of size, will be kinetic limited such that there is little or no dependence of hybridization efficiency on spot size. Most microarrays and assays, however, operate somewhere between these two extremes. The results in Figure 3 illustrate this intermediate behavior. After 2 h of hybridization there remains an approximately exponential dependence of efficiency on feature size for spots larger than 200 to 300 μm, while hybridization efficiency on features smaller than this display increasing insensitivity to the capture spot size. This issue may be examined in more detail by turning to a central tenet of the

hypothesis used to predict the phenomenon now confirmed by this work, specifically that smaller spots will capture target analyte faster than larger spots because of an expression relating the target analyte surface flux q (mol cm^{-2} s^{-1}) to the capture spot radius a as $q = 2DC_{To}/\pi a$ [1,2]. This expression for the flux of target onto the surface may be derived from the mass-transfer limiting solution presented in the next section, and is valid only at the center of the spot. As discussed above, under mass transfer limiting conditions the flux does not remain constant across the spot surface, but in fact, monotonically increases with radial distance from the center. To investigate whether the system under study does, indeed, suffer from mass transfer limitations, the results of the full reaction-diffusion model are applied to predict the flux at the center of the feature, shown in Figure 6.

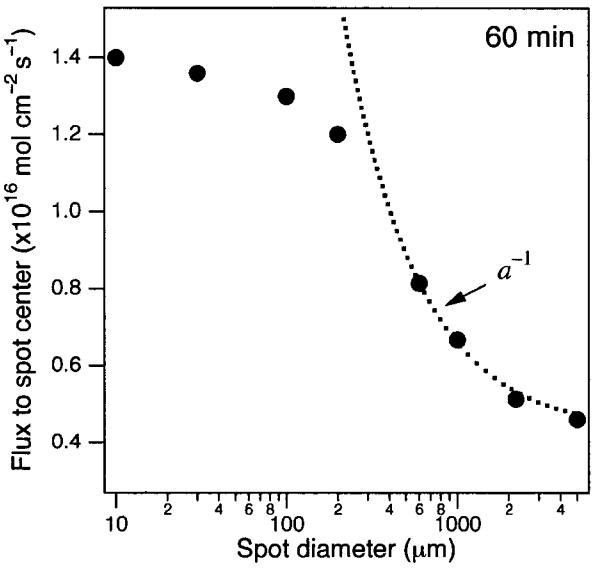

Figure 6. Predicted target flux at the center of the immobilized probe spot (circles) as a function of feature size, after 1 h of hybridization. The dashed line is a nonlinear regression of the data confirming the implication arising from Figure 3 that the larger spots are mass transfer limited, while the smaller spots ($\leq$ 200 mm) approach kinetically limiting behavior.

The circles represent results obtained from the numerical solution, and the dashed line is a nonlinear regression of that data, assuming $q \propto a^{-1}$. Consistent with the hybridization efficiency data of Figure 3, the predicted target flux at the spot center indicates mass transfer limiting behavior in the system for features larger than 200 to 300 μm. However, for features smaller than this the system transitions to kinetic limited behavior. As this occurs the actual hybridization rate becomes significantly lower than predicted via mass transfer limited theory. The prediction that hybridization rate and efficiency become insensitive to spot size under kinetic limitations is consistent with experimental measurements of binding kinetics in flow cells designed for operation in the kinetically limited regime [17]. This previous work determined that, for spots ranging from 1145 μm to 80 μm, fractional coverage (measured as mean % binding) was almost independent of spot size for experiments up to 27 min duration under flow.

It may be concluded from the experiments and numerical simulations that an optimal feature size exists for any system involving surface capture, binding or hybridization of a specific target analytes to affinity probes immobilized within a discrete region on a surface. The criterion for fractional coverage or hybridization efficiency is not its maximum, since, as shown in Figure 3, this quantity increases monotonically up to the smallest feature size considered. Instead, the optimum feature size is the point at which the system begins to transition from mass transfer limiting to kinetic limiting behavior. When the rates of diffusion and hybridization are comparable, the affinity capture system is functioning as close to ideal as possible. Further increases in capture efficiency are possible as the surface feature size is further decreased, but the technical challenges associated with engineering such features with requisite precision and

acquiring sufficient signal upon hybridization may make the pursuit of additional gains problematic.

The optimal surface capture feature size may be estimated without performing hybridization studies or detailed numerical simulations, provided that necessary parametric data are available. The relative rates of hybridization and mass transfer are characterized by a dimensionless parameter, the Damköhler number, defined as $Da = k_1 a C_{Po}/\mathrm{D}$. The desired feature size is the value of a for which (approximately) $0.5 \leq Da \leq 1$, that is, conditions for which the assay system displays *slightly* kinetic limiting behavior. Using the parameters associated with the system considered here it is estimated that the radius a should be between 60 and 120 μm, consistent with the results shown in Figures 5 and 6.

In this regard, microarray spots currently employed in most commercial assay formats (50~ 200 μm diameters) are in the range of optimal size for surface capture assay in terms of probe/analyte capture efficiency. Further increases in probe/analyte reaction efficiency by reducing feature size to nm size is not as promising as reducing size from macroscopic (e.g., ~mm~cm diameters) to 50~ 200 μm sizes because of transition from mass transfer limiting behavior to kinetic limited behavior in the range of microarray spot sizes. However, nm to μm size surface capture features provide other promising characteristics other than improved assay sensitivity (e.g., high feature densities, high reporting content), but also face other more technical challenges (reliable fabrication, detection). Beyond optimal surface feature size analysis, our numerical model can also be used to predict incubation/hybridization times, sensitivity, and fractional occupancy for

microarray-based assays and other surface-capture bioassays before performing experiments.

Materials and Methods

Materials

All DNA oligonucleotides (TriLink Biotechnologies, San Diego, CA) were HPLC-purified. The 20-mer oligonucleotide probe 5'-CTGAACGGTAGCATCTTGAC-3' was selected because it forms a stable duplex with its complementary pair 5'-GTCAAGATGCTACCGTTCAG-3'(oligo2) at room temperature, with minimal interference due to self-complementarity or secondary structure [18, 19]. Thiolated DNA probe (5'-terminal thiol group with a hexamethylene spacer (5'-HS-C6-oligo1-3') is end-labeled with ^{32}P at its 3' terminus using [$\alpha^{32}P$]-ddATP (Amersham Biosciences, Piscataway, NJ) in presence of terminal transferase [6]; complementary target oligo2 and non-complementary control oligo1 is end-labeled with ^{32}P at 5' ends using [$\gamma^{32}P$]-ATP (Amersham Biosciences) in presence of T4 polynucleotide kinase (Promega Corp., Madison, WI) [10]. Labeled oligonucleotides were purified with an oligo mini-spin column (Roche Diagnostics Corp.). Concentrations of ^{32}P-labeled oligonucleotides were measured with a TriCarb 1500 liquid scintillation analyzer for specific activity determinations. For fluorescence detection, probe is 3' thiolated (C3 propyl spacer) with 5'-fluorescent Cy3 label (5'-Cy3-olgo1-C3-SH-3', as received from vendor); complementary target is supplied 3'-labeled with fluorescent Cy5 dye (5'-oligo2-Cy5-3'). After probe DNA immobilization and hybridization with target

DNA, fluorescent dyes on both probe and target DNA extend away from the gold substrate, minimizing gold-fluorescent dye quenching [12]. 11-mercapto-1-undecanol (97%, Aldrich) was used as received. 1X TE-NaCl buffer contains 1M NaCl, 10mM Tris-HCl, 1mM EDTA (pH = 7.0). Chromium (99.5% Aldrich) and gold wire (99.999% Aldrich) were used to coat silicon wafers. Millipore-quality water (18 MΩ · cm) was used for all experiments.

Photolithographic preparation of gold spot arrays

Arrays of gold spots with controlled diameters (42, 100, 600, 2000 micron diameters) were fabricated on silicon substrates using routine photolithography. Semiconductor grade polished silicon wafers were first cleaned in piranha solution for 30 minutes, after which the wafer was rinsed with de-ionized water, and blown dry with nitrogen. A bi-layer photoresist stack (Microchem LOR 10B, Shipley 1818) was spin-coated onto the wafer, and exposed through a high-resolution (2700 dpi) laser-printed positive transparency mask to irradiate the array pattern on the substrate using ultraviolet light. This pattern was then developed according to the manufacturer's recommendations. Gold (30 nm thick) was deposited onto a 6 nm Ti adhesion layer using e-beam sputtering, after which a chemical lift-off procedure removed the photoresist layers to reveal the arrayed gold spots. The wafer was then rinsed with methanol, blown dry with nitrogen, and plasma-cleaned (O_2 and Ar, 0.3 Torr total gas pressure, 100 W power, 5 min) prior to DNA probe exposure.

^{32}P-Radiometric assay of both DNA surface density and hybridization efficiency on gold

Metal-coated silicon pieces with different diameter deposited gold spots were plasma-cleaned using O_2/Ar plasma for 5 min before DNA exposure. To quantify immobilized DNA probe surface density, probe DNA solutions at 1 μM concentrations (^{32}P-labeled 5'-HS-C6-oligo1-3'diluted with unlabeled identical 5'-HS-C6-oligo1-3') were prepared in 1X TE-NaCl buffer. Substrates were immersed into DNA solutions for 5 hours, rinsed copiously with 1X TE-NaCl buffer and water, dried with N_2, then backfilled with 11-mercapto-1-undecanol (MCU, 10 μM in water) for 1 hour to fill vacant gold sites and prevent non-specific DNA capture ([6,10,12]). After MCU backfilling, samples were rinsed with water, dried with N_2 and exposed to a storage phosphor imager (Amersham) simultaneously with known ^{32}P-ATP standards for radioactivity surface measurements. To quantify surface density of target DNA hybridization, substrates were first immersed in probe solutions containing only 5'-HS-C6-oligo1-3' at 1μM concentration for 5 hours, then rinsed, dried, backfilled, rinsed again and dried. Immediately thereafter, these samples were backfilled with 11-mercapto-1-undecanol (MCU, 10μM in water) for 1 hour to fill vacant gold sites, then rinsed again with water and dried with N_2. These samples were then immersed in target DNA solutions (1 nM ^{32}P-labeled oligo2 diluted with unlabeled oligo2) in 1X TE-NaCl buffer for 30 min, 1 hour and 2 hours. Individual samples were removed at these three assay time points, rinsed copiously with cold 1X TE-NaCl buffer (pure water rinse dissociates the DNA duplex [7], data not shown), dried with N_2 and exposed to a storage phosphor imager

(Amersham) simultaneously with ^{32}P-ATP standards for radioactivity surface measurements.

Gray-scale pixelated images of surface ^{32}P density were obtained using a STORM™ (Amersham Biosciences) scanner and analyzed using ImageQuant software (v. 5.1, Amersham Biosciences). Quantitation of sample DNA surface density using gray-scale image analysis was performed by constructing calibration curves for each labeling reaction as described previously [6]. DNA surface density values were averaged from two or three individual spots in each experiment. For studies of hybridization efficiency as a function of spot radius, surface density profiles as a function of spot radius for both immobilized DNA probe and hybridized target were obtained from intensity line profiles drawn across the center of 2-mm diameter spot ^{32}P-scanned images using ImageQuant™ software. More than 3 spots (with 2 to 4 straight line profiles per spot) were analyzed for both DNA probe and target density profiles for each time point in each experiment.

Fluorescence assay of DNA hybridization efficiency on gold spots

Plasma-cleaned substrates were immersed in DNA probe (1μM, 5'-Cy3-olgo1-C3-SH-3') in 1X TE-NaCl for 5 hours, rinsed copiously with 1X TE-NaCl buffer and water, dried with N_2, then backfilled with MCU (aqueous, 10 μM) for 1 hour. After backfilling, rinsing and drying, samples were then immersed in DNA target (1 nM, 5'-oligo2-Cy5-3') in 1X TE-NaCl buffer. Individual samples were removed at three assay time points (30 min, 1 hour and 2 hours) rinsed copiously with 1X TE-NaCl buffer, then ice cold 0.1X TE-NaCl buffer then dried with N_2. Ice-cold diluted buffer more effectively removes residual salt crystals from drying, minimizing fluorescence scattering noise, without any observable influence on double-stranded DNA yields. Samples were scanned

using a ScanArray Express Microarray Imager (Perkin Elmer, Fremont, CA). The microarray scanned fluorescence images were then processed using ImageQuant™ software.

Numerical model

In this unstirred quiescent system, DNA analyte transport through aqueous media to a discrete immobilized surface probe region occurs solely by diffusion. Once an analyte molecule reaches the surface where probe exists it will reversibly hybridize at a finite rate, removing it from solution. The processes of analyte diffusion and solid-phase hybridization are described through a continuum species conservation equation and mass flux boundary condition, respectively, and for the configuration being modeled, the equations are written in a somewhat unusual boundary-fitted, orthogonal coordinate system known as oblate spheroidal coordinates [20]. The main reason for selecting this coordinate system is the ability to apply a numerical scheme to solve the governing equation and boundary conditions that will most accurately resolve transport and reactions for spots of arbitrary size, in this case ranging from millimeters down to 100 nm. As shown in Figure 7, the circular spot on the surface where probe is immobilized corresponds to the coordinate surface $\xi = 0$ for $0 \le \eta \le \pi/2$ and $0 \le \phi \le 2\pi$. The passive, non-reacting plane surrounding the spot corresponds to $\eta = \pi/2$ for $\xi > 0$, and the axis of revolution is $\eta = 0$, $\xi > 0$. Assuming the system is axisymmetric, i.e., all variables are independent of ϕ, the analyte diffusion equation and boundary conditions may be cast in terms of ξ and η [21]. The form of the governing differential equation may then be simplified through application of the transform $x = \sinh\xi$ and $y = \cos\eta$, mapping the

curvilinear coordinate system in Figure 7 onto a rectangle. Using the transformation, together with basic trigonometric and hyperbolic identities, it is possible to write the axisymmetric analyte diffusion equation as [21]

$$\frac{\partial w}{\partial t} = \frac{\mathrm{D}}{a^2(x^2+y^2)}\left[(1+x^2)\frac{\partial^2 w}{\partial x^2}+2x\frac{\partial w}{\partial x}+(1-y^2)\frac{\partial^2 w}{\partial y^2}-2y\frac{\partial w}{\partial y}\right], \qquad (1)$$

where $w(x,y,t)$ is the dimensionless analyte concentration, a (cm) is the radius of the probe spot, and $\mathcal{D}$ (cm^2/s) is the effective binary diffusion coefficient of analyte in solution. The dimensionless target concentration is defined as $w = C_T/C_{To}$, where C_{To} (mol/cm^3) is the initial analyte concentration and $C_T(x,y,t)$ is the unknown distribution of analyte.

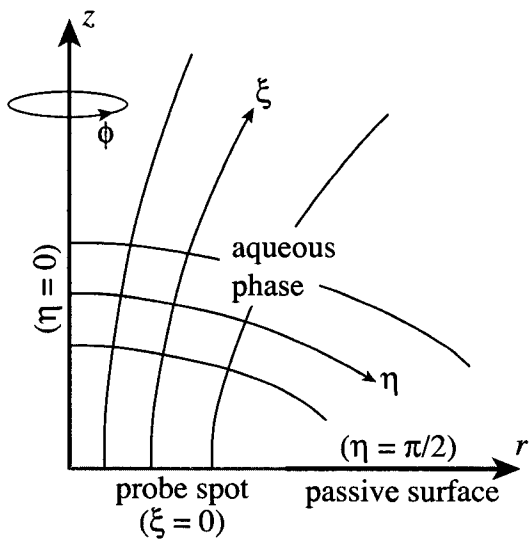

Figure 7. Oblate spheroidal coordinates (ξ, η) are used to describe the geometry near the probe spot. The coordinate system is similar to spherical, with ξ the radial coordinate and η the angular coordinate. Cylindrical coordinates (r, z) are shown as well.

Boundary conditions

Four boundary conditions and an initial condition must be associated with equation (1). Initially, at time $t = 0$, the analyte is uniformly distributed in solution at its

initial concentration, C_{To}. On the passive surface surrounding the spot ($y = 0$) a zero mass flux condition is applied, and at the axis of rotation ($y = 1$) the axisymmetry condition is imposed. The system is modeled as being significantly larger in lateral (radial horizontal) extent than linear (vertical). To capture this geometry and to impose boundary conditions away from the surface, the transformed coordinate pair (x, y) is related to the cylindrical coordinates (r, z) as $z = a\,x\,y$ and $r = a\sqrt{(1+x^2)(1-y^2)}$. The cylindrical coordinates are also shown in Figure 7. Then, a zero mass flux condition is applied at the upper boundary $z = H$ and a bulk concentration condition is applied at large, but finite values of r.

At the probe surface ($x = 0$) a mass balance is applied to relate the flux of target from the aqueous phase with the forward and reverse rates of hybridization. Several approaches have been used to formulate this condition, including its treatment as a thin disk into which analyte diffuses before reacting [22-24], but in many studies the spot is treated as a planar surface on which solid-phase hybridization occurs [25-27]. In its simplest form the hybridization reaction may be treated as a one-step, reversible reaction between target and probe with rate constants k_1 and k_{-1} [28]. The forward reaction rate is presumed to be proportional to the local analyte concentration, $C_T(0,y,t)$, and the surface density of unhybridized probe strands, $C_P(y, t)$. Similarly, the reverse rate is assumed to be proportional to the surface density of hybridized probe-target pairs, $C_{PT}(y, t)$. Defining the fraction of hybridized probe-target paris as $\theta = C_{PT}/C_{Po}$, where C_{Po} is the initial surface density of unhybridized probes, the mass conservation boundary condition at the probe surface may be written in the transformed coordinate system as:

$$\frac{\mathsf{D}}{ayC_{Po}}\frac{\partial w}{\partial x} = k_1 w(1-\theta) - \hat{k}_{-1}\theta \qquad \text{at } x = 0,\ 0 \le y \le 1, \tag{2}$$

where $\hat{k}_{-1} = k_{-1}/C_{To}$. Equation (2) assumes that, at any position y on the spot surface, there is conservation of hybridization sites such that $C_P + C_{PT} = C_{Po}$. The surface surrounding the probe spot is assumed to be passive so that its boundary condition is $\partial w/\partial y = 0$ at $y = 0, x > 0$. The presence of the function $\theta(y, t)$ in (2) requires that an additional constraint be specified, and this can be applied in the form of a mass-action expression for C_{PT}. In transformed variables this equation is

$$\frac{1}{C_{To}}\frac{\partial\theta}{\partial t} = k_1 w(1-\theta) - \hat{k}_{-1}\theta \qquad \text{at } x = 0,\ 0 \le y \le 1. \tag{3}$$

The hybridized fraction θ is not assumed to be constant across the surface of the spot, and as shown in the results above, this quantity can vary significantly with radial position, i.e., with y. In formulating the hybridization kinetics as shown in (2) and (3) it is important to recognize that the hybridization details are masked by the assumed single step sequence, and more important, the dissociation constant K_D may be two to ten orders of magnitude different from the bulk solution hybridization value [28, 29].

Model parameters were selected to match as close as possible the experimental conditions described above. A correlation exists for the diffusion coefficients of oligomers in aqueous milieu [30], such that $D = 4.9 \times 10^{-6} bp^{-0.72}$ (cm^2/s), where bp is the number of base pairs. This correlation was applied because of evidence that the diffusion coefficients of relatively small ssDNA oligomers are not substantially different from those of double-stranded DNA oligomers of the same size [31]. Based on a survey of multiple data [28] the dissociation constant was chosen such that the solid phase hybridization value was three orders of magnitude less than the bulk solution value; for this system the constant was chosen to be $K_D = 10^{-7}$ M, consistent with data in a recent

study [32]. The one adjustable parameter in the model is k_1, since this kinetic solid phase hybridization rate constant has not been measured. A value found to reasonable here, one several orders of magnitude lower than anticipated in bulk solution hybridization (approximately 10^5 to 10^6 M^{-1} s^{-1} [28]) is $k_1 = 10^3$ M^{-1} s^{-1}. Last, the values of C_{To} and C_{Po} were taken from experiment; as noted in the previous section it was necessary to incorporate radial position dependence of C_{Po} into the model.

Numerical solution

The system of equations (2) through (4) was solved via a time-implicit, finite volume algorithm, second-order accurate in space and first-order accurate in time. The size of the (x,y) grid had an inverse dependence on feature size, ranging from 301×91 for a 5 mm probe spot to 4001×191 for a 100 nm spot. For a given spot size, grid densities were increased until the solution did not change by more than 0.01% after 2 h of simulated hybridization. The time step was chosen by the same mechanism; it was halved until the same criterion as for grid size was met.

The mass transfer-limiting case

As discussed in the Introduction, virtually all DNA, antibody, and protein surface capture arrays with millimeter and sub-millimeter features are severely mass transfer limited; that is, these devices operate at an extremum where the rate at which hybridization occurs is (essentially) infinitely fast compared to the rate at which analyte can diffuse to the surface. In this limit an analyte molecule disappears from solution the instant it arrives at the probe spot, and (2) may be replaced with a simpler boundary condition that captures this instantaneous depletion adjacent to the surface: $C_T = 0$ or

$w = 0$ at $x = 0$. Physically, this approximation arises from diffusion being the rate limiting step in the solid-phase hybridization process; from (2) it is clear that the magnitude of the right hand side is limited to the maximum possible concentration gradient, which will occur when the analyte concentration is zero at the probe spot surface.

If this alternate boundary condition is imposed, bulk analyte transport is decoupled from the actual state of the surface—as measured by $\theta(y, t)$—and (3) becomes extraneous. However, a consequence of this treatment is that the hybridization reaction becomes irreversible, and will always proceed at the analyte diffusion rate as described by the left hand side of (2), subject to the constraint $w(0, y, t) = 0$. As shown below, this reaction behavior will invariably be correct for large enough surface features at the early stages of hybridization. But as the system progresses asymptotically toward equilibrium the actual net rate will increasingly diverge from mass transfer limited behavior.

Under mass transfer limited operation, if the fluid domain is large enough in extent (rigorously, semi-infinite) it can be argued that the system operates at pseudo steady state, since the analyte concentration is assumed to always approach zero at the probe surface. In that circumstance the diffusion equation and boundary conditions map directly to an analogous heat transfer problem, for which an analytical solution was developed in cylindrical coordinates [33]. The equivalent solution for this system is

$$w(r,z) = 1 - \frac{2}{\pi}\int_0^\infty e^{-\lambda z} J_0(\lambda r)\sin\lambda a \frac{d\lambda}{\lambda}, \tag{4}$$

where $w = C_T/C_{To}$, J_0 is a Bessel function of the first kind of order zero, and λ is the integration variable. This expression was used in the previous section to investigate the degree to which actual behavior, as described by equations (2), (3), and (4), aligns with that predicted in this limit.

Acknowledgements

This work was supported by NIH Grant EB00726. The authors thank Ms. Diana Findley and Ms. Jessica Elzea for their contributions to the numerical model development, and Mr. N. Scott Lynn for preparation of the gold spot arrays.

References

(1) Ekins, R. P. *Clinical chemistry* **1998**, *44*, 2015-2030.

(2) Ekins, R. P.; Berger, H.; Chu, F. W.; Finckh, P.; Krause, F. *Nanobiology* **1998**, *4*, 197-220.

(3) Ekins, R. P. *Clin. Chim. Acta* **1960**, *5*, 453-459.

(4) Petrovykh, D. Y.; Kimura-Suda, H.; Tarlov, M. J.; Whitman, L. J. *Langmuir* **2004**, *20*, 429-440.

(5) Petrovykh Dmitri, Y.; Perez-Dieste, V.; Opdahl, A.; Kimura-Suda, H.; Sullivan, J. M.; Tarlov Michael, J.; Himpsel, F. J.; Whitman Lloyd, J. *J. Am. Chem. Soc.* **2006**, *128*, 2-3.

(6) Steel, A. B.; Levicky, R. L.; Herne, T. M.; Tarlov, M. J. *Biophys. J.* **2000**, *79*, 975-981.

(7) Levicky, R.; Herne, T. M.; Tarlov, M. J.; Satija, S. K. *J. Am. Chem. Soc.* **1998**, *120*, 9787-9792.

(8) Georgiadis, R.; Peterlinz, K. P.; Peterson, A. W. *J. Am. Chem. Soc.* **2000**, *122*, 3166-3173.

(9) Kimura-Suda, H.; Petrovykh, D. Y.; Tarlov, M. J.; Whitman, L. J. *J. Am. Chem. Soc.* **2003**, *125*, 9014-9015.

(10) Gong, P.; Harbers, G. M.; Grainger, D. W. *Anal. Chem.* **2006**, *78*, 2342-2351.

(11) Shumaker-Parry, J. S.; Zareie, M. H.; Aebersold, R.; Campbell, C. T. *Anal. Chem.* **2004**, *76*, 918-929.

(12) Gong, P.; Lee, C.-Y.; Gamble, L. J.; Castner, D. G.; Grainger, D. W. *Anal. Chem.* **2006**, *78*, 3326-3334.

(13) Rosi, N. L.; Mirkin, C. A. *Chem Rev* **2005**, *105*, 1547-1562.

(14) Ekins, R. P.; Chu, F. W. *Clin Chem* **1991**, *37*, 1955-1967.

(15) Wightman, R. M.; Wipf, D. O. In *Electroanal. Chem.*; Bard, A. J., Ed.; Marcel Dekker: NY, 1989; Vol. 15, pp 267-353.

(16) Saito, Y. *Review of Polarography* **1968**, *15*, 177-187.

(17) Sapsford, K. E.; Liron, Z.; Shubin, Y. S.; Ligler, F. S. *Anal. Chem.* **2001**, *73*, 5518-5524.

(18) Mazzola, L. T.; Frank, C. W.; Fodor, S. P. A.; Mosher, C.; Lartius, R.; Henderson, E. *Biophys. J.* **1999**, *76*, 2922-2933.

(19) Forman, J. E.; Walton, I. D.; Stern, D.; Rava, R. P.; Trulson, M. O. *ACS Sym. Ser.* **1998**, *682*, 206-228.

(20) Happel, J.; Brenner, H. In *Prentice-Hall international series in the physical and chemical engineering sciences.*; Prentice-Hall: Englewood Cliffs, N.J.,, 1965, pp 512-516.

(21) Morse, P. M.; Feshbach, H. *Methods of Theoretical Physics*; McGraw-Hill: New York, 1953.

(22) Edwards, D. A. *Bulletin of Mathematical Biology* **2001**, *63*, 301-327.

(23) Bhanot, G.; Louzoun, Y.; Zhu, J.; DeLisi, C. *Biophys. J.* **2003**, *84*, 124-135.

(24) Gadgil, C.; Yeckel, A.; Derby, J. J.; Hu, W.-S. *J. Biotechnol.* **2004**, *114*, 31-45.

(25) Lagerholm, B. C.; Thompson, N. L. *Biophys. J.* **1998**, *74*, 1215-1228.

(26) Shvartsman, S. Y.; Wiley, H. S.; Deen, W. M.; Lauffenburger, D. A. *Biophys. J.* **2001**, *81*, 1854-1867.

(27) Smart, J. L.; McCammon, J. A. *Biophys. J.* **1998**, *75*, 1679-1688.

(28) Levicky, R.; Horgan, A. *Trends in Biotechnology* **2005**, *23*, 143-149.

(29) Tarlov, M. J.; Steel, A. B. In *Biomolecular Films: Design, Function, and Applications*; Rusling, J. F., Ed.; Marcel Dekker: New York, 2003, pp 545-608.

(30) Lukacs, G. L.; Haggie, P.; Seksek, O.; Lechardeur, D.; Freedman, N.; Verkman, A. S. *J Biol Chem* **2000**, *275*, 1625-1629.

(31) Stellwagen, E.; Stellwagen, N. C. *Electrophoresis* **2002**, *23*, 2794-2803.

(32) Vanderhoeven, J.; Pappaert, K.; Dutta, B.; Vanhummelen, P.; Baron, G. V.; Desmet, G. *Electrophoresis* **2004**, *25*, 3677-3686.

(33) Carslaw, H. S.; Jaeger, J. C. In *Conduction of Heat in Solids,* 2nd ed.; Oxford University Press: Oxford, 1986 Conduction of Heat in Solids, pp 214-217.

CHAPTER V

SUMMARY AND PROPOSED FUTURE WORK

This dissertation research focuses on effects of fabrication variables on the bioassay performance of protein and DNA microarrays immobilized on various substrate surfaces. Several factors have been investigated for their influences on microarray bioassays in order to improve microarray performance important to clinical applications.

Major accomplishments of this dissertation research:

- Micron-patterned DNA and protein arrays have been successfully printed onto maleimide –modified silicon nitride surfaces, demonstrated by analyte surface capture assays.
- Poly (vinyl alcohol) (PVA, M.W. 9000) improves capture antibody performance of microarrays of anti-h-IL-1β, anti-h-TNFα and anti-h-IL-4 on both OptArray^{TM} and Codelink^{TM} commercial slides. Mechanisms are not clear.
- Covalent binding dominates DNA microarray immobilization, whereas printed proteins bind to substrate surfaces (maleimide-modified silicon nitride and commercial polymer microarray slides) through physical adsorption or other interactions, where covalency is unimportant.

- Inverse relationships between analyte flux /surface capture efficiency and capture feature size were validated by combinations of a full reaction-diffusion numerical model and a DNA oligomer/gold experimental system.

Questions remaining to be addressed:

- Non-equilibrium dynamics and mechanisms for proteins " drying down" on surfaces during microarray printing.
- Capture efficiencies for capture antibodies printed in microarrays.
- Antibody conformational changes with different hydroxylated printing additives.

Proposed future work:

- Investigate dynamics of protein microarray printing/drying on surfaces:
  Real time detection techniques (camera, confocal-fluorescence microscope) coupled with microarray contact printer and hand spotter should prove useful to investigate nano-droplet evaporation processes, and antibody spot distribution using different printing additives. Polymer (PVA, PEG) additives labeled with different fluorescent dyes could also be used to observe simultaneous distribution of both additives and antibodies under fluorescence microscopy to investigate influences of these additives on antibody immobilization and distribution in microspots. AFM can be used to measure thicknesses of protein layers formed in bulk immobilization and microarray printing.
- Absolute analyte binding efficiencies of capture antibodies printed in microarrays:
  Dual isotope labels (^{125}I, ^{32}P, ^{14}C) can be used to label both capture antibodies and antigens to compare in both bulk immobilization and microarray printing conditions on selected microarray slides. Absolute surface densities of both capture antibodies

and capture antigens can be measured and correlated with fluorescence signals obtained using corresponding fluorescent dye-labeled antibodies and antigen capture systems.

- Orientated antibody immobilization:

  Protein A, G and A/G[1, 2] and Mix&Go® (Bio-Layer, Brisbane, Australia)[3] can all be used for site-specific antibody (IgG) immobilization. Nitroliotriacetic acid (NTA)[4, 5] or streptavidin functionalized surfaces[6] can be used for immobilization of oriented protein molecules with poly-His tags or biotin tags, respectively. However, these surfaces are all designed assuming bulk immobilization conditions. These surfaces can be tested in the above experiments for printed and solution adsorbed IgG orientation.

- Antibody conformational changes with hydroxylated printing/drying additives:

  AFM can be used as a force sensor to pull adsorbed proteins from a surface to understand protein conformation and orientation. Self-interference fluorescence microscopy (SFEE) can measure the average position of fluorescent dyes of antibodies on microarraying slides to differentiate folded and unfolded antibodies on surfaces [7].

References:

(1) Dodge, A.; Fluri, K.; Verpoorte, E.; de Rooij, N. F. *Anal. Chem.* **2001**, *73*, 3400-3409.

(2) Oh, B. K.; Kim, Y. K.; Park, K. W.; Lee, W. H.; Choi, J. W. *Biosens Bioelectron* **2004**, *19*, 1497-1504.

(3) http://www.bio-layer.com/.

(4) Cha, T.; Guo, A.; Jun, Y.; Pei, D.; Zhu, X. Y. *Proteomics* **2004**, *4*, 1965-1976.

(5) Sigal, G. B.; Bamdad, C.; Barberis, A.; Strominger, J.; Whitesides, G. M. *Anal. Chem.* **1996**, *68*, 490-497.

(6) Lue, Y.-P. R.; Yeo, S.-Y. D.; Tan, L.-P.; Uttamchandani, M.; Chen, G. Y.-J.; Yao, S. Q. In *Protein microarrays*; Schena, M., Ed.; Jones and Bartlett: Sudbury, Mass., 2005, pp 13-42.

(7) Moiseev, L.; Unlu, M. S.; Swan, A. K.; Goldberg, B. B.; Cantor, C. R. *Proc Natl Acad Sci U S A* **2006**, *103*, 2623-2628.

APPENDIX A

DRUG/DEVICE COMBINATIONS FOR LOCAL DRUG THERAPIES AND INFECTION PROPHYLAXIS

Reprinted with permission from: Wu, P.; Grainger, D. W. *Biomaterials* **2006**, *27*, 2450-2467.

This Appendix contains the manuscript of a review paper published in *Biomaterials*, formatted according to requirement of *Biomaterials*. References are formatted in the designated Vancouver form. The manuscript was written by Peng Wu and edited by David W. Grainger. This chapter is a review of implantable combination devices-- those comprising drug-releasing components together with functional prosthetic implants.

Drug/Device Combinations for Local Drug Therapies and Infection Prophylaxis

Peng Wu, David W. Grainger

Abstract

Combination devices -- those comprising drug releasing components together with functional prosthetic implants -- represent a versatile, emerging clinical technology promising to provide functional improvements to implant devices in several classes. Landmark anti-microbial catheters and the drug-eluting stent have heralded the entrance, and significantly, routes to FDA approval, for these devices into clinical practice. This review describes recent strategies creating implantable combination devices. Most prominent are new combination devices representing current orthopedic and cardiovascular implants with new added capabilities from on-board or directly associated drug delivery systems are now under development. Wound coverings and implantable sensors will also benefit from this combination enhancement. Infection mitigation, a common problem with implantable devices, is a current primary focus. On-going progress in cell-based therapeutics, progenitor cell exploitation, growth factor delivery and advanced formulation strategies will provide a more general and versatile basis for advanced combination device strategies. These seek to improve tissue-device integration and functional tissue regeneration. Future combination devices might best be completely re-designed *de novo* to deliver multiple bioactive agents over several spatial and temporal

scales to enhance prosthetic device function, instead of the current 'add-on' approach to existing implant device designs never originally intending to function in tandem with drug delivery systems.

Table of Contents

Introduction to combination devices

Drug/medical device combination products represent an emerging new trend in implantable therapeutics. Combination devices have drawn increasing attention from both pharmaceutical and medical device companies as a strategy to overcome several long-standing clinical problems involving complications associated with device implantation. Using locally controlled drug delivery, combination products have already found applications in various areas of cardiovascular disease, diabetes, orthopedics and cancer [1]. Drug and device combinations can be designed in coordinated strategies to elicit mutually reinforcing effects and provide, in certain circumstances, significant medical advantages over administering both the drug and the device in their conventional, separate forms. Formal regulatory recognition and development of the combination device design motif world-wide is relatively new [2], With flexible performance features and biotechnology both advancing on many contributing fronts, combination products represent a promising new opportunity for improving implanted prosthetic device performance and associated quality of life issues.

According to the U.S. FDA's definition, "a combination device comprises two or more regulated components, i.e., drug/device, biologic/device, or drug/device/biologic, that are physically, chemically, or otherwise combined or mixed and produced as a single entity; or two or more separate products packaged together in a single package or as a unit and comprised of drug and device products, device and biological products, or biological and drug products." [2] With increasing clinical and commercial interest in combining medical devices with pharmacological agents for joint marketing, both the

European union and the U.S. FDA have recently established new policies and guidelines for these combination products [2]. FDA approval of the drug-eluting coronary stent (DES, i.e., Cordis' CYPHER™, Johnson & Johnson, USA) in 2003 opened the gate for broadly adapting similar technology to combine the device and pharma worlds that have remained largely separate to date. While combination device approvals in Europe (i.e., "CE mark") pre-date introductions elsewhere, formation of the U.S. FDA's Office of Combination Products in 2003 recognized the need for a dedicated group to manage the regulation of combination products. Clear precedents and approval protocols should now spur significant growth in the combination products market estimated to reach $9.5 billion by 2009 according to a recent report [1]. Effective exploitation of capabilities of both medical devices and drug delivery in combination approaches requires intelligent incorporation of new technology, changes and refinement of both existing drug delivery systems and medical devices, shifts from traditional devices and drug forms, and compliance with new FDA and E.U. regulations [2]. Product efficacy is not as simple as a linear combination of status quo technologies in both the device and delivery arenas: neither current product has been designed or utilized with the intent of exploiting the benefits of the other, and as such cannot necessarily maximize benefit from a simple add-on combination. As combination products are currently developed in diverse medical areas, comprehensive understanding of appropriate controlled release strategies with distinct therapeutic advantages to more complex combination products is critical. This article reviews current controlled drug release techniques from local devices, especially those relevant existing first-generation combination products, as a basis for identifying needs and improving designs for next-generation products.

Device-based local drug release versus systemic administration

Combination devices are predicated on the principle of local controlled drug delivery from an implanted prosthetic device whose primary purpose is functional or structural replacement of host tissue. Optimal dual function (i.e., drug release and prosthetic performance) are ideally coordinated and designed to work in tandem. Hence, drug release properties from the device are not simply adjunct to device implantation, and must be thoroughly understood. Drugs are clinically administered in diverse ways, including topical (nasal, cutaneous, ocular, aural), oral, intravenous, intramuscular, subcutaneous, sublingual, and other local administration routes [3]. While many delivery strategies facilitate systemic drug bioavailability, local release seeks to provide therapeutic drug concentrations only to intended target sites for prolonged times required to produce the desired pharmacological outcome. Due to numerous acknowledged advantages (see Table 1), local drug release strategies are frequently considered to address thrombosis, osteomyelitis, periodontitis, biomedical device-related infections and other microbial pathologies, or inflammatory complications that are refractory to most conventional methods of systemic drug administration once established.

An ideal drug delivery system should (a) provide effective drug doses continually to target site, and (b) offer possibilities for continuously therapeutic drug release over prolonged periods [4]. Drug release rates and durations depend upon each clinical context, including the therapy sought, disease or pathogen, device design, tissue implant site, and drug susceptibility and clearance mechanisms. These considerations then

require careful assessment of target site pharmacokinetics, effective dosage and release kinetics requirements, formulation of device design factors to enable effective drug dose

Table 1: Advantages of local drug release strategies over systemic drug therapy

1. Lower doses required
2. Greater control over toxicity and bioavailability of dose
3. Less susceptibility to promoting antibiotic resistance
4. Extended duration of release
5. Possibilities to combine local and systemic drugs with different kinetics
6. Controlled release from surfaces of combination devices directly to site
7. Avoidance of systemic drug exposure
8. Direct mitigation of device-centered infection using combination device release

delivery without impairing device performance, as well as analysis of site, side-effects and toxicity, and selection of clinically effective drugs in each context. In treating thrombosis, for example, the adherent clot or coagulation film can deter drug release from the device. In the case of implant-based infections, increased complexity associated with wound site compromised healing biology and microbial colonization, anticipated primary and secondary pathogens, tissue site drug toxicity and local metabolism, and infection susceptibility must all be considered in drug selection, dosing and release mechanisms.

Drug release properties from many current devices are currently unsatisfactory or at least, sub-optimal, primarily due to poor design, biomaterial selection, drug release mechanism, drug selections, matrix/device fabrication methods and manufacturing

specific to local host implant site environmental characteristics. Additionally, drug dosing requirements for extended release regimens (e.g., months to years) cannot be readily accommodated by simply adapting known release technologies to existing medical implant designs. Many factors need to be considered for dosing strategies including therapeutic indices, bioavailability, toxicity thresholds, and efficacy in the context of the therapy sought (e.g., pro-angiogenic, anti-coagulation, anti-inflammatory, anti-fibrotic and anti-microbial) and the tissue site. Special therapeutic conditions warrant further design considerations. For example, the release of "sub-therapeutic" or "sub-inhibitory" drug concentrations (e.g., those below the minimum therapeutic or inhibitory concentration (MTC and MIC, respectively)) from biomaterials devices into surrounding tissue or fluids might actually exacerbate infectious complications or induce resistance in wound-site bacteria [5]. Therefore, local antibiotic release profiles should ideally exhibit initial high release rates (burst release) to counter any initial elevated infection risk immediately post-surgery or implantation, followed by a long period of drug release within the therapeutically efficacious dosing zone to continually hinder latent infection [6].

Device-related infection

All implanted medical devices, from transient, easily inserted and retrieved contact lenses, urinary catheters and endotracheal tubes, to more permanently surgically implanted cardiac valves, embolic coils, vascular grafts, hip, knee and shoulder joints, pacemakers, coronary stents, and plastic surgery augmentation devices suffer from recognized risks of "device-related" or "implant-associated" infection [7]. This risk is both acute and chronic, with periods of latency extending the entire life of the patient.

Pathogen-device colonization occurs too often, resulting in host patient morbidity and device removal, or mortality. Bacteria encounter the implant via several mechanisms: (a) exogenous pathogens from skin, surgical instrumentation or the local environment, gaining direct access to the implant site during device placement, or (b) ubiquitous, systemically circulating, non-pathogenic but opportunistic bacteria spontaneously alter their phenotype to become pathogenic at the implant site. The former event produces immediate colonization while the latter event can occur at any time post-implantation, even years after device placement (so-called "latent infection"). The host implant site offers a continued opportunistic environment for bacterial colonization: surgical trauma instantly reduces tissue transport and perfusion, enhances inflammatory reactions, blood clotting, edema, alters homeostasis, and produces an abrupt, non-integrated biomaterial-tissue interface. All of these factors favor microbial survival and colonization of the site. In short, the implant site overcomes acute phase reactions but chronically never resolves to a true healing mode that stabilizes the site. Additionally, most implant materials and designs manifest poorly controlled, dynamic interfacial responses in physiological milieu that favor microbial surface colonization. [8] Adhesion of ubiquitous host planktonic bacteria to device surfaces through their extension of fibrils, expression of new sessile surface receptor patterns, and secretion of polysaccharide adhesins is the first step in device-site infection [9]. After surface attachment, rapid bacterial proliferation produces sister cells eventually forming resident colonies. Many pathogens, once sessile, use quorum sensing mechanisms to adapt [10, 11]; some create protective, complex mucopolysaccharide barrier films known as "biofilms" to enhance colony stability and escape the host immune response. Once a biofilm is formed, bacteria can shed to become

free satellites that migrate and attach to other, non-colonized surfaces. Through quorum signaling the biofilm structure also facilitates cell-to-cell communication, furthering phenotypic alterations, adaptation against immune response, and cross-breeding that promotes genetic exchange and antibiotic-resistance transfer processes [7]. Bacteria within a mature adherent biofilm colony are very difficult to eliminate, refractory to administered antimicrobials, host immune mechanisms and clearance. Systemization of implant-induced infection is a serious complication (sepsis). Hence, removal of the device is often required to effectively treat the infection both locally and systemically [12].

Nosocomial infections occur in more than two million hospitalizations in the U.S. each year, with the average hospital cost near US $15,000 [13-15]. Increased clinical use of both long-established and new innovative medical implanted devices increases every year with consequent higher infection incidence. With more extensive use of medical devices in aging populations, accompanied by serious infection problems associated with these medical devices, design and study of improved methods for direct, controlled, and local release of drugs to prevent device-related infections remains a compelling priority. Innovative, effective drug/device combination products are required for improved performance of medical devices, decreasing health care costs, avoiding systemic administration of high levels of antimicrobial drugs and reducing further risks of antibiotic-resistance.

Two main strategies have attempted to reduce incidence of device-related infections: anti-adhesive biomaterials using physicochemical surface modification methods (including non-drug containing coatings, films and ion treatments -- not covered

in this review), and direct incorporation of drugs into or onto the medical device [16], either immobilized or released. Depending on the intended medical device application, cost-effectiveness and usage period, drugs are combined with medical devices using different formulation methods.

Drug-eluting stents

Since first clinical introduction in 1977,[17] percutaneous coronary intervention (PCI) has always been limited by restenosis. As the most common therapeutic treatment for coronary artery disease (CAD), PCI procedures now number more than 1.5 million annually in the United States [18]. Deploying a rigid but compliant endovascular scaffold that prevents vessel shrinkage and recoil post-intervention (i.e., an endovascular stent) mitigates incidence of restenosis compared to balloon angioplasty alone [19, 20]. The stent has produced perhaps the greatest clinical impact in combination device technology to date, generating a new billion-dollar cardiovascular device market impacting millions of patients annually. Nonetheless, vessel restenosis remains a major complication of stent placement, so-called "in-stent restenosis", requiring re-intervention at rates up to 50% in several patient classes, depending on the anatomical placement, pathophysiology, size and lesion complexity [21, 22]. To date, most systemically administered drugs have shown disappointing results in preventing in-stent restenosis [23-25] generally attributed to poor drug bioavailability, toxicity, and insufficient drug concentration at injury sites. Substantial effort has been directed toward optimization and testing of novel drug eluting stents (DES), which represent a highly visible and successful precedent combination device clinical technology.

Sirolimus, also called rapamycin, is perhaps the most successful and extensively studied stent-released drug to date because of its demonstrated effectiveness against in-stent hyperplasia following coronary stent deployment [26]. Sirolimus is a potent inhibitor of cytokine and growth factor-mediated smooth muscle cell proliferation. Its mechanism of action is via receptor-based antagonism of the intracellular enzyme, mTOR (mammalian target of rapamycin [27]), the downstream mediator of the cell's PI3K/Akt phosphorylation signaling pathway that regulates many basic cell functions. Receptor-based inhibition of mTOR results in cell-cycle arrest in the late G1 to S phases, a potent anti-proliferative and anti-hyperplastic event [28]. Sirolimus-eluting stents have demonstrated dramatically reduced rates of restenosis compared to conventional bare metal stents in several clinical trials involving 238 ~ 1058 patients with 6 to 12 months follow-up time [29-32]. Following Europe's lead, FDA's approval of Cordis' CYPHER™ sirolimus-eluting stent (2003) opened the gate for adapting new technology combining both device and pharmaceutical designs in the United States. The FDA-approved and CE-certified CYPHER™ stent is now routinely deployed in millions of PCI cases annually throughout Europe, the Middle East, Canada, Asia-Pacific, Latin America and United States. The remarkable success of the sirolimus-eluting stent spurred substantial interest in developing improved drug-eluting stents with anti-mitotic sirolimus analogues [26]. Various immunosuppressive drugs (sirolimus, everolimus, tacrolimus, ABT-578), anti-proliferative drugs (paclitaxel, antinomycin, angiopeptin et al.), anti-migratory drugs (batimastat) and gene therapeutic reagents (antisense and siRNA, vascular endothelial growth factor (VEGF), endothelial nitric oxide synthase (eNOS and related genes)) have been combined with stents and investigated for their local release

and anti-restenotic effects [33-36]. Very recently, the FDA approved Boston Scientific's TAXUS Express^{2TM} paclitaxel-eluting coronary stent [37], touting consistently low re-vascularization rates throughout the stent, equivalent deliverability with the CYPHER™ system, and immediate post-procedure magnetic resonance imaging (MRI). Such *in situ* device imaging capability (e.g., MRI for metallic implants) provides new detailed diagnostic information on device placement and lesion site healing. However, recent data [38] suggest that sirolimus-eluting stents exhibit superior performance in reducing incidence of stent thrombosis compared to the paclitaxel-eluting stents.

As all clinically approved cardiovascular stents to date comprise expandable metallic wire woven or etched tubular designs for endovascular placement, anti-restenotic drugs for delivery to the vascular wall can be directly adsorbed onto the stent struts or incorporated into a matrix or coating on-stent, and continually released after stent deployment. The stent directly contacts the vessel wall and protrudes into the endovascular tissue bed close to cellular agents implicated in restenosis. Hence, stent-released drugs are locally available to target smooth muscle cells in the vessel wall with high local concentrations and minimal systemic bioavailability and toxicity. Most drug-on-stent impregnation techniques and polymer coatings are proprietary, but must be demonstrated biocompatible or at least biologically inert. Although sirolimus and paclitaxel-eluting stents demonstrate clinical effectiveness now up to 2 years after implantation [39], evidence for actual implant site healing and normal tissue homeostasis are lacking. Long-term concerns over late neo-intimal formation and stent-based thrombosis still remain in drug-eluting stent sites once drug elution is exhausted and chronic inflammatory responses dominate. Completely biodegradable drug-eluting stents

may prove ideal in this regard for long-term applications if mechanical and safety concerns can be resolved, providing initial restenotic prevention while eventually resorbing completely to eliminate thrombosis risks and allow complete endoluminal healing [33, 40]. Next-generation commercial drug-eluting stents will use a FDA- and EU-approved degradable polymeric coating (polylactic acid) over metallic stents for drug encapsulation and release [41]. The Champion^{TM} stent (Guidant, Santa Clara, CA) is one example currently in trials. With restriction of this absorbable polymer to the abluminal (outer) surface of each strut, drug and polymer are not exposed to flowing blood in the arterial lumen, a primary cause of current stent thrombosis with rates of 4-6% often requiring aggressive systemic anticoagulant therapy (and associated risk factors) [41]. Notably, eventual degradation of bioresorbable polymers ensures predictable systemic drug elimination over a finite time without drug retention, while reducing potential risks for late adverse events months to years after implantation [42].

Current commercial drug-eluting stents are coated with a thin (~microns) non-degradable polymer coating (e.g., polyisobutylene or polymethacrylate copolymers). These coatings are compositionally balanced for drug partitioning, solubility and release, as well as processing and endoluminal compatibility. Loaded with micrograms of drug (e.g., currently approved for paclitaxcel or sirolimus, ~140 micrograms/cm^2) per device, these coatings usually exhibit similar drug release kinetics: an early significant burst release (24-36 hours) followed by slow continuous release over a longer period of time (typically up to six weeks). Varying drug selections, drug-loading methods, concentrations, coating chemistries and designs, application methods, and polymer composition will influence initial burst rates, overall release duration, bioavailability and

therapeutic potential [43, 44]. Even anatomical factors and disease pathology influence drug delivery. [45] However, to realize more complicated kinetic release profiles, including multi-step pulsatile or slower, extended release, more complex, versatile and programmable drug-eluting stent systems are needed. A newly designed metallic stent containing unique honeycomb strut elements with inlaid stacked layers of degradable polylactide-co-glycolide (PLGA) reservoirs containing paclitaxel has demonstrated programmable release kinetics. A biphasic release profile was created by the addition of blank layers of PLGA polymer within the reservoir stacks. Early burst and late release behavior for paclitaxel were adjusted both dependently and independently, controlled by drug loading concentration, numbers of layers, and positioning of the various layers within the polymer reservoir stack. With this strategy, two or more different drugs can be loaded in separate reservoir layers and released separately in different time periods [46].

As one of the earliest products to be reviewed and approved by the FDA as a combination product, drug-eluting stents provide an excellent device platform for local drug delivery and an outstanding example of a successful prototypical combination product. Clinical recognition and rapid success are attributed to their deployment directly against and into the vessel wall target tissue, prolonged tissue contact with minimal drug doses required for efficacy. Several specific design factors for anti-restenosis efficacy include stent-strut material, stent configuration, polymer coating material, drug properties, drug encapsulation and release strategy. While early bare metal stents represented early prototypes to coat to release drugs, more recent DES designs are based on drug selection and programmed release designs intimately related into the *de novo* stent strut and frame components. [46] While current DES technology appears successful

against in-stent restenosis, further improvements and novel innovation in combination *de novo* implant device designs are required to address challenging interventional cardiology and radiology problems at peripheral vasculature sites [47], particularly venous and multiple lesion sites [48, 49], with more versatile therapeutic and pharmacological profiles, and in other tissues, including needed biliary stent applications [50].

Antimicrobial central venous catheters

Central venous catheters are used frequently in critical care situations for delivery of critical fluids, parenteral nutrition, and drug administration in a variety of hospital settings. In the United States alone, 5 million central venous catheters are inserted into patients every year. Unfortunately, these catheters are also a major cause of nosocomial infections: 100,000 to 500,000 catheter-related bloodstream infections (CRBI) occur annually, with ~US $3,700 to ~US $28,000 medical remediation costs depending on the original central venous catheter placed. At least 25,000 patients die each year of CRBI [51, 52]. Systemic or oral administration of antimicrobial agents is not a clinically preferred route to reduce CRBI infections. Properly designed combinations of antimicrobial agents delivered from these catheters could instead provide efficacious concentrations of antimicrobial agents locally at placement site without requiring high systemic anti-infective dosing. Antimicrobial central venous catheters are generally not considered as drug/device combination products, as their original FDA approval and emergence into clinical use preceded the more recently imposed combination product review approach used currently. However, many different tactics used for attaching or impregnating antimicrobial agents (including both antiseptics and antibiotics) onto/into

catheters should provide precedents and inspiration for future improved combination products in various clinical areas.

Two main strategies for incorporating antimicrobials onto catheter surfaces have been employed and have shown promising results [53]. To enhance solubility and bioavailability, many antibiotics are synthetically designed as anionic derivatives (e.g., using carboxylate, phosphate, or sulfate substituents) analogous to that of many natural glycosaminoglycans (e.g., heparins, chondroitins), phosphorylated proteins, and other biological molecules [54]. The first application method, simple drug coating, uses antibiotics' anionic charges to bind them electrostatically to medical device surfaces via intermediate layers of adsorbed cationic surfactants, such as tridodecylmethylammonium choloride (TDMAC). Hydrophobic alkylated regions of these surfactants adsorb to catheter polymer device surfaces by physical attraction, presenting cationic charges on the surface available for anionic antibiotic complexation [55, 56]. The second method, drug impregnation, incorporates antimicrobials into the polymer device bulk material directly prior to injection molding or extrusion in the same manner that common device fillers such as pigments or stabilizers are added to extrudable plastic resins [57]. Excipients to retard or enhance drug release rates can also be co-formulated in principle, although in practice, total mass loading of all additives is limited by gross effects on polymer matrix physical properties. These strategies have allowed incorporation of various antimicrobials to catheters, and investigation of their anti-infective efficiency. Combinations of antimicrobials are preferred over single agents due to concerns over promoting antimicrobial resistance [58]. So far, the most effective agents used to treat catheter-related infection are the combination of minocycline/rifampicin (MR) antibiotics

[59, 60] and the combination of chlorhexidine/silver sulfadiazine (C-SS) antiseptics [61]. Central venous catheters coated or impregnated with both antibiotic and antiseptic combinations have been FDA and CE approved and commercialized (e.g., C-SS: ARROWgard®, Arrow International, Reading, PA; MR: BioGuard Spectrum™ catheter, Cook Critical Care, Bloomington, IN).

The ARROWgard™ catheter impregnates C-SS on its external surface whereas the BioGuard Spectrum™ catheter is coated with MR on both internal and external surfaces using TDMAC [53]. Both MR and C-SS combinations have demonstrated broad-spectrum antimicrobial activity against Gram positive and Gram negative organisms, and fungi . Many *in vitro* and *in vivo* studies comparing microbial adherence and CRBI incidence between MR and C-SS catheters using different infection models have been reported in the past decade. Randomized clinical trials [60, 62] demonstrated superior performance of minocycline/rifampicin-impregnated catheters versus C-SS coated catheters in resisting CRBI, particularly in patients requiring vascular access for over seven days. While both MR [59, 63-65] and C-SS [61, 66-72] catheters exhibited significantly reduced CRBI in a number of pre-clinical and clinical studies, conflicting results have led to doubts regarding the safety of C-SS catheters [58, 73-76]. However, minocycline/rifampicin and C-SS catheter antimicrobial coatings are not entirely equivalent for clinical comparison. Higher levels of chlorhexidine seem to improve the performance of C-SS coated catheters (C-SS$^+$ catheters) [77] using a novel agar infection model that simulates rat subcutaneous infection. In comparison with C-SS catheters, C-SS$^+$ catheters exhibited higher chlorhexidine release and retention, resulting in significantly lower bacterial adhesion than the C-SS catheter at both day 7 and day 14. In

this study, C-SS$^+$ catheters exhibited effective resistance against many tested organisms, including *E. aerogenes*, *C. albicans*, *P. aeruginosa*, *S. aureus*, *S. epidermidis*, and rifampicin-resistant *S. epidermides*, whereas MR catheters were effective only against *S. aureus* and *S. epidermidis*. Another *in vitro* study [78] also showed superior efficacy of C-SS$^+$ catheters versus MR catheters against Gram positive *S. aureus* and *S. epidermidis*.

Both MR (BioGuard Spectrum^{TM}) and C-SS (Arrowgard^{TM}) catheters are acknowledged to reduce bacterial adhesion and CRBI infection significantly more than uncoated catheters. However, according to FDA public health notices, chlorhexidine has the potential for serious hypersensitivity reactions. Recently, miconazole- and rifampicin incorporated into polyurethane central venous catheters using a new diffusion process exhibited superior activities against Gram positive, Gram negative and *C. albicans in vitro*. Anti-infective efficacy of this new antimicrobial catheter remained stable at room temperature for more than one year, and the antimicrobial activity half-life exceeded 3 weeks [79]. Recently, significantly reduced CRBI were reported compared to standard unmodified polyurethane central venous catheters using a randomized controlled clinical trial. No adverse effects or antimicrobial resistance were observed [80].

Application of the C-SS- or MR-coated, or any anti-microbially treated, catheter elicits concerns about selective local emergence of organisms resistant to the associated antimicrobials. Antibiotic-resistant bacteria continually emerge at increasing rates as a result of widespread and too-often indiscriminate clinical use of antibiotics [81-83]. Bacterial resistance to antiseptics (chlorhexidine and silver sulphadiazine) and antibiotics (minocycline and rifampicin) has been reported on central venous catheters *in vitro* [84]. Resistance in *S. epidermidis* was found to develop more easily for the antibiotic

combination than for antiseptics, and more readily for rifampicin than minocycline. Although no clinical emergence of resistant bacteria has been reported using these or any other treated catheters to date, continual monitoring to locally releasing devices should be vigilantly pursued to determine resistance profiles of bacteria recovered from colonized catheters.

Intravascular catheter materials can also be modified to accommodate anti-microbial combinations. All catheter materials must be biocompatible, withstanding implant conditions within the vascular system without deteriorating or causing patient complications. Several biomedical polymers including polyethylene, fluoropolymer, polyvinyl chloride (PVC), silicones, elastomeric hydrogels and polyurethanes have been used in catheter fabrication with notable clinical success [85-87]. Certain specific properties must be considered when developing in-dwelling vascular devices, for example, thromboresistance, flexibility, smooth surface, lack of kink memory, no chemical leaching and reasonable cost. These fixed catheter materials properties also influence amounts of antimicrobials incorporated and their release kinetics. To increase amounts of adsorbed antibiotics, side-chain functional groups (acidic, basic and ionic groups) have been introduced into device polymer backbones to produce specific interactions with acidic and basic functional groups on the antibiotics, amoxicillin and rifampin [88]. Antibiotic loading and release behavior were influenced both by strength of drug-polymer interaction and the resultant water swelling of the polymer matrix. Specifically, when antibiotic-polymer interaction is dominated by ionic interactions, adsorption of antibiotics onto the polymer is favored by strongly positively and

negatively charged groups on the polymer surface, whereas for polar antibiotic-polymer interactions, amounts of surface-bonded antibiotics depend on matrix hydrophilicity.

While clinical trials have now shown that patient infections are significantly reduced by using antimicrobial catheters (mainly BioGuard Spectrum^{TM}, Arrowgard^{TM}) [61, 66, 89], these results are difficult to translate to other clinical situations [90]. Two recent reports [91, 92] declared that studies of antimicrobial central venous catheters suffer from methodological and statistical flaws. Multiple factors beyond device design can substantially influence the risk of CRBI, including patient profiles, catheter care, and insertion protocols. Several issues associated with use of antimicrobial central venous catheters remain to be addressed for unequivocal clinical acceptance. These include lack of clear, convincing clinical trial data, significant cost differential, potential toxicity and risk of increased antimicrobial resistance.

Antimicrobial urinary catheters

Urethral catheters are used for bladder drainage as a treatment option for patients with urinary retention, general surgery recovery, bladder obstruction, paralysis or a loss of sensation in the perineal area. More than 30 million urinary catheters were employed in the United States annually. One out of 4 hospitalized patients receives an in-dwelling urinary catheter [93]. Millions of catheter-associated urinary tract infections (CUTI) occur annually, with an average cost of US ~$3000 to ~US $4000 each [94]. Nonetheless, CUTI are generally considered assumed to be benign with low attributable mortality [95] but significant collective cost and morbidity. Bacterial migration on and adhesion to inserted devices are important factors in CUTI.

Many efforts have focused on catheter surface modification in order to impede initial adhesion and biofilm formation, and reduce CUTI incidence. The most extensive clinical testing has combined catheters with antimicrobial agents. One simple, common method to reduce CUTI involves immersing the urinary catheter into an antimicrobial solution prior to urethral insertion. Immersion of these devices (typically flexible polymer) into antimicrobial solutions to allow direct drug sorption onto and into the device surface constitutes the most straightforward method for loading antimicrobial agents into medical devices. Several studies [96, 97] concluded that medical devices, including prostatic stents and urethral catheters, immersed in solutions of the broad-spectrum antibiotic, ciprofloxacin (commonly used to treat sinusitis, otitis media, urinary tract infections and prostatitis), can significantly reduce bacterial adhesion and consequently reduce CUTI risks. As these antimicrobial agents are only physically ad- or ab-sorbed to device surfaces, this method is unlikely to load drugs for prolonged release to prevent bacterial infection over long periods: loading is low, release is rapid, and dose depletion occurs quickly. Nonetheless, certain practical clinical advantages exist. Suitable catheters can be treated by drug solution immersion immediately prior to clinical placement, providing early, short-term protection against infection, flexibility and direct control to clinicians in certain situations.

Silver and its salts have been the most commonly used antimicrobial agent applied to urinary catheters. Solubilized silver ion ($Ag^{+}_{(aq)}$) is the bioactive form, released in many different ways from silver-containing coatings as an anti-infective in multiple clinical contexts [98]. To clarify mixed clinical results of silver-coated urinary catheters, a meta-analysis with a total of 2,355 patients was performed [99] and

demonstrated significantly improved performance of silver alloy catheters but not standard silver oxide urinary catheters over control catheters in treating CUTI. One possible reason is that silver alloy remains in the catheter for a longer time [100]. In the United States, silver oxide catheters are no longer available. A recent comprehensive assessment of impregnated catheters intended for short-term use in hospitalized adults using eight differently designed trials compared silver alloy catheters with standard catheters [101]. Risk of asymptomatic bacteriuria was significantly reduced in the silver alloy group at less than 1 week of catheterization, but to a reduced degree at greater than 1 week. However, emergence of bacterial resistance to silver was not tested in any of these trials. Two new FDA-approved hydrogel/silver urinary catheters developed by C.R. Bard (Covington, GA) provide protection against CUTI. The Bardex I.C. (latex), and LubriSil I.C. (silicone) catheters both feature a proprietary lubricious hydrogel surface coating over a layer of metallic silver applied to both inner and outer catheter surfaces. This unique combination permits smooth intra-urethral insertion and enhanced infection protection, proven to reduce CUTI incidence in several *in vitro* [102] pre-clinical[103], and clinical studies [104, 105]. Outside of silver, catheters impregnated with urinary antiseptic, nitrofurazone, [103] and the broad-spectrum antibiotic combination proven effective in central venous catheters (see section above), minocycline and rifampin [106] exhibited significant reductions in CUTI in randomized human trials.

Since conclusions regarding the efficacy of systemic antimicrobial agents to prevent CUTI are not clear, novel technologies for incorporating antimicrobial agents into urinary catheters for release may continue to provide new combination product advances for preventing CUTI. Current combination devices however are far from a final

definitive answer for CUTI. While silver-based medical technologies are very common in multiple formulations and delivery strategies [98], silver-resistant bacteria are common in environments where silver ion is ubiquitous (e.g., mining wastes). Concern over pressure that creates such silver-resistant strains in medical practice is now evident [107]. These concerns are applicable to other anti-infective agents including chlorhexidine [108] and nitrofuroxan [109]. Urinary catheters that release more potent antimicrobial agents in more diverse ways should be pursued, and issues similar to those mentioned for central venous catheters should best be carefully considered and addressed in future designs.

Orthopedic device-based drug delivery

Bone defects resulting from disease, trauma, surgical intervention, or congenital deficiencies represent a substantial clinical challenge world-wide for orthopedic reconstructive surgeons. This also presents an immense opportunity for bioengineers, tissue engineers and drug delivery specialists to more rapidly produce bone. The preferred treatment for such defects is autologous bone graft, but harvest is painful, supply is limited, and risks of infection, nerve loss, functional impairments, hemorrhage, and cosmetic defects are significant. Additionally, orthopedic hardware placement for fixation and stabilization fractured bones during healing, or to functionally replace complete tissues (e.g., in total joint replacements) represents millions of implanted devices annually. Bone-implant integration (i.e., direct bone-implant bonding [110]) and long-term stabilization is a common clinical problem with substantial complications including infection, bone resorption, and loosening [111-113]. Frequently, despite mechanical stabilization using fixation devices, fractures are either slow-healing or non-union (~5-10% [114]). Hence, recent advances in drug delivery are now being used in

tandem with orthopedic implants with future prospects as new combination devices to promote and accelerate bone neogenesis, more reliable bone healing and functional tissue replacement [115]. Delivery of small molecule osteo-inductive molecules as well as biological derived growth factors, anti-osteoporotic agents, and osteo-synthetic genetic materials (DNA, siRNA) to bone injury sites are reported [116-119]. Because few reports demonstrate efficacy for exogenous osteogenic factors delivered simply as topical solutions in large animal models, matrix-based delivery of these molecules is now common [118, 120, 121]. Osteo-precursor cell-based local delivery is now also reported for bone engineering [118, 122-124]. These biotechnology approaches seek to accelerate and enhance bone defect healing and bone-implant stabilization through rapid local osteogenesis induced through local release of cells, mitogenic and morphogenic agents [125]. Orthopedic drug delivery vehicles are most often physically de-coupled from the device (e.g., separate collagen sponge or tricalcium phosphate granules delivering growth factors directly adjacent to or placed into spinal implant cage [120]) by either design or previous regulatory requirements. However, new methods to effectively integrate and combine delivery strategies into orthopedic, periodontal fixation or total joint replacement devices for controlled, local release and new bone-generating therapeutic potential at the implant site would be clinically useful.

Bone infection (osteomyelitis) is a local or generalized infection of bone and bone marrow typically caused by bacteria introduced from trauma, surgery, implant use, by direct colonization from a proximal infection or via systemic circulation. Osteomyelitis in an implant context is also prevalent and clinically difficult to treat, often refractory to antimicrobials: the biofilm mode of pathogen growth on an implant surface protects

sessile bacterial colonies against host immune response and antimicrobial therapy through complex environmental factors [126]. Conventional therapy with systemic antibiotics is expensive, prone to complications and often unsuccessful [127]. Major problems treating osteomyelitis include poor antimicrobial distribution at the site of infection due to limited blood circulation to infected skeletal tissue, and inability to directly address the biofilm pathogen scenario. High systemic dosage of antibiotics to facilitate sufficient tissue and biofilm penetration is not preferable because of possible serious toxic side effects. Controlled antimicrobial release systems in orthopedic combination devices represent alternatives to conventional systemic treatments, and include antibiotic-eluting bioceramics, drug-impregnated bone cements, and natural and synthetic anti-microbially loaded polymers [128].

One commonly used infection management method with orthopedic implants utilizes antibiotics loaded into clinically ubiquitous bone cement, polymethylmethacrylate (PMMA), or PMMA beads. These non-biodegradable polymer cements have been employed clinically to prevent or treat osteomyelitis in various forms for nearly four decades [129-131]. Several commercial antibiotic-impregnated bone cements based primarily on PMMA/MMA are now CE- approved, including Simplex™ P with erythromycin and colistin tobramycin (Stryker, UK) sold in Europe for more than 20 years, and gentamicin-containing Palacos™ PMMA cement (refobacin palacos r-Knochenzement®, Merck, Austria). A gentamicin-containing PMMA bead, Septopal® (E. Merck, Germany) is also commercially available in Europe [126, 132]. Until recently, no antibiotic-containing bone cement was approved for use in the United States. Instead, surgeons commonly added antibiotics off-label to bone cement directly in the operating

suite. In 2003, the first pre-blended bone cement containing an antibiotic (Simplex P with tobramycin developed by Stryker Howmedica Osteonics) was approved for use in the United States. Later in 2003, Biomet, Inc. (Warsaw, IN, USA) announced FDA clearance of their Palacos G^{TM} antibiotic-loaded bone cement.

More detailed information about antibiotic-loaded PMMA cement and beads is found in excellent recent reviews [126, 132-135]. PMMA can be loaded to deliver a variety of widely used antimicrobials and some other bioactive "agents" including anti-osteoporetic agents, proteins (model protein, albumin) and peptides (e.g., growth factors) [136]. The intention in these non-degradable matrices is to slowly release the soluble mixed bioactive reagents from the solidified, often-glassy, non-swelling PMMA bone cement monolith surrounding the implant over time. Loaded drugs are usually released in a typical bi-phasic fashion: an initial burst release followed by a long, tail of low, and importantly, largely incomplete release that continues for days to months. Small molecule antimicrobial release behavior from PMMA is influenced by relative loading amount [137], bulk porosity [138], surface area and surface roughness of the bone cement [138-140]. Addition of soluble lactose to PMMA produces increased antimicrobial release by percolation-based porous diffusion [137]. All of these observations lead to the conclusion that PMMA bone cement drug release occurs through solvent pore penetration, soluble matrix dissolution and solubilized drug outward diffusion via networks of continuous, accessible pores within an otherwise largely insoluble, dense, glassy bulk PMMA matrix.

In vivo studies have demonstrated that antimicrobial-loaded bone cement can prevent infection from intra-operative challenge within a short time after implantation

[139, 141-143]. This effectiveness in preventing infections is further illustrated in prospective, randomized and controlled clinical trials comparing antibiotic-loaded bone cement to drug-free bone cement control groups [144, 145]. Tobramycin is an aminoglycoside closely related to gentamicin with a similar spectrum of activity, slightly more effective against *Pseudomonas* [146] but less ototoxic and nephrotoxic than gentamicin [147, 148]. Its elution characteristics are judged superior to those of gentamicin [149]. A recent clinical study testing the pharmacokinetics and safety profile of tobramycin bone cement [150] demonstrated local tobramycin concentrations more than 200 times higher than systemic levels only 1 hour after administration. Systemic drug absorption was minimal with rapid urine excretion. However, despite some promise, drawbacks also limit clinical enthusiasm for use of antimicrobial-loaded bone cement. For example, gentamicin and tobramycin are used most frequently by surgeons for incorporation into bone cement in Europe and United States, respectively [135, 151-155]. Pharmacokinetic studies indicate that antibiotic release from gentamicin-impregnated PMMA cement or beads is far from satisfactory [156-158]. Less than 50% of the antibiotic load is released from implants within 4 weeks, and no continuous release was observed thereafter, indicating significant bioavailability problems. Recently, 19 of 28 bacterial strains cultured directly from a clinically retrieved gentamicin-loaded bone cement were gentamicin resistant, raising concerns for the effectiveness of gentamicin-incorporated implants [159].

Antimicrobial peptides represent a new alternative drug class for incorporation into PMMA cement implants. Antimicrobial peptide Dhvar-5, an antifungal peptide found in human saliva, has been incorporated into PMMA beads, and its release behavior

and antimicrobial efficacy have been investigated *in vitro* [160]. Its C-terminal net positive charge can disrupt and penetrate the negatively charged bacterial cell wall. The Dhvar-5 release profile is characterized as a high concentration initial burst followed by a continuous release with gradually decreased concentration over a 28-day period. Up to 91% of incorporated Dhvar-5 was released from PMMA beads in one month. Large fractional Dhvar-5 release observed in this study was explained by the freeze-dried amorphous powder formulation with a relatively high volume fraction compared to gentamicin sulfate. It was hypothesized that at higher concentrations, Dhvar-5 creates a porous network throughout the bead, allowing percolation-based pore diffusion from the bead core.

Regardless of the different antimicrobial agents mixed into PMMA liquid resins and its long tradition in orthopedic device fixation, inherent limitations reduce clinical enthusiasm for these combination implants. PMMA is not biodegradable, so with any clinical failure, secondary surgery is necessary to remove the PMMA before new bone can regenerate in the defect. PMMA polymerization exhibits a well-known, prominent exotherm [161]. Both this heat and residual MMA monomer can kill healthy surrounding bone cells and possibly inactivate the antibiotic if PMMA is used in the popular "doughy" form [131]. Other criticisms are the low PMMA bonding strength to the implant surface and known soft tissue encapsulation of PMMA. In cases of loosening and removal, bone substance will also be lost. Biomimetic synthetic hydroxyapatites (HAP) [162] are a more attractive natural candidate as composite materials for bone cement due to their intrinsic non-toxicity, high biocompatibility and ability to support growth of new bone tissue [163, 164]. HAP attempts to produce the same elementary inorganic chemical

solid chemical composition as bone and tooth mineral. Past work [131] investigated release behavior of cephalexin- and norfloxacin- loaded HAP cement *in vitro*. Drug release patterns of these antibiotic-loaded HAP cements correlated well with the Higuchi model [165]. The 4.8wt% norfloxacin-loaded cement provided continuous antibiotic release to 250 hours with complete release estimated to be 3 weeks. Anionic collagen:HAP composite pastes for antibiotic controlled release have been developed using inorganic salts, $Ca(NO_3)_2.4H_2O$ and $(NH_4)_2PO_4$, mixed with anionic collagen at a mass ratio of 20:1 followed by addition of ciprofloxacin [164]. Antibiotic release rate is controlled by the porosity and tortuosity in the composite, permitting drug release throughout the healing process. Other synthetic hydroxyapatite cements such as β-tricalcium phosphate or calcium phosphate bioceramics, either alone [166, 167] or associated with natural [168] or synthetic polymers [169], have also been studied to treat bone infection with some claims to success. These composites provide potential bulk compositional versatility for antibiotic-releasing formulations.

Biodegradable polymer cements and implants draw increasing interest because of their advantages over PMMA cements or PMMA beads in principle. First, because biodegradable beads resorb at controllable rates, surgical removal and soft tissue reconstruction are unnecessary. Second, these polymers are able to provide longer release periods and higher antimicrobial agent concentrations to more completely treat particular orthopedic infections, and third, biodegradability can be varied from weeks to years, permitting different types of infections to be treated over different time scales [170-173]. Biodegradable FDA-approved polyesters, the poly(α–hydroxy acids) poly-L-lactic acid (PLA), poly(glycolic acid) (PGA), and poly(lactic–co-glycolic acid) (PLGA) (also called

polylactide, polyglycolide, and poly(lactide-co-glycolide) respectively) continue to attract immense pharmaceutical and biomedical interest [174-177]. Currently, a number of FDA-approved clinically marketed products utilize PLA and PLGA as excipients to facilitate sustained bioactive drug release in several major device areas [178]. Specifically, in applications for treating osteomyelitis, poly(D,L-lactide) (PDLLA), PLA, PLGA, PEG, PLA-PLGA block copolymers and other copolymers are manufactured into biodegradable beads, microspheres, melt-extruded cylinders, suspension-extruded/coated cylinders and drug-releasing coatings and matrix films [135], as used for example on orthopedic devices [179, 180]. Several *in vitro* and *in vivo* studies have investigated antibiotic-loaded bone implants containing biodegradable polymers [4, 128, 130, 173]. Predictably, release kinetics were found to be influenced by polymer molecular weight, mass ratio of polymer to antibiotic, bead size, copolymer composition, and various manufacturing parameters [173]. PGA, PLA and PLGA polyesters are all strongly hydrophobic, placing practical constraints on formulating devices with sufficient drug loading and dispersion for reliable delivery of antimicrobials. To increase hydrophilicity and other physico-chemical properties to improve drug-polymer compatibility of these popular polyesters, various block copolymer excipients or matrix analogs comprising biodegradable polyesters and poly(ethylene glycol) (PEG) additives have been developed. PLA and PLA-PEG copolymer monolithic disk implants containing gentamicin sulfate were compared *in vitro* [130]. PLA-PEG copolymers released antibiotics faster and exhibited more pronounced inhibitory effects against *E. coli* over PLA homopolymers matrices, due to increased PEG-PLA hydrophilicity, hydration rates, drug dispersion, and PEG-assisted swelling characteristics.

Biodegradable polyhydroxyalkanoates (PHA) have also drawn substantial interest, claimed to be superior to PLGA for two primary reasons. First, as a polyester of biological origin, PHA is considered environmentally preferable. Second, PHA can be chemically and physically tailored to produce diverse physicochemical properties of clinical relevance, such as piezoelectricity claimed to induce new bone formation on load-bearing sites, and drug loading compatibility for release control [181, 182]. Sulperazone® (sulbactam-cefoperazone 1:1)- and Duocid® (sulbactam-ampicillin 1:1)-loaded poly(3-hydroxybutyrate-co-4-hydroxyvalerate), (P(3-HB-co-4-HB)) rods were reported [183] as effective biodegradable implants to treat osteomyelitis. In this *in vivo* study, a hemolytic strain of *S. aureus* was directly delivered into the medullary cavity of rabbit tibiae. Surgery sites were almost completely healed at 6 weeks using these antibiotic-loaded P(3-HB-co-4-HB) intramedullary implants.

The increasing clinical use of orthopedic devices, their well-known integration issues with host tissues, and needs for improved bone defect solutions all provide new, compelling opportunities for developing novel combination device-drug delivery products with long-term osteoinductive and antimicrobial efficiency integrated into functional orthopedic implants. This challenge, combined with exciting new developments in bone biology and molecular medicine, provides a versatile set of new components for novel device designs. While biologically derived mitogens and morphogens are current attractive candidates (since modern proteomics, genomics and signaling mechanistic elucidation has identified and validated their innate biological importance), they exhibit certain unattractive recombinant cost development structures and more practical bioactivity and stability issues associated with any bioactive protein

formulated into a polymer delivery system. Hence, more attractive pharma options include discovery of potent non-biological mitogen and morphogen small molecule surrogates that recapitulate the relevant biological signaling cascades *in vivo* without need for exogenous specific chemokine or cytokine release [184]. This would allow significant dose and formulating flexibility currently unavailable.

Mitogenic and morphogenic agent release for device integration and tissue regeneration

As described above in orthopedic applications, the expanding availability of increasingly diverse types of endogenous growth factors (cytokines, chemokines) and elucidation of their innate biological control mechanisms have prompted an explosion of interest in their adaptations for use in producing clinically important amounts of tissue in regenerative medicine and tissue engineering [185]. Another important application would be to enhance and accelerate implant device-tissue integration to mitigate clinical problems as discussed above in section 7 [186-188]. Continual discoveries in both cytokine mitogens (producing cell proliferation) and morphogens (producing cell phenotypic alterations and differentiation), and chemokines across virtually all major tissue types have prompted generic approaches to growth factor delivery using controlled release [189] as well as specific growth factors delivered for specific goals, including neovasculogenesis [190, 191], bone neogenesis [125], and neurogenesis [192], along with many other tissue engineering examples [193]. Because of the short half-life, pleiotropism, dynamic interaction and inter-controls in signaling, and rapid turnover of many growth factors *in vivo*, exogenesis introduction of these bioactive agents to promote local controlled tissue responses, tissue engineering and regenerative medicine must

consider strategies to control growth factor release and therapeutically relevant bioavailability. Current costs for producing and formulating these agents also limits dosing.

Combination devices are ideally suited to overcome many of these challenges to either release or induce the local cellular environment around the implanted device to produce therapeutic levels of mitogens or morphogens directly at tissue sites, from device surfaces, and within tissue engineered matrices. The challenges are not trivial: reliable protein and gene delivery is difficult (even locally), formulation into release matrices is inefficient, control of natural cycles and pharmacodynamics is not possible, and current knowledge about how to recapitulate specific cell signaling cascades to produce effective tissue growth without adverse side effects (angioma, fibrosis, ectopic mineralization) is woefully incomplete. Nonetheless, this represents an important frontier where true bioactive molecular and cellular signaling might be exploited onto and into implanted devices using natural cascades to therapeutic ends. Important clinical endpoints are therapeutic angiogenesis, enhanced functional tissue regeneration, and improved device integration and biocompatibility with host tissue.

Other drug/device combination products

Wound dressings

CardioTech International, Inc. (Woburn, MA, USA) just received FDA approval to market an antibiotic-containing hydrogel wound and burn dressing intended for use in the management of partial and full-thickness wounds including venous stasis ulcers, diabetic ulcers, pressure sores, blisters, superficial wounds, abrasions, lacerations and

donor sites. The wound contact surface comprises a hydrogel containing mixed antibiotic components including neomycin sulfate, bacimicin zinc and polymyxin B sulphate (10,000 Units). A second outer layer consists of a polymeric film [194]. The combination of wound dressing with direct antibiotic release provides obvious advantages over traditional wound dressings in preventing bacterial infection, especially in high-risk patients.

Cerebrospinal shunts

Infection remains a major clinical complication for use of cerebrospinal fluid (CSF) shunts and is usually managed by shunt removal, temporary insertion of an external drainage and implantation of a new shunt system. Morbidity and costs associated with this cyclic replacement process throughout the life of patients with hydrocephalus are profound. Rifampin-loaded silicone ventricular catheters capable of releasing rifampin in bacteriocidal concentrations beyond 2 months were used to prevent *S. epidermidis* and *S. aureus* colonization and infection *in vitro* and *in vivo* in a rabbit CSF infection model [195]. In contrast to control groups, no animals with rifampin-loaded catheters exhibited clinical signs of infection. After animal sacrifice, no culturable bacteria (e.g., from catheter, brain tissue, CSF, blood) were found in drug-releasing shunts, in contrast to control catheters.

Dexamethasone release and fibrosis

Implant-localized fibrosis results frequently from foreign body reactions. While some implant devices (e.g., hernial or abdominal repair meshes) may actually become stabilized by such avascular in-growth, other devices including many catheters and

sensors that require specific communication with host tissues are significantly and adversely affected. Corticosteroids including dexamethasone have therefore been used to reduce acute inflammatory events responsible for fibrosis, including attenuation of inflammatory cell cascades, fibroblastic recruitment and collagen production in implant sites.[196]. Locally released drug from polymer coatings on the implant, or polymer-drug microspheres in the wound site have been reported for cardiac pacing electrode tips (pacemaker leads) and implantable electro-biosensors monitoring blood glucose levels in diabetes management. Devices lacking local device-based drug release are affected by implant-associated fibrosis that limits device-tissue communication, either electrically or biochemically. Double-blinded clinical studies compared identical electrode configurations (Medtronic, Minneapolis, MN) with and without loaded steroid (dexamethasone) over long time periods *in vivo* (6-months to 2-year follow-up periods) [197, 198]. Constant pacing pulse duration thresholds were shown for the steroid-releasing leads, while control leads without steroids showed a significant rise in pacing thresholds. A more recent clinical study confirmed excellent performance of pacemaker leads containing dexamethasone sodium phosphate and dexamethasone acetate [199]. PLGA microspheres alone or PLGA microsphere/poly(vinyl alcohol (PVA) hydrogel composites releasing dexamethasone have been implanted subcutaneously into rats and investigated *in vitro* and *in vivo* as a conjunctive therapy with implantable sensors [200, 201]. Dexamethasone release from PLGA microsphere/PVA hydrogel composites exhibited approximately zero-order kinetics. These composites demonstrated some *in vivo* capability to modulate both acute and chronic inflammatory responses, and minimized fibrosis adjacent to the implants [200, 201]. Such composite coating design

provides some versatility for combination devices for altering drug dosing via microsphere loading into the hydrogel matrix, as well as through microsphere composition, and mixed microsphere-based dual drug administration. By contrast, glucose reporting performance of biomedical polyurethane-coated amperometric glucose sensors subdermally implanted into dogs for weeks was not significantly affected by local dexamethasone release from the polyurethane [202].

New approaches to deliver antimicrobial agents

Several studies have aimed to construct novel triggered drug delivery systems that release antimicrobials at specific locations at required times. These new systems are usually triggered by certain endogenous host infection responses such as inflammation-related enzymes, thrombin activity or microbial proteases. Drug-conjugated polymers [203] synthesized using 1,6-hexane diisocyanate (HDI), polycaprolactone diol (PCL), and the fluoroquinolone antibiotic, ciprofloxacin, polymerized into the polymer backbone release drug as the polymer degrades by an inflammatory cell-derived enzyme, cholesterol esterase. Microbiological assessment showed that released ciprofloxacin possessed antimicrobial activity against *P. aeruginosa* after 10 days. However, in this polymer design, the enzyme does not specifically cleave precisely at the drug conjugation position in the polymer backbone. Additionally, general hydrolysis can also degrade the polymer. Hence, fragments of ciprofloxacin bonded to different PCL and/or HDI fragments may not display antimicrobial activity and could also induce cell toxicity. Combinations of different enzymatically labile polymer-drug linkages and modification of the degradable polymer chemistry may solve this problem [204]. Significant increases in thrombin-like activity were reported in *S. aureus*-infected wounds [205]. These

workers then developed a novel peptide to link an insoluble polymer matrix with antimicrobials specifically cleaved by thrombin [206]. A poly(vinyl alcohol)-peptide-gentamicin conjugate was developed and investigated both *in vitro* and *in vivo*. Released gentamicin amounts were dependent on local thrombin concentration associated with *S. aureus* infection with bacteriocidal effects observed in animal models of *S. aureus* infection.

These two sophisticated, new polymer-drug conjugate examples provide some new directions for future controlled, local antimicrobial release strategies. Triggered or stimuli-sensitive approaches to new combination medical devices, prompting antimicrobial or more general drug release with pre-programmed temporal and spatial profiles are possible. Poly(vinyl alcohol) is a candidate occlusive wound dressing material; HDI and PCL could also be co-processed to form a biodegradable implantable device. Furthermore, new discoveries in microbiological phenotypes, proteomics and infection mechanisms should allow development of new pathogen-specific cleavable conjugates, new classes of drugs and new anti-adhesive or anti-proliferative pharmacological targets exploited in combination with implantable devices. This strategy could borrow from better-developed enzyme-cleavable or targeted pharmaceutical approaches for polymer-prodrug formulations in other therapeutic areas [207-209].

Conclusions

With the recent proven clinical success of precedent DES systems, recognition of the therapeutic value of locally released antimicrobials in several clinical device classes including catheters and bone cements, and launch of an antibiotic wound dressing, local

drug delivery/device combination therapy is becoming an exciting new biomedical frontier, with associated diverse creative strategies newly available. For many reasons, the surface of any indwelling medical device provides an excellent platform for the formation of bacterial colonies or biofilms, producing life-threatening infections across most types of implanted devices. In the case of anti-microbial strategies, many different biomaterial approaches, different polymer coating chemistries and architectures, and different antibiotics have been studied and, taken together, exhibit unique opportunities to help mitigate device-related infections. These medical devices also provide drug reservoirs for local delivery to infection sites with minimal systemic toxicity, and capabilities for advanced pharmacokinetics, drug mixtures, complex release mechanisms and site-sensitive stimulated release controls. For other types of medical device functional and integrative challenges, combination approaches that utilize new developments in local cell, tissue and molecular biology manipulation might be accomplished. These include new activities from delivered mitogens and morphogens, controlled apoptosis and differentiation, enhanced host cell recruitment, tissue regeneration, wound healing, vasculogenesis, and tissue-implant integration, along with limited destructive inflammatory reactions, infection and fibrosis. Increasing appreciation for host tissue biology in the implant site will lead to breakthroughs in this area where combination therapies might readily assist.

With the establishment of US FDA's Office of Combination Products and other equivalent oversite organizations world-wide, exciting device precedents, clinical successes, and corresponding new codes, pharmaceutical companies and device manufactures are actively seeking development opportunities for new drug/device

combination products based on their existing drug and device products. This could result in a blurring of business plans between traditional drug and biomedical device companies as the two approaches slowly converge in the combination sector, and readily require the synergy of closely partnered interaction (or even mergers) to fully capitalize on innovative combination products. Additionally, combination devices up for FDA approval that exploit advantages of an already-approved therapeutic entity could enjoy expedited approval [1]. While this provides the most direct route to product, improved performance might better be gained from *de novo* device design that anticipates and exploits drug delivery and device *in vivo* performance from *de novo* design conception.

In order to take experimental model studies into reliable clinical use, many further issues must be considered and resolved. Device biomaterials must remain biocompatible in the presence of drug modifications, and in some cases, biodegradable materials are preferred to produce required drug release control and duration. Bacterial resistance to antimicrobials, especially to locally released antibiotics must be carefully considered and monitored precisely at the point of delivery. Mechanical and other functional medical device performance properties must not be compromised by combination with drug/antimicrobial release and associated manufacturing processes. Significantly, the commonly observed disconnect between *in vitro* and *in vivo* efficacy and pharmacology testing must be overcome with direct validation in a clinical context: mechanisms of action and therapeutic benefit should be clearly elucidated and not remain anecdotal.

Acknowledgements

The authors appreciate useful perspectives from H. Busscher and J. van Horn (Royal University of Groningen, The Netherlands), K. Ward (iSense, Inc., USA), and H.

Schweitzer (Colorado State University, USA), and constructive review comments from referees to improve the communication quality.

References

[1] Dubin CH. A One-Two Punch: Drug/Medical Device Combination Products are Taking Healthcare in a New Direction. Is the Pharmaceutical Industry Prepared? Drug Deliv Technol 2004;4(4).

[2] United States Food and Drug Administration; 21 CFR ?3.2(e); European Commission DG Enterprise, Directorate G, Unit 4, MEDDEV 2.1/3 rev 2 (Council Directive 90/385/EEC, 65/65/EEC and 93/42/EEC), see http://europa.eu.int/comm/enterprise/medical_devices/meddev/2_1_3___07-2001.pdf.

[3] Ansel HC, Popovich NG, Loyd V. Allen J. Pharmaceutical Dosage Forms and Drug Delivery Systems. 6 ed. Media: Williams & Wikins, 1995.

[4] Liu S-J, Ueng SW-N, Lin S-S, Chan E-C. In vivo release of vancomycin from biodegradable beads. J Biomed Mater Res 2002;63(6):807-813.

[5] Gransden WR. Antibiotic resistance. Nosocomial gram-negative infection. J Med Microbiol 1997;46(6):436-439.

[6] Zhang X, Wyss UP, Pichora D, Goosen MFA. Biodegradable controlled antibiotic release devices for osteomyelitis: optimization of release properties. J Pharm Pharmacol 1994;46(9):718-724.

[7] Khardori N, Yassien M. Biofilms in device-related infections. J Ind Microbiol 1995;15(3):141-147.

[8] Gristina AG, Naylor P, Myrvik Q. Infections from biomaterials and implants: a race for the surface. Med Prog Technol 1988-89;14(3-4):205-224.

[9] Stoodley P, Sauer K, Davies DG, Costerton JW. Biofilms as complex differentiated communities. Annu Rev Microbiol 2002;56:187-209.

[10] Finch RG, Pritchard DI, Bycroft BW, Williams P, Stewart GSAB. Quorum sensing: a novel target for anti-infective therapy. J Antimicrob Chemother 1998;42(5):569-571.

[11] March JC, Bentley WE. Quorum sensing and bacterial cross-talk in biotechnology. Curr Opin Biotechnol 2004;15(5):495-502.

[12] Barton AJ, Sagers RD, Pitt WG. Bacterial adhesion to orthopedic implant polymers. J Biomed Mater Res 1996;30(3):403-410.

[13] Roberts RR, Scott RD, 2nd, Cordell R, Solomon SL, Steele L, Kampe LM, et al. The use of economic modeling to determine the hospital costs associated with nosocomial infections. Clin Infect Dis 2003;36(11):1424-1432.

[14] Stone PW, Larson E, Kawar LN. A systematic audit of economic evidence linking nosocomial infections and infection control interventions: 1990-2000. Am J Infect Control 2002;30(3):145-152.

[15] Haley RW, Culver DH, White JW, Morgan WM, Emori TG. The nationwide nosocomial infection rate. A new need for vital statistics. Am J Epidemiol 1985;121(2):159-167.

[16] Pascual A. Pathogenesis of catheter-related infections: lessons for new designs. Clin Microbiol Infect 2002;8(5):256-264.

[17] Gruntzig A. Transluminal dilatation of coronary-artery stenosis. Lancet 1978;1:263.

[18] Fattori R, Piva T. Drug-eluting stents in vascular intervention. Lancet 2003;361(9353):247-249.

[19] Fischman DL, Leon MB, Baim DS, Schatz RA, Savage MP, Penn I, et al. A randomized comparison of coronary-stent placement and balloon angioplasty in the treatment of coronary artery disease. Stent Restenosis Study Investigators. N Engl J Med 1994;331(8):496-501.

[20] Serruys PW, de Jaegere P, Kiemeneij F, Macaya C, Rutsch W, Heyndrickx G, et al. A comparison of balloon-expandable-stent implantation with balloon angioplasty in patients with coronary artery disease. Benestent Study Group. N Engl J Med 1994;331(8):489-495.

[21] Meads C, Cummins C, Jolly K, Stevens A, Burls A, Hyde C. Coronary artery stents in the treatment of ischaemic heart disease: a rapid and systematic review. Health Technol Assess 2000;4(23):1-153.

[22] Indolfi C, Mongiardo A, Curcio A, Torella D. Molecular Mechanisms of In-Stent Restenosis and Approach to Therapy with Eluting Stents. Trends Cardiovasc Med 2003;13(4):142-148.

[23] Serruys PW, Foley DP, Jackson G, Bonnier H, Macaya C, Vrolix M, et al. A randomized placebo-controlled trial of fluvastatin for prevention of restenosis after successful coronary balloon angioplasty: Final results of the fluvastatin angiographic restenosis (FLARE) trial. Eur Heart J 1999;20(1):58-69.

[24] Serruys PW, Foley DP, Pieper M, Kleijne JA, De Feyter PJ. A multicentre randomized placebo controlled clinical trial of trapidil for prevention of restenosis after coronary stenting, measured by 3-D intravascular ultrasound. Eur Heart J 2001;22(20):1938-1947.

[25] Holmes DR, Jr., Savage M, LaBlanche JM, Grip L, Serruys PW, Fitzgerald P, et al. Results of prevention of restenosis with tranilast and its outcomes (PRESTO) trial. Circulation 2002;106(10):1243-1250.

[26] Birkenhauer P, Yang Z, Gander B. Preventing restenosis in early drug-eluting stent era: Recent developments and future perspectives. J Pharm Pharmacol 2004;56(11):1339-1356.

[27] Chan S. Targeting the mammalian target of rapamycin (mTOR): a new approach to treating cancer. Br J Cancer 2004;91(8):1420-1424.

[28] Poon M, Badimon Juan J, Fuster V. Overcoming restenosis with sirolimus: from alphabet soup to clinical reality. Lancet 2002;359(9306):619-622.

[29] Morice M-C, Serruys PW, Sousa JE, Fajadet J, Hayashi EB, Perin M, et al. A randomized comparison of a sirolimus-eluting stent with a standard stent for coronary revascularization. N Engl J Med 2002;346(23):1773-1780.

[30] Moses JW, Leon MB, Popma JJ, Fitzgerald PJ, Holmes DR, O'Shaughnessy C, et al. Sirolimus-eluting stents versus standard stents in patients with stenosis in a native coronary artery. N Engl J Med 2003;349(14):1315-1323.

[31] Schofer J, Schluter M, Gershlick AH, Wijns W, Garcia E, Schampaert E, et al. Sirolimus-eluting stents for treatment of patients with long atherosclerotic lesions in small coronary arteries: double-blind, randomised controlled trial (E-SIRIUS). Lancet 2003;362(9390):1093-1099.

[32] Lemos P, A., Serruys P, W., van Domburg RT, Saia F, Arampatzis CA, Hoye A, et al. Unrestricted utilization of sirolimus-eluting stents compared with conventional bare stent implantation in the "real world": the rapamycin-eluting stent evaluated at rotterdam cardiology hospital (RESEARCH) registry. Circulation 2004;109(2):190-195.

[33] Tanabe K, Regar E, Lee CH, Hoye A, van der Giessen WJ, Serruys PW. Local drug delivery using coated stents: New developments and future perspectives. Curr Pharm Des 2004;10(4):357-367.

[34] Yamaguchi T. Drug-eluting stent trial. Cardiac Practice 2004;15(4):417-419.

[35] Schwartz RS, Chronos NA, Virmani R. Preclinical restenosis models and drug-eluting stents :still important, still much to learn. J Am Coll Cardiol 2004;44(7):1373-1385.

[36] Robinson KA, Chronos NA, Schieffer E, Palmer SJ, Cipolla GD, Milner PG, et al. Endoluminal local delivery of PCNA/cdc2 antisense oligonucleotides by porous balloon catheter does not affect neointima formation or vessel size in the pig coronary artery model of postangioplasty restenosis. Cathet Cardiovasc Diagn 1997;41(3):348-353.

[37] Stone GW, Ellis SG, Cox DA, Hermiller J, O'Shaughnessy C, Mann JT, et al. A polymer-based, paclitaxel-eluting stent in patients with coronary artery disease. N Engl J Med 2004;350(3):221-231.

[38] Morice M-C. REALITY Trial Data. American College of Cardiology Annual Meeting 2005.

[39] Degertekin M, Serruys Patrick W, Tanabe K, Lee Chi H, Sousa JE, Colombo A, et al. Long-term follow-up of incomplete stent apposition in patients who received sirolimus-eluting stent for de novo coronary lesions: an intravascular ultrasound analysis. Circulation 2003;108(22):2747-2750.

[40] Eberhart RC, Su S-H, Nguyen Kytai T, Zilberman M, Tang L, Nelson KD, et al. Bioresorbable polymeric stents: current status and future promise. J Biomater Sci Polym Ed 2003;14(4):299-312.

[41] Herrmann R, Schmidmaier G, Markl B, Resch A, Hahnel I, Stemberger A, et al. Antithrombogenic coating of stents using a biodegradable drug delivery technology. Thromb Haemost 1999;82(1):51-57.

[42] Hietala E-M, Salminen U-S, Stahls A, Valimaa T, Maasilta P, Tormala P, et al. Biodegradation of the copolymeric polylactide stent: long-term follow-up in a rabbit aorta model. J Vasc Res 2001;38(4):361-369.

[43] Rodgers Campbell DK. Drug-eluting stents: role of stent design, delivery vehicle, and drug selection. Rev Cardiovasc Med 2002;3 Suppl 5:S10-15.

[44] Hwang C-W, Wu D, Edelman Elazer R. Impact of transport and drug properties on the local pharmacology of drug-eluting stents. International journal of cardiovascular interventions 2003;5(1):7-12.

[45] Hwang C-W, Edelman ER. Arterial ultrastructure influences transport of locally delivered drugs. Circ Res 2002;90(7):826-832.

[46] Finkelstein A, McClean D, Kar S, Takizawa K, Varghese K, Baek N, et al. Local drug delivery via a coronary stent with programmable release pharmacokinetics. Circulation 2003;107(5):777-784.

[47] Shammas NW, Dippel EJ. Evidence-based Management of Peripheral Vascular Disease. Curr Atheroscler Rep 2005;7(5):358-363.

[48] Carter AJ, Robinson K, Gibson L, Haller S, Brodeur A, Collingwood R, et al. Experimental Feasibility and Efficacy of a Novel Modular Segmented Stent with In-situ Programmable Length and Drug Elution from a Biodegradable Polymer Coating. Am J Cardiol 2005;96(suppl 7A):7H.

[49] Lorenzo A. Xtent debuts customizable stents to positive reviews. Med Dev Daily 2005;9(203):1.

[50] van Berkel AM, van Marle J, Groen AK, Bruno MJ. Mechanisms of biliary stent clogging: confocal laser scanning and scanning electron microscopy. Endoscopy 2005;37(8):729-734.

[51] Chatzinikolaou I, Raad II. Central venous catheter related infections: the role of antimicrobial catheters. Molecular and Cellular Biology of Critical Care Medicine 2003;3(Immunology and Infectious Disease):187-215.

[52] Viot M. Intravenous access: related problems in oncology. Int J Antimicrob Agents 2000;16(2):165-168.

[53] Pai MP, Pendland SL, Danziger LH. Antimicrobial-coated/bonded and -impregnated intravascular catheters. Ann Pharmacother 2001;35(10):1255-1263.

[54] Jagpal R, Greco RS. Studies of a graphite-benzalkonium-oxacillin surface. Am Surg 1979;45(12):774-779.

[55] Greco RS, Harvey RA. The role of antibiotic bonding in the prevention of vascular prosthetic infections. Ann Surg 1982;195(2):168-171.

[56] Kamal GD, Pfaller MA, Rempe LE, Jebson PJ. Reduced intravascular catheter infection by antibiotic bonding. A prospective, randomized, controlled trial. JAMA 1991;265(18):2364-2368.

[57] Zhang X. Anti-infective coatings reduce device-related infections. Antimicrob/Anti-infect Mater 2000:149-180.

[58] Schierholz JM, Rump AF, Pulverer G, Beuth J. Anti-infective catheters: novel strategies to prevent nosocomial infections in oncology. Anticancer Res 1998;18(5B):3629-3638.

[59] Raad I, Darouiche R, Hachem R, Mansouri M, Bodey GP. The broad-spectrum activity and efficacy of catheters coated with minocycline and rifampin. J Infect Dis 1996;173(2):418-424.

[60] Darouiche RO, Raad II, Heard SO, Thornby JI, Wenker OC, Gabrielli A, et al. A comparison of two antimicrobial-impregnated central venous catheters. Catheter Study Group. N Engl J Med 1999;340(1):1-8.

[61] Veenstra DL, Saint S, Saha S, Lumley T, Sullivan SD. Efficacy of antiseptic-impregnated central venous catheters in preventing catheter-related bloodstream infection: a meta-analysis. JAMA 1999;281(3):261-267.

[62] Marik PE, Abraham G, Careau P, Varon J, Fromm RE, Jr. The ex vivo antimicrobial activity and colonization rate of two antimicrobial-bonded central venous catheters. Crit Care Med 1999;27(6):1128-1131.

[63] Raad I, Darouiche R, Dupuis J, Abi-Said D, Gabrielli A, Hachem R, et al. Central venous catheters coated with minocycline and rifampin for the prevention of catheter-related colonization and bloodstream infections. A randomized, double-blind trial. Ann Intern Med 1997;127(4):267-274.

[64] Raad II, Darouiche RO, Hachem R, Abi-Said D, Safar H, Darnule T, et al. Antimicrobial durability and rare ultrastructural colonization of indwelling central catheters coated with minocycline and rifampin. Crit Care Med 1998;26(2):219-224.

[65] Raad II, Hanna HA. Intravascular catheter-related infections new horizons and recent advances. Arch Intern Med 2002;162(8):871-878.

[66] Maki DG, Stolz SM, Wheeler S, Mermel LA. Prevention of central venous catheter-related bloodstream infection by use of an antiseptic-impregnated catheter. A randomized, controlled trial. Ann Intern Med 1997;127(4):257-266.

[67] Bach A, Schmidt H, Boettiger B, Schreiber B, Boehrer H, Motsch J, et al. Retention of antibacterial activity and bacterial colonization of antiseptic-bonded central venous catheters. J Antimicrob Chemother 1996;37(2):315-322.

[68] George SJ, Vuddamalay P, Boscoe MJ. Antiseptic-impregnated central venous catheters reduce the incidence of bacterial colonization and associated infection in immunocompromised transplant patients. Eur J Anaesthesiol 1997;14(4):428-431.

[69] Heard SO, Wagle M, Vijayakumar E, McLean S, Brueggemann A, Napolitano LM, et al. Influence of triple-lumen central venous catheters coated with chlorhexidine and silver sulfadiazine on the incidence of catheter-related bacteremia. Arch Intern Med 1998;158(1):81-87.

[70] Loo S, van Heerden PV, Gollege CL, Roberts BL, Power BM. Infection in central lines: antiseptic-impregnated vs standard non-impregnated catheters. Anaesth Intensive Care 1997;25(6):637-639.

[71] Tennenberg S, Lieser M, McCurdy B, Boomer G, Howington E, Newman C, et al. A prospective randomized trial of an antibiotic- and antiseptic-coated central venous catheter in the prevention of catheter-related infections. Archives of surgery (Chicago, Ill : 1960) 1997;132(12):1348-1351.

[72] van Heerden PV, Webb SA, Fong S, Golledge CL, Roberts BL, Thompson WR. Central venous catheters revisited--infection rates and an assessment of the new Fibrin Analysing System brush. Anaesth Intensive Care 1996;24(3):330-333.

[73] Logghe C, Van Ossel C, D'Hoore W, Ezzedine H, Wauters G, Haxhe JJ. Evaluation of chlorhexidine and silver-sulfadiazine impregnated central venous catheters for the prevention of bloodstream infection in leukaemic patients: a randomized controlled trial. J Hosp Infect 1997;37(2):145-156.

[74] Pemberton LB, Ross V, Cuddy P, Kremer H, Fessler T, McGurk E. No difference in catheter sepsis between standard and antiseptic central venous catheters. A prospective randomized trial. Archives of surgery (Chicago, Ill : 1960) 1996;131(9):986-989.

[75] Ciresi DL, Albrecht RM, Volkers PA, Scholten DJ. Failure of antiseptic bonding to prevent central venous catheter-related infection and sepsis. Am Surg 1996;62(8):641-646.

[76] Ellis ME, Rhydderch D, Zwaan F, Guy ML, Baillie F. High incidence of line-related infection and mechanical failure of an antiseptic impregnated central venous catheter in highly immunocompromised patients. Scand J Infect Dis 1996;28(1):91-93.

[77] Gaonkar TA, Modak SM. Comparison of microbial adherence to antiseptic and antibiotic central venous catheters using a novel agar subcutaneous infection model. J Antimicrob Chemother 2003;52(3):389-396.

[78] Yorganci K, Krepel C, Weigelt JA, Edmiston CE. In vitro evaluation of the antibacterial activity of three different central venous catheters against Gram-positive bacteria. Eur J Clin Microbiol Infect Dis 2002;21(5):379-384.

[79] Schierholz JM, Fleck C, Beuth J, Pulverer G. The antimicrobial efficacy of a new central venous catheter with long-term broad-spectrum activity. J Antimicrob Chemother 2000;46:45-50.

[80] Yuecel N, Lefering R, Maegele M, Max M, Rossaint R, Koch A, et al. Reduced colonization and infection with miconazole-rifampicin modified central venous catheters: a randomized controlled clinical trial. J Antimicrob Chemother 2004;54(6):1109-1115.

[81] Levy SB. Antibiotic resistance - the problem intensifies. Adv Drug Deliv Rev 2005;57(10):1446-1450.

[82] Costerton JW, Stewart PS. Battling biofilms. Sci Am 2001;285(1):74-81.

[83] Virk A, Steckelberg JM. Clinical aspects of antimicrobial resistance. Mayo Clin Proc 2000;75(2):200-214.

[84] Tambe SM, Sampath L, Modak SM. In vitro evaluation of the risk of developing bacterial resistance to antiseptics and antibiotics used in medical devices. J Antimicrob Chemother 2001;47(5):589-598.

[85] Trooskin SZ, Mikulaschek AW. Biomaterials used for catheters. Implant Biol 1994:267-286.

[86] Szycher M, Editor. Biocompatible Polymers, Metals, and Composites. Lancaster, PA: Technomic, 1983.

[87] Crocker KS, Devereaux GB, Ashmore DL, Coker MH. Clinical evaluation of elastomeric hydrogel peripheral catheters during home infusion therapy. J Intraven Nurs 1990;13(2):89-97.

[88] Piozzi A, Francolini I, Occhiaperti L, Venditti M, Marconi W. Antimicrobial activity of polyurethanes coated with antibiotics: a new approach to the realization of medical devices exempt from microbial colonization. Int J Pharm 2004;280(1-2):173-183.

[89] Raad I, Buzaid A, Rhyne J, Hachem R, Darouiche R, Safar H, et al. Minocycline and ethylenediaminetetraacetate for the prevention of recurrent vascular catheter infections. Clin Infect Dis 1997;25(1):149-151.

[90] Pearson ML, Abrutyn E. Reducing the risk for catheter-related infections: a new strategy. Ann Intern Med 1997;127(4):304-306.

[91] Crnich CJ, Maki DG. Are antimicrobial-impregnated catheters effective? Don't throw out the baby with the bathwater. Clin Infect Dis 2004;38(9):1287-1292.

[92] McConnell SA, Gubbins PO, Anaissie EJ. Are antimicrobial-impregnated catheters effective? Replace the water and grab your washcloth, because we have a baby to wash. Clin Infect Dis 2004;39(12):1829-1833.

[93] Haley RW, Hooton TM, Culver DH, Stanley RC, Emori TG, Hardison CD, et al. Nosocomial infections in U.S. hospitals, 1975-1976: estimated frequency by selected characteristics of patients. Am J Med 1981;70(4):947-959.

[94] Cho YW, Park JH, Kim SH, Cho Y-h, Choi JM, Shin HJ, et al. Gentamicin-releasing urethral catheter for short-term catheterization. J Biomater Sci Polym Ed 2003;14(9):963-972.

[95] Darouiche RO. Device-associated infections: a macroproblem that starts with microadherence. Clin Infect Dis 2001;33(9):1567-1572.

[96] Cormio L, La Forgia P, Siitonen A, Ruutu M, Tormala P, Talja M. Immersion in antibiotic solution prevents bacterial adhesion onto biodegradable prostatic stents. Br J Urol 1997;79(3):409-413.

[97] Cormio L, La Forgia P, La Forgia D, Siitonen A, Ruutu M. Bacterial Adhesion to Urethral Catheters: Role of Coating Materials and Immersion in Antibiotic Solution. Eur Urol 2001;40(3):354-359.

[98] Melaiye A, Youngs WJ. Silver and its application as an antimicrobial agent. Expert Opinion on Therapeutic Patents 2005;15(2):125-130.

[99] Saint S, Elmore JG, Sullivan SD, Emerson SS, Koepsell TD. The efficacy of silver alloy-coated urinary catheters in preventing urinary tract infection: a meta-analysis. Am J Med 1998;105(3):236-241.

[100] Liedberg H. Catheter induced urethral inflammatory reaction and urinary tract infection. An experimental and clinical study. Scand J Urol Nephrol Suppl 1989;124:1-43.

[101] Brosnahan J, Jull A, Tracy C. Types of urethral catheters for management of short-term voiding problems in hospitalised adults. J Urol 2005;173(3):846-847.

[102] Ahearn DG, Grace DT, Jennings MJ, Borazjani RN, Boles KJ, Rose LJ, et al. Effects of hydrogel/silver coatings on in vitro adhesion to catheters of bacteria associated with urinary tract infections. Curr Microbiol 2000;41(2):120-125.

[103] Maki DG, Tambyah PA. Engineering out the risk for infection with urinary catheters. Emerg Infect Dis 2001;7(2):342-347.

[104] Bologna RA, Tu LM, Polansky M, Fraimow HD, Gordon DA, Whitmore KE. Hydrogel/silver ion-coated urinary catheter reduces nosocomial urinary tract infection rates in intensive care unit patients: a multicenter study. Urology 1999;54(6):982-987.

[105] Verleyen P, De Ridder D, Van Poppel H, Baert L. Clinical application of the Bardex IC Foley catheter. Eur Urol 1999;36(3):240-246.

[106] Darouiche RO, Smith JA, Jr., Hanna H, Dhabuwala CB, Steiner MS, Babaian RJ, et al. Efficacy of antimicrobial-impregnated bladder catheters in reducing catheter-associated bacteriuria: a prospective, randomized, multicenter clinical trial. Urology 1999;54(6):976-981.

[107] Silver S. Bacterial silver resistance: molecular biology and uses and misuses of silver compounds. FEMS Microbiol Rev 2003;27(2-3):341-353.

[108] Richards CL, Hoffman KC, Bernhard JM, Winslow SD, Norman JC, Whalen RL. Development and characterization of an infection inhibiting urinary catheter. ASAIO J 2003;49(4):449-453.

[109] Al-Habdan I, Sadat-Ali M, Corea James R, Al-Othman A, Kamal Baher A, Shriyan Devdas S. Assessment of nosocomial urinary tract infections in orthopaedic patients: a prospective and comparative study using two different catheters. Int Surg 2003;88(3):152-154.

[110] Nishiguchi S, Kato H, Fujita H, Oka M, Kim HM, Kokubo T, et al. Titanium metals form direct bonding to bone after alkali and heat treatments. Biomaterials 2001;22(18):2525-2533.

[111] Sporer SM, Paprosky WG. Biologic fixation and bone ingrowth. Orthop Clin North Am 2005;36(1):105-111, vii.

[112] Hirakawa K, Jacobs Joshua J, Urban R, Saito T. Mechanisms of failure of total hip replacements: lessons learned from retrieval studies. Clin Orthop 2004;(420):10-17.

[113] Morscher EW. Failures and successes in total hip replacement--why good ideas may not work. Scandinavian journal of surgery 2003;92(2):113-120.

[114] Praemer A, Furner S, Rice DP. Musculoskeletal Conditions in the United States. Park Ridge, IL: American Academy of Orthopedic Surgeons, 1992.

[115] Gerstenfeld LC, Cullinane DM, Barnes GL, Graves DT, Einhorn TA. Fracture healing as a post-natal developmental process: Molecular, spatial, and temporal aspects of its regulation. J Cell Biochem 2003;88(5):873-884.

[116] Samartzis D, Khanna N, Shen Francis H, An Howard S. Update on bone morphogenetic proteins and their application in spine surgery. J Am Coll Surg 2005;200(2):236-248.

[117] Luginbuehl V, Meinel L, Merkle HP, Gander B. Localized delivery of growth factors for bone repair. Eur J Pharm Biopharm 2004;58(2):197-208.

[118] Leach JK, Mooney DJ. Bone engineering by controlled delivery of osteoinductive molecules and cells. Expert Opin Biol Ther 2004;4(7):1015-1027.

[119] Kandziora F, Bail H, Schmidmaier G, Schollmeier G, Scholz M, Knispel C, et al. Bone morphogenetic protein-2 application by a poly(D,L-lactide)-coated interbody cage: in vivo results of a new carrier for growth factors. J Neurosurg 2002;97(1, Suppl.):40-48.

[120] Seeherman H, Wozney J, Li R. Bone morphogenetic protein delivery systems. Spine 2002;27(16 Suppl 1):S16-23.

[121] Hannallah D, Peterson B, Lieberman Jay R, Fu Freddie H, Huard J. Gene therapy in orthopaedic surgery. J Bone Joint Surg Am 2002;84(6):1046-1061.

[122] Winn SR, Schmitt JM, Buck D, Hu Y, Grainger D, Hollinger JO. Tissue-engineered bone biomimetic to regenerate calvarial critical-sized defects in athymic rats. J Biomed Mater Res 1999;45(4):414-421.

[123] Arinzeh TL, Tran T, McAlary J, Daculsi G. A comparative study of biphasic calcium phosphate ceramics for human mesenchymal stem-cell-induced bone formation. Biomaterials 2005;26(17):3631-3638.

[124] Petite H, Viateau V, Bensaid W, Meunier A, de Pollak C, Bourguignon M, et al. Tissue-engineered bone regeneration. Nat Biotechnol 2000;18(9):959-963.

[125] Mistry AS, Mikos AG. Tissue engineering strategies for bone regeneration. Adv Biochem Eng Biotechnol 2005;94:1-22.

[126] Winnger DA, Fass RJ. Antibiotic-impregnated cement and beads for orthopedic infections. Antimicrob Agents Chemother 1996;40(12):2675-2679.

[127] Frutos CP, Diez PE, Barrales-Rienda JM, Frutos G. Validation and in vitro characterization of antibiotic-loaded bone cement release. Int J Pharm 2000;209(1-2):15-26.

[128] Baro M, Sanchez E, Delgado A, Perera A, Evora C. In vitro-in vivo characterization of gentamicin bone implants. J Controlled Release 2002;83(3):353-364.

[129] Trippel SB. Antibiotic-impregnated cement in total joint arthroplasty. J Bone Joint Surg Am 1986;68(8):1297-1302.

[130] Huang YY, Chung TW. Microencapsulation of gentamicin in biodegradable PLA and/or PLA/PEG copolymer. J Microencapsul 2001;18(4):457-465.

[131] Yu D, Wong J, Matsuda Y, Fox JL, Higuchi WI, Otsuka M. Self-setting hydroxyapatite cement: a novel skeletal drug delivery system for antibiotics. J Pharm Sci 1992;81(6):529-531.

[132] Harper EJ. Bioactive bone cements. Proc Inst Mech Eng [H] 1998;212(2):113-120.

[133] Stengel D, Bauwens K, Sehouli J, Ekkernkamp A, Porzsolt F. Systematic review and meta-analysis of antibiotic therapy for bone and joint infections. Lancet Infectious Diseases 2001;1(3):175-188.

[134] Edmiston CE, Jr., Goheen MP. Studying bacterial adhesion to antibiotic impregnated polymethyl methacrylate. In: An YH, Friedman RJ, editors. Handbook of Bacterial Adhesion. Totowa, NJ: Humana Press Inc., 2000. p. 599-608.

[135] Kanellakopoulou K, Giamarellos-Bourboulis EJ. Carrier systems for the local delivery of antibiotics in bone infections. Drugs 2000;59(6):1223-1232.

[136] Downes S. Methods for improving drug release from poly(methyl methacrylate) bone cement. Clin Mater 1991;7(3):227-231.

[137] Virto MR, Frutos P, Torrado S, Frutos G. Gentamicin release from modified acrylic bone cements with lactose and hydroxypropylmethylcellulose. Biomaterials 2002;24(1):79-87.

[138] van de Belt H, Neut D, Uges DRA, Schenk W, van Horn JR, van der Mei HC, et al. Surface roughness, porosity and wettability of gentamicin-loaded bone cements and their antibiotic release. Biomaterials 2000;21(19):1981-1987.

[139] Picknell B, Mizen L, Sutherland R. Antibacterial activity of antibiotics in acrylic bone cement. J Bone Joint Surg Br 1977;59-B(3):302-307.

[140] Masri BA, Duncan CP, Beauchamp CP, Paris NJ, Arntorp J. Effect of varying surface patterns on antibiotic elution from antibiotic-loaded bone cement. J Arthroplasty 1995;10(4):453-459.

[141] Elson RA, Jephcott AE, McGechie DB, Verettas D. Bacterial infection and acrylic cement in the rat. J Bone Joint Surg Br 1977;59-B(4):452-457.

[142] Nijhof MW, Stallmann HP, Vogely HC, Fleer A, Schouls LM, Dhert WJA, et al. Prevention of infection with tobramycin-containing bone cement or systemic cefazolin in an animal model. J Biomed Mater Res 2000;52(4):709-715.

[143] Nijhof MW, Fleer A, Hardus K, Vogely HC, Schouls LM, Verbout AJ, et al. Tobramycin-containing bone cement and systemic cefazolin in a one-stage revision. Treatment of infection in a rabbit model. J Biomed Mater Res 2001;58(6):747-753.

[144] Josefsson G, Gudmundsson G, Kolmert L, Wijkstrom S. Prophylaxis with systemic antibiotics versus gentamicin bone cement in total hip arthroplasty. A five-year survey of 1688 hips. Clin Orthop 1990;(253):173-178.

[145] Chiu F-Y, Chen C-M, Lin Chien-Fu J, Lo W-H. Cefuroxime-impregnated cement in primary total knee arthroplasty: a prospective, randomized study of three hundred and forty knees. J Bone Joint Surg Am 2002;84-A(5):759-762.

[146] Scott CP, Higham PA. Antibiotic bone cement for the treatment of Pseudomonas aeruginosa in joint arthroplasty: Comparison of tobramycin and gentamicin-loaded cements. J Biomed Mater Res B Appl Biomater 2003;64B(2):94-98.

[147] Scott CP, Higham PA, Dumbleton JH. Effectiveness of bone cement containing tobramycin. An in vitro susceptibility study of 99 organisms found in infected joint arthroplasty. J Bone Joint Surg Br 1999;81(3):440-443.

[148] Wade A, Reynolds JE. The Extra Pharmacopoeia: Incorporating Squire's "Companion". 27 ed. London: The Pharmaceutical Press, 1977.

[149] Nelson CL, Griffin FM, Harrison BH, Cooper RE. In vitro elution characteristics of commercially and noncommercially prepared antibiotic PMMA beads. Clin Orthop 1992;(284):303-309.

[150] Sterling GJ, Crawford S, Potter JH, Koerbin G, Crawford R. The pharmacokinetics of Simplex-tobramycin bone cement. J Bone Joint Surg Br 2003;85(5):646-649.

[151] Buchholz HW, Elson RA, Heinert K. Antibiotic-loaded acrylic cement: current concepts. Clin Orthop 1984;(190):96-108.

[152] Marks KE, Nelson CL, Lautenschlager EP. Antibiotic-impregnated acrylic bone cement. J Bone Joint Surg Am 1976;58(3):358-364.

[153] Walenkamp GH. Chronic osteomyelitis. Acta Orthop Scand 1997;68(5):497-506.

[154] Heck D, Rosenberg A, Schink-Ascani M, Garbus S, Kiewitt T. Use of antibiotic-impregnated cement during hip and knee arthroplasty in the United States. J Arthroplasty 1995;10(4):470-475.

[155] Fish DN, Hoffman HM, Danziger LH. Antibiotic-impregnated cement use in U.S. hospitals. Am J Hosp Pharm 1992;49(10):2469-2474.

[156] Wahlig H, Dingeldein E, Bergmann R, Reuss K. The release of gentamicin from polymethylmethacrylate beads. An experimental and pharmacokinetic study. J Bone Joint Surg Br 1978;60-B(2):270-275.

[157] Hoff SF, Fitzgerald RH, Kelly PJ. The depot administration of penicillin G and gentamicin in acrylic bone cement. J Bone Joint Surg Am 1981;63-A(5):798-804.

[158] Bunetel L, Segui A, Cormier M, Percheron E, Langlais F. Release of gentamicin from acrylic bone cement. Clin Pharmacokinet 1989;17(4):291-297.

[159] Neut D, Van de Belt H, Stokroos I, Van Horn JR, Van der Mei HC, Busscher HJ. Biomaterial-associated infection of gentamicin-loaded PMMA beads in orthopedic revision surgery. J Antimicrob Chemother 2001;47(6):885-891.

[160] Faber C, Stallmann HP, Lyaruu DM, de Blieck JMA, Bervoets TJM, van Nieuw Amerongen A, et al. Release of antimicrobial peptide Dhvar-5 from polymethyl methacrylate beads. J Antimicrob Chemother 2003;51(6):1359-1364.

[161] Yang J-M, You J-W, Chen H-L, Shih C-H. Calorimetric characterization of the formation of acrylic type bone cements. J Biomed Mater Res 1996;33(2):83-88.

[162] Ricci J, Alexander H, Nadkarni P, Hawkins M, Turner J, Rosenblum S, et al. Biological Mechanisms of Calcium Sulfate Replacement by Bone. In: Davies JE, editor. Bone Engineering. Toronto, Canada: EM Squared Incorporated, 2000. p. 332-344.

[163] Hench LL. Bioceramics: from concept to clinic. J Am Ceram Soc 1991;74(7):1487-1510.

[164] Martins VCA, Goissis G, Ribeiro AC, Marcantonio E, Jr., Bet MR. The controlled release of antibiotic by hydroxyapatite-anionic collagen composites. Artif Organs 1998;22(3):215-221.

[165] Higuchi T. Mechanism of sustained-action medication. Theoretical analysis of rate of release of solid drugs dispersed in solid matrices. J Pharm Sci 1963;52(12):1145-1149.

[166] Kurashina K, Kurita H, Kotani A, Takeuchi H, Hirano M. In vivo study of a calcium phosphate cement consisting of a-tricalcium phosphate/dicalcium phosphate dibasic/tetracalcium phosphate monoxide. Biomaterials 1997;18(2):147-151.

[167] Gao TJ, Lindholm TS, Kommonen B, Ragni P, Paronzini A, Lindholm TC. Microscopic evaluation of bone-implant contact between hydroxyapatite, bioactive glass and tricalcium phosphate implanted in sheep kiaphyseal defects. Biomaterials 1995;16(15):1175-1179.

[168] Flautre B, Pasquier G, Blary MC, Anselme K, Hardouin P. Evaluation of hydroxyapatite powder coated with collagen as an injectable bone substitute: microscopic study in rabbit. J Mater Sci Mater Med 1996;7(2):63-67.

[169] Domb AJ, Manor N, Elmalak O. Biodegradable bone cement compositions based on acrylate and epoxide terminated poly(propylene fumarate) oligomers and calcium salt compositions. Biomaterials 1996;17(4):411-417.

[170] Ali SAM, Doherty PJ, Williams DF. Mechanisms of polymer degradation in implantable devices. 2. Poly(DL-lactic acid). J Biomed Mater Res 1993;27(11):1409-1418.

[171] Nie L, Nicolau DP, Nightingale CH, Browner BD, Quintiliani R. In vitro elution of ofloxacin from a bioabsorbable polymer. Acta Orthop Scand 1995;66(4):365-368.

[172] Lin SS, Ueng SW, Liu SJ, Chan EC, Chao EK, Tsai CH, et al. Development of a biodegradable antibiotic delivery system. Clin Orthop 1999;(362):240-250.

[173] Liu S-J, Ueng SW-N, Chan E-C, Lin S-S, Tsai C-H, Wei F-C, et al. In vitro elution of vancomycin from biodegradable beads. J Biomed Mater Res 1999;48(5):613-620.

[174] Gander B, Meinel L, Walter E, Merkle HP. Polymers as a platform for drug delivery: reviewing our current portfolio on poly(lactide-co-glycolide) (PLGA) microspheres. Chimica 2001;55(3):212-217.

[175] Anderson JM, Shive MS. Biodegradation and biocompatibility of PLA and PLGA microspheres. Adv Drug Deliv Rev 1997;28(1):5-24.

[176] Ikada Y, Tsuji H. Biodegradable polyesters for medical and ecological applications. Macromol Rapid Commun 2000;21(3):117-132.

[177] Huh KM, Cho YW, Park K. PLGA-PEG block copolymers for drug formulations. Drug Deliv Technol 2003;3(5):42, 44-49.

[178] Mi F-L, Shyu S-S, Lin Y-M, Wu Y-B, Peng C-K, Tsai Y-H. Chitin/PLGA blend microspheres as a biodegradable drug delivery system: a new delivery system for protein. Biomaterials 2003;24(27):5023-5036.

[179] Wildemann B, Sander A, Schwabe P, Lucke M, Stoeckle U, Raschke M, et al. Short term in vivo biocompatibility testing of biodegradable poly(D,L-lactide)-growth factor coating for orthopedic implants. Biomaterials 2005;26(18):4035-4040.

[180] Darouiche RO, Farmer J, Chaput C, Mansouri M, Saleh G, Landon GC. Anti-infective efficacy of antiseptic-coated intramedullary nails. J Bone Joint Surg Am 1998;80(9):1336-1340.

[181] Pouton CW, Akhtar S. Biosynthetic polyhydroxyalkanoates and their potential in drug delivery. Adv Drug Deliv Rev 1996;18(2):133-162.

[182] Lee SY. Plastic bacteria? Progress and prospects for polyhydroxyalkanoate production in bacteria. Trends Biotechnol 1996;14(11):431-438.

[183] Gursel I, Korkusuz F, Turesin F, Alaeddinoglu NG, Hasirci V. In vivo application of biodegradable controlled antibiotic release systems for the treatment of implant-related osteomyelitis. Biomaterials 2001;22(1):73-80.

[184] Schmoekel HG, Weber FE, Schense JC, Graetz KW, Schawalder P, Hubbell JA. Bone repair with a form of BMP-2 engineered for incorporation into fibrin cell ingrowth matrices. Biotechnol Bioeng 2004;89(3):253-262.

[185] Deuel TF, Zhang N. growth factors. In: Lanza RP, Langer R, Vacanti J, editors. Principles of tissue engineering. 2nd ed. San Diego, CA: Academic Press, 2000. p. 129-141.

[186] Sumner DR. Fixation of implants. In: Callaghan JJ, Rosenberg AG, Rubash HE, Simonian PT, Wickiewicz TA, editors. The adult knee. Philadelphia: Lippincott Williams & Wilkins, 2003. p. 289.

[187] Jacobs JJ, Goodman SB, Sumner DR, Hallab NJ. Biological response to orthopaedic implants. In: Sheldon RS, editor. Orthopaedic Basic Science,Anonymous. Rosemont, Illinois: American Academy of Orthopaedic Surgeons, 2000. p. 401.

[188] Moucha CS, Urban RM, Turner TM, Jacobs JJ, Sumner DR. Fixation of Implants. In: Shanbhag A, Rubash HE, Jacobs JJ, editors. Joint replacements and bone resorption: pathology, biomaterials and clinical practice. New York: Marcel Dekker, 2005.

[189] Richardson TP, Murphy WL, Mooney DJ. Polymeric delivery of proteins and plasmid DNA for tissue engineering and gene therapy. Crit Rev Eukaryot Gene Expr 2001;11(1-3):47-58.

[190] Bouhadir KH, Mooney DJ. Promoting angiogenesis in engineered tissues. J Drug Target 2001;9(6):397-406.

[191] Young JL, Dean DA. Nonviral gene transfer strategies for the vasculature. Microcirculation 2002;9(1):35-49.

[192] Perez-Martin M, Azcoitia I, Trejo Jose L, Sierra A, Garcia-Segura Luis M. An antagonist of estrogen receptors blocks the induction of adult neurogenesis by insulin-like growth factor-I in the dentate gyrus of adult female rat. Eur J Neurosci 2003;18(4):923-930.

[193] Lanza RP, Langer R, Vacanti J. Principles of tissue engineering. 2nd ed. San Diego, CA: Academic Press, 2000.

[194] Hess CT. The Art of Skin and Wound Care Documentation. Adv Skin & Wound Care 2003;18(1):43-53.

[195] Hampl J, Schierholz J, Jansen B, Aschoff A. In vitro and in vivo efficacy of a rifampin-loaded silicone catheter for the prevention of CSF shunt infections. Acta Neurochir (Wien) 1995;133(3-4):147-152.

[196] Labhasetwar V, Levy RJ. Implants for site-specific drug delivery. Journal of applied biomaterials : an official journal of the Society for Biomaterials 1991;2(3):211-212.

[197] Mond H, Stokes K, Helland J, Grigg L, Kertes P, Pate B, et al. The porous titanium steroid eluting electrode: a double blind study assessing the stimulation threshold effects of steroid. Pacing and clinical electrophysiology : PACE 1988;11(2):214-219.

[198] Wish M, Swartz J, Cohen A, Cohen R, Fletcher R. Steroid-tipped leads versus porous platinum permanent pacemaker leads: a controlled study. Pacing and clinical electrophysiology : PACE 1990;13(12 Pt 2):1887-1890.

[199] Singarayar S, Kistler Peter M, De Winter C, Mond H. A comparative study of the action of dexamethasone sodium phosphate and dexamethasone acetate in steroid-eluting pacemaker leads. Pacing and clinical electrophysiology : PACE 2005;28(4):311-315.

[200] Patil SD, Papadimitrakopoulos F, Burgess DJ. Dexamethasone-loaded poly(lactic-co-glycolic) acid microspheres/poly(vinyl alcohol) hydrogel composite coatings for inflammation control. Diabetes Technology & Therapeutics 2004;6(6):887-897.

[201] Hickey T, Kreutzer D, Burgess DJ, Moussy F. In vivo evaluation of a dexamethasone/PLGA microsphere system designed to suppress the inflammatory tissue response to implantable medical devices. J Biomed Mater Res 2002;61(2):180-187.

[202] Ward WK, Troupe JE. Assessment of chronically implanted subcutaneous glucose sensors in dogs: the effect of surrounding fluid masses. ASAIO journal (American Society for Artificial Internal Organs : 1992) 1999;45(6):555-561.

[203] Woo GLY, Mittelman MW, Santerre JP. Synthesis and characterization of a novel biodegradable antimicrobial polymer. Biomaterials 2000;21(12):1235-1246.

[204] Harten RD, Svach DJ, Schmeltzer R, Uhrich KE. Salicylic acid-derived poly(anhydride-esters) inhibit bone resorption and formation in vivo. J Biomed Mater Res A 2005;72A(4):354-362.

[205] Tanihara M, Suzuki Y, Nishimura Y, Suzuki K, Kakimaru Y, Fukunishi Y. A Novel Microbial Infection-Responsive Drug Release System. J Pharm Sci 1999;88(5):510-514.

[206] Tanihara M, Suzuki Y, Nishimura Y, Suzuki K, Kakimaru Y. Thrombin-sensitive peptide linkers for biological signal-responsive drug release systems. Peptides (New York) 1998;19(3):421-425.

[207] Grainger DW. Controlled-release and local delivery of therapeutic antibodies. Expert Opin Biol Ther 2004;4(7):1029-1044.

[208] Minko T, Kopeckova P, Kopecek J. Mechanisms of anticancer action of HPMA copolymer-bound doxorubicin. Macromol Symp 2001;172:35-47.

[209] Griffith LG. Emerging design principles in biomaterials and scaffolds for tissue engineering. Ann N Y Acad Sci 2002;961(Reparative Medicine):83-95.